EMPIRICAL CHARACTERIZATION OF BALLISTIC IMPACT FLASH

THESIS

Thomas P. Talafuse, First Lieutenant, USAF

AFIT-OR-MS-ENS-11-23

DEPARTMENT OF THE AIR FORCE

AIR UNIVERSITY

AIR FORCE INSTITUTE OF TECHNOLOGY

Wright-Patterson Air Force Base, Ohio

AFIT-OR-MS-ENS-11-23

EMPIRICAL CHARACTERIZATION OF BALLISTIC IMPACT FLASH

THESIS

Presented to the Faculty of the
Department of Operational Sciences
Graduate School of Engineering and Management
Air Force Institute of Technology
Air University
Air Education and Training Command
in Partial Fulfillment of the Requirements for the
Degree of Master of Science in Operations Research

Thomas P. Talafuse, B.S.
First Lieutenant, USAF

March, 2011

AFIT-OR-MS-ENS-11-23

EMPIRICAL CHARACTERIZATION OF BALLISTIC IMPACT FLASH

Thomas P. Talafuse, B.S.
First Lieutenant, USAF

Approved:

//SIGNED//	18 MARCH 11
Dr. Raymond R. Hill (Advisor)	Date
//SIGNED//	18 MARCH 11
Maj Shay R. Capehart (Reader)	Date

Abstract

Fires onboard aircraft are leading mechanisms for mishaps and losses during peacetime and combat operations. Typical ignition sources causing fires onboard aircraft include electrical sparks and hot surfaces. However, impact and penetration of common threats encountered during combat operations, such as armor piercing incendiary projectiles and missile fragments, generate short-lived, but thermally-intense clouds (flashes) capable of igniting fires. Fire simulations supporting system-level survivability analyses depend on accurate characterization of these flash clouds, however, such accurate representations are not currently available.

This research presents the modeling approach developed to estimate the boundary model representations of impact flashes. The research presents generalized meta-modeling approaches to estimate flash size radii (in both the X and Y dimension), flash position, flash size duration, and flash orientation. The empirical model was developed using actual test data obtained via live-fire testing conducted by the 46th Test Group, Aerospace Survivability Analysis Branch. The time series response data from a set of live-fire test events were validated, analytical methods used to develop that response data based on impact event image processing were refined, and the data were then used to create fourth-order time series models of the response data for each of the test events. The collective of these time series models were then characterized by their parameter sets and a meta-model of those parameterizations was built as a function of test event setup parameters (e.g., projectile speed, angle of attack, and impact material) These final models were transitioned to the customer and are being linked to physics-based thermal models. The end result will be a first-ever projectile impact flash cloud representation suitable for survivability analyses.

Acknowledgements

Special thanks goes to my research advisor, Dr. Raymond Hill, for his tireless guidance and mentorship during this program of study. Without his help and direction, this research would have never been completed.

Thanks also to the sponsor unit, the Aerospace Survivability Branch of the 46th Test Group at Wright-Patterson AFB, specifically Mr. Jaime Bestard. In sponsoring this research, my education horizons were vastly expanded and I was able to apply my learning to a real-world problem. I hope my efforts will be of value to current and future Americans in harm's way.

Table of Contents

List of Figures

List of Tables

EMPIRICAL CHARACTERIZATION OF BALLISTIC IMPACT FLASH

1. Introduction

1.1 Background

The capability of an aircraft to avoid or withstand a man-made hostile environment is, obviously, a major concern for any air force. This phenomenon is referred to as "aircraft combat survivability" [1]. An aircraft's survivability can be measured through two primary factors. The first, susceptibility, focuses on the inability of an aircraft to avoid the elements of an enemy's air defense that make up the man-made hostile mission environment, such as approaching missiles, guns, etc. The second factor, vulnerability, refers to the inability of an aircraft to withstand the damage caused by the man-made hostile environment. That is, the likelihood that an aircraft will survive given that it has been hit [1].

One way an enemy attempts to impair an aircraft is through kinetic energy penetrators. Such penetrators include armor piercing incendiary (API) rounds, or fragments from an exploding warhead. The kinetic energy of these fragments involved in a ballistic impact is dissipated in various forms, mainly through deformation of the target, friction, and heat [2]. Energy dissipated by heat results in various phenomena, such as the oxidation of spall (i.e., flakes broken off from the projectile or target) and/or the combustion of incendiary mixtures. Flash occurs as the spall and subsequent fragmentation from the impact have enough thermal energy to oxidize the materials involved and is capable of igniting flammable mixtures [2]. Figure 1 illustrates the phenomenon of a fragment striking a target, with an impact-side

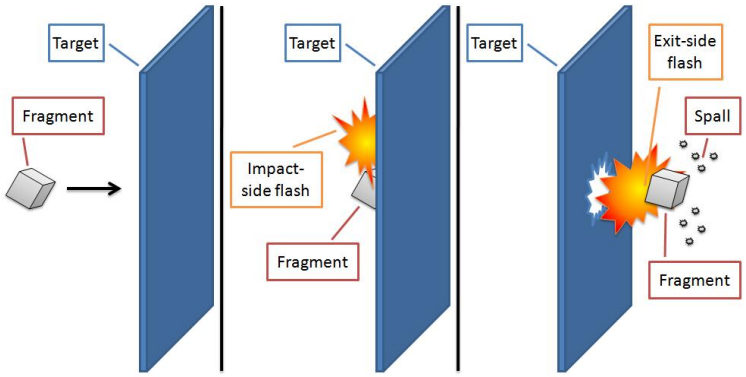

Figure 1 Fragment Flash Phenomenon [2]

flash occurring as material is oxidized on impact, and a subsequent exit-side flash from oxidation of both target material and spall.

Studying the effects these fragments have on military aircraft is one method of enhancing the survivability of those military aircraft. Analysts at the Aerospace Survivability and Safety Operating Location (46th TG/OL-AC) at Wright-Patterson Air Force Base have analyzed fragment penetration prediction for several years. They have sought to standardize a data collection methodology and to develop valid flash characterization models. Current models were developed before the availability of digital high-speed video and can only roughly predict flash duration and size. High-speed video provides the capability to conduct post-test analyses to estimate flash characteristics. With this increase in technology, a new model should be capable of predicting flash shape, position, size, orientation, and the thermal energy contained within the flash for the duration of the event.

Recent efforts have focused on developing models to characterize the boundaries of ballistic impact flashes. Using tests performed by the 46th Test Group, Aerospace Survivability Analysis Branch, high-speed video data were analyzed and reduced to time series parameters describing the ellipses enclosing the flash cloud at each frame [2]. These ellipses provide measures of flash size, position, and orientation. These data, coupled with the associated experimental settings, provide a set of predictive data for ballistic impact flash characterization. Subsequent re-

gression analysis was performed on the data and an empirical model was derived to characterize ballistic impact flash size [4].

1.2 Problem Statement

While past research has established a satisfactory method of characterizing individual ballistic impact flashes, prediction methodologies are needed to develop effective survivability models. No model currently exists that characterizes these ballistic flash instances. To overcome this inadequacy, a methodology is defined and used to realize a model capable of predicting ballistic impact flash characteristics is built and assessed for both Air Force and joint survivability analyses.

This effort builds directly on the data reduction results of Bestard & Kocher's (2010) and preliminary work by Henninger (2010). Bestard and Kocher's demonstrate the ability to use numerical methods to fit a series of ellipses to a flash event over the duration of the event [2]. These ellipses are then used to derive flash measurements as a function of time. Henninger's research established that a specific flash radius can be modeled appropriately using regression-based techniques. This approach extends these past results to a more generalized case, predicting ballistic impact flash characteristics based upon a set of initial conditions.

2. Literature Review

This chapter addresses the existing methodologies used for designed experiments, as it is the foundation for data collection used in the model design. Additionally, as this is a follow-on research effort, much of Henninger's literature review is applicable to the current problem. In order to present a thorough understanding of the subject in this document, Henninger's review is re-introduced. This chapter provides a broad survey of ballistic impact flash characterization studies to date, with a focus on four AFIT theses from the 1991-1993 timeframe.

2.1 Designed Experiments

A designed experiment is a test or series of tests in which purposeful changes are made to the input variables of a process or system so that we may observe and identify the reasons for changes that may be observed in the output response [7]. The full listing of such tests is often referred to as a test matrix. In developing a test matrix, the number of variables and the values they assume must be taken into account. To conduct a full factorial test (all possible combinations of variables tested) many experiments are needed. For example, if there are six variables, with two levels, a high and low value associated to each variable, the number of experiments required to conduct a full factorial would be 2^6, or 64 experiments. When some of the variables have more than two possible values the number of experiments grows even larger.

Full factorial designs can be too large in practical cases. To obtain meaningful results without conducting all possible experimental combinations, the techniques of response surface methodology (RSM) and designed experiments are employed. These techniques allow for a subset of the experiments to be performed which have been chosen to maximize the amount of information returned.

2.2 Reynolds 1991

Reynolds [8] focused on modeling the incendiary functioning (IF) of Soviet armor piercing incendiary (API) projectiles impacting graphite/epoxy composite panels. Until his effort, most studies had concentrated on metal targets. Reynolds used multivariate analysis and response surface methodology approaches to uncover a negative correlation between projectile residual mass and incendiary functioning.

Historically, most vulnerability assessments prior to Reynolds' thesis relied on a government study from the 1960s called Project THOR. This study revealed that target material and projectile characteristics (weight, speed, angle, etc.) were both important factors in determining projectile penetration. Project THOR, however, did not examine incendiary or high-explosive effects [8].

The Penetration Equations Handbook for Kinetic-Energy Penetrators, published by the Joint Technical Coordinating Group for Munitions Effectiveness (JTCG/ME), used the results from Project THOR and presented extensive data and equations to determine whether or not an API round will function given a specific target material. The handbook breaks down the prediction of incendiary functioning into five categories: incendiary fails to function, functions completely, partially functions, slow-burns, or has a delayed function. For projectiles other than those tested, there are correction factors that can be applied to the equations. However, these data and other models are not accurate for targets made of composite materials [8].

Reynolds studied data from a test effort using the Soviet 12.7mm API round fired at different angles against various composite material thicknesses. The API round is designed to allow the outer jacket over the nose to peel away during impact, thereby igniting the incendiary material in the nose. The heavy steel (or other metal) core of the round then continues on its path. Ideally, the API round penetrates the skin of an aircraft, with the core subsequently rupturing fuel or hydraulic lines or

fuel tanks, at which point a proper incendiary flash created upon initial impact with the skin would cause ignition of those escaping fluids [8].

In his analysis, Reynolds used four predictor variables: impact velocity (IV), impact mass (IM), ply thickness (PLY), and impact obliquity angle (ANG) [8]. These variables were used to derive formulas for residual mass (RM), residual velocity (RV), and incendiary function (IF).

Reynolds data included some test shots where the incendiary function occurred on the entry side of the target. The analysis derived two separate regression models: one (type I) that classified entry-side functioning as actual functioning that could ignite fuel, and another (type II) that classified it as a non-function. The equations are listed below.

$$\begin{aligned} IF(typeI) = &- 9.305985 + 0.226584 * PLY + 0.001116 * ANG^2 \\ &+ 0.0000039451 * IV * IM - 0.000064 * IV * PLY \\ &+ 0.000015 * IV * ANG - 0.000073 * IM * ANG \\ &- 0.00044 * PLY * ANG \end{aligned} \tag{1}$$

$$\begin{aligned} IF(typeII) = &- 8.219702 - 0.001746 * PLY^2 + 0.000313 * ANG^2 \\ &- 0.000014 * IV * PLY + 0.000041 * IV * ANG \\ &+ 0.000426 * IM * PLY - 0.002008 * PLY * ANG \end{aligned} \tag{2}$$

The discriminant analysis called for rounding the results from the above equations, yielding values that fell into the following five IF categories:

0 - No Function

1 - Delayed Function

3 - Slow Burn

4 - Partial Function

5 - Complete Function

Reynolds effort improved upon the JTCG/ME with respect to composite targets, but left room for improvement in predicting what type of incendiary functioning will occur [8].

2.3 Knight 1992

Knight [5] expanded Reynolds effort and continued to analyze API projectile function. Knight specifically used regression analysis, discriminant analysis, and neural networks to better predict residual velocity, residual mass, and incendiary functioning of 12.7mm and 14.5mm API rounds on graphite/epoxy composite panels.

Knight's test shots were accomplished by the Wright Laboratories Survivability Enhancement Branch. For incendiary functioning, 281 shots were deemed valid. High-speed flash photography was used to document IF, with three separate IF classifications:

#1: 2-group classification (nonfunctioning and functioning)

#2: 2-group classification (nonfunction (entry-side functions included) and mixed)

#3: 3-group classification (entry-side, nonfunctions, and mixed)

The mixed category included complete, delayed, slow burn, and partial functioning shots [5].

To summarize Knights findings, a neural network algorithm was chosen as the best method to classify each shot into one of three categories: frontal (entry side function), mixed functioning (includes all types of function), and nonfunctions. The misclassification rate was 8.25%.

2.4 Lanning 1993

Lanning [6] studied API projectile effects when penetrating two composite panels. IF was examined only in that it directly relates to residual projectile mass.

Lanning states that incendiary effects are not a quantifiable variable [6]. The technology available at the time to record the incendiary flash made it an inexact science. At the time, seven IF categories were used: non-function, partial, slow burn, frontal, delayed, complete and total.

Using two panels expanded the possible results since each panel could see a different IF category. Since Lanning only had 52 data points, the number of IF categories was reduced to two. This made incendiary function a binary variable. Discriminant analysis and neural networks were used, with promising results. Generally, it was found that composite panels require a higher projectile velocity in order to produce flashes, and that they produce flashes of a longer duration than aluminum panels.

2.5 Blythe 1993

Blythe [3] attempted to establish a methodology for predicting flash characteristics of projectile impacts with composite materials, along with residual mass and velocity. Blythe indicates that exit-side flashes had not been studied much prior to that time. He mentions studies by Ritter in 1986 and 1989 of steel fragments impacting metal and graphite/epoxy targets that focused on flash duration, temperature, and pressure. He also highlighted the current method for predicting the probability of kill for kinetic projectiles, the Computation of Vulnerable Areas and Repair Times (COVART) computer model [3].

The test shots used 20mm and 30mm guns to shoot steel fragments into aluminum and composite targets. Exit-side flashes were first observed with mid-velocity shots (7,000 feet/second) for the aluminum target and not until the high-velocity shots for the composite (10,000 feet/second). Additionally, the flash peaked much more quickly with the aluminum target (0.2 milliseconds) than with the composite target (1.1 milliseconds) [3]. While no model for predicting exit-side flashes was

produced, Blythe recommended focusing on the 7,000-9,000 feet/seconds regime for composites, and using discriminant analysis for developing the prediction model [3].

2.6 Bestard & Kocher 2010

Technological advances now allow capturing ballistic impact flashes on high-speed digital video. Bestard & Kocher [2] used image processing algorithms to perform frame-by-frame analysis of flashes and enclose the flash instance within an ellipse. Figure 2 illustrates this image processing encapsulation. Due to the noisy nature of the flash, they used numerically stable methods based on least squares minimization. Measurements of ellipse axes provide flash size estimates, along with data on ellipse orientation and location, all as a function of time.

Figure 2 Video Frame with Entry and Exit Flashes and Fitted Ellipses

Given a set of n boundary data points ($\tilde{x}_i$ and $\tilde{y}_i$), the definition of an ellipse is

$$F(x, y) = p_1x^2 + p_2xy + p_3y^2 + p_4x + p_5y + p_6 = 0, p_2^2 - 4p_1p3 < 0. \quad (3)$$

Bestard & Kocher [2] expressed the ellipse-specific fitting problem as a constrained minimization problem

$$\min_{\vec{a}} \|\mathbf{D}\vec{a}\| \text{ subject to } \vec{a}^T\mathbf{C}\vec{a} = 1 \quad (4)$$

where

$$\mathbf{D} = \begin{bmatrix} \tilde{x}_1^2 & \tilde{x}_1\tilde{y}_1 & \tilde{y}_1^2 & \tilde{x}_1 & \tilde{y}_1 & 1 \\ \vdots & \vdots & \vdots & \vdots & \vdots & \vdots \\ \tilde{x}_n^2 & \tilde{x}_n\tilde{y}_n & \tilde{y}_n^2 & \tilde{x}_n & \tilde{y}_n & 1 \end{bmatrix}, \vec{a} = \begin{bmatrix} \vec{a}_1 \\ \vec{a}_2 \end{bmatrix}, \vec{a}_1 = [p_1\ p_2\ p_3]^T, \vec{a}_2 = [p_4\ p_5\ p_6]^T \tag{5}$$

and

$$\mathbf{C} = \begin{bmatrix} \mathbf{C_1} & \mathbf{0} \\ \mathbf{0} & \mathbf{0} \end{bmatrix}, \mathbf{C_1} = \begin{bmatrix} 0 & 0 & 0 \\ 0 & -1 & 0 \\ 2 & 0 & 0 \end{bmatrix} \tag{6}$$

The optimal solution of the system corresponds to the eigenvector of $\vec{a}$.

This algorithm provides a time series of ellipse positions (S), sizes (A), and orientations (ϕ) for each test event whose parameters are given by:

$$S(t_i) = \sqrt{x_{0,i}^2 + y_{0,i}^2}\,,\ A(t_i) = \pi r_{x,i} r_{y,i},\ and\ \phi(t_i) = \frac{1}{2} arccot\left(\frac{p_1 - p_3}{p_2}\right) \tag{7}$$

where:

$$\begin{aligned} x_{0,i} &= \frac{2p_3p_4 - p_2p_5}{4\beta}, \\ y_{0,i} &= \frac{2p_1p_5 - p_2p_4}{4\beta}, \\ r_{x,i} &= \sqrt{\frac{\alpha}{\beta(p_3 - p_1) - \gamma}}, \\ r_{y,i} &= \sqrt{\frac{\alpha}{\beta(p_1 - p_3) - \gamma}} \end{aligned} \tag{8}$$

and:

$$\begin{aligned}\alpha =&\frac{1}{2}(p_1p_5^2 + p_3p_4^2 + p_6p_2^2 - p_2p_4p_5 - 4p_1p_3p_6),\\ \beta =&(\frac{p_2^2}{4} - p_1p_3)\sqrt{(1 + \frac{p_2^2}{(p_1 - p_3)^2}},\\ \gamma =&(p_3 + p_1).\end{aligned} \tag{9}$$

Bestard & Kocher tried to generalize the overall displacement and flash size. They concluded that the components of the flash trajectory (i.e., the x and y components) were hard to establish, but that the overall displacement (S) generally follows a logarithmic trajectory [2]. They observed that fragment flashes on the impact side show rapid growth and slower decay while exit side flashes exhibit slower growth and decay. Data were collected on the magnitude of the major radius and minor radius for entry-side flash, where the major radius is the semi-major axis and the minor radius the semi-minor axis of the ellipse. No distribution was fit to these components, however, Bestard & Kocher observed that a Weibull distribution provided a relatively good fit to the overall area of the flash cloud for entry-side flash [2]. While the Weibull distribution shape captured the shape of the flash time-series data, using the Weibull distribution is not appropriate for subsequent survivability modeling. A function of time that adequately captures the shape of the flash time-series is needed.

Bestard & Kocher also concluded that orientation of the flash clouds are not clear and with orientation ranges between 0° and 90°, the most plausible simplification of these variations is to consider a constant orientation, found by taking the average of the orientation time series [2].

2.7 Henninger 2010

Henninger [4] sought a time-based empirical function to model the flash-event time-series data. Henninger examined test data from eight shots of steel frag-

ments against bismaleidmide resin (BMI) targets collected by the 46th Test Group, Aerospace Survivability Analysis Branch, to demonstrate the ability to model the life of a flash radius as a time series model, with time as the regressor. The designed experiment varied the same four factors used in previous research: projectile weight, projectile velocity, target panel thickness, and impact obliquity. He focused solely on the entry-side flash radius and did not delve into the position, orientation, duration, or thermal aspects of the flash and assumed separate models for both the X-axis and Y-axis. Henninger's original idea was to develop a model for flash radius of the form

$$FlashRadius = f(time) + N(0, \sigma^2) \tag{10}$$

where $f(time)$ is the regression-based model and $N(0, \sigma^2)$ is some normally distributed error that captures the inherent noise within the flash radii. Analysis showed that a quartic model provided a good fit to flash radius, as seen in Figure 3, and

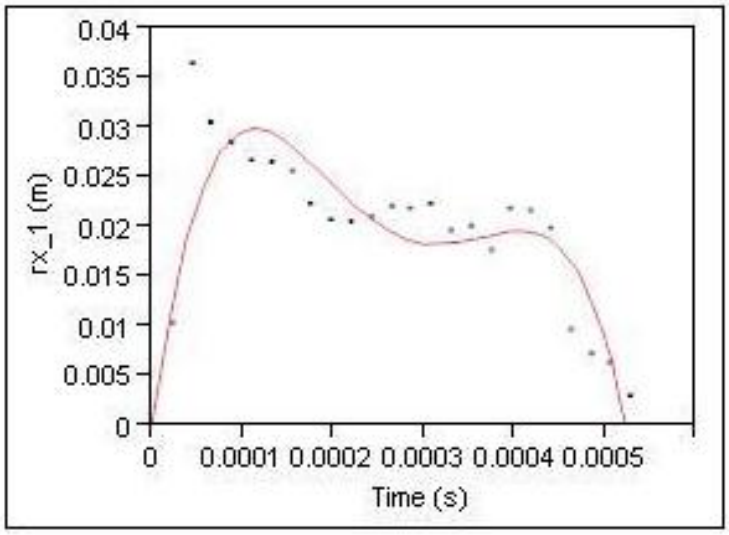

Figure 3 Quartic Fit of X-radius vs. Time

takes the form

$$r_{x_i}(t) = \beta_{x_1} t + \beta_{x_2} t^2 + \beta_{x_3} t^3 + \beta_{x_4} t^4 + \epsilon_{x_i} \tag{11}$$

$$r_{y_i}(t) = \beta_{y_1} t + \beta_{y_2} t^2 + \beta_{y_3} t^3 + \beta_{y_4} t^4 + \epsilon_{y_i}. \tag{12}$$

Henninger fit a quartic model to replicates with the same design settings. He found that this model had an averaging effect between the two sets of data and was not as accurate in modeling the flash radius. This can be seen in Figure 4. He also combined data sets across projectile weights, with similar results.

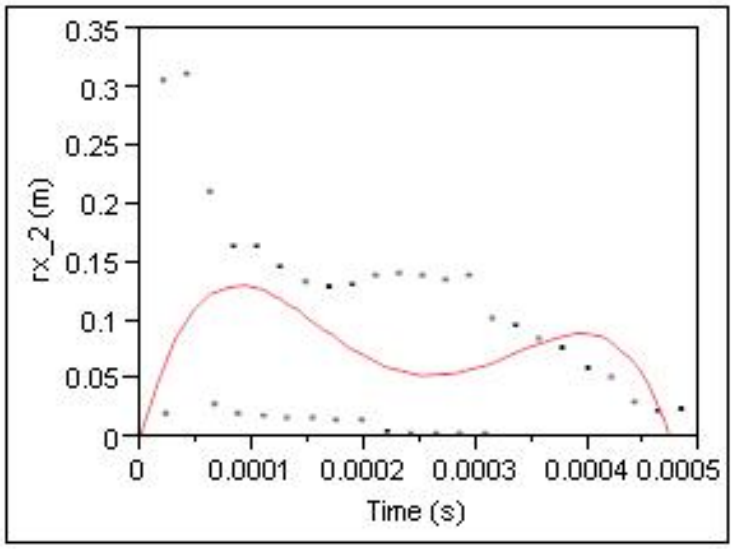

Figure 4 Combined Model: X-Radius vs. Time

Henninger concluded that aggregating the data added to the error but did not add to the fidelity of the model. Furthermore, residuals from the model indicated non-constant variance and were not normally distributed, leading Henninger to believe that a better model for flash radius would most likely be of the form

$$FlashRadius = f(time) + g(time) \tag{13}$$

where $g(time)$ represents the error in terms of a time series model [4].

2.8 COVART

The Computation of Vulnerable Area Tool (COVART) model predicts the ballistic vulnerability of vehicles (fixed-wing, rotary-wing, and ground targets), given ballistic penetrator impact. Each penetrator is evaluated along each shotline (line-of-sight path through the target). Whenever a critical component is struck by the penetrator, the probability that the component is defeated is computed using user defined conditional probability-of-component dysfunction given a hit (Pcd/h) data. COVART evaluates the vulnerable areas of components, sets of components, systems, and the total vehicle. In its simplest form, vulnerable area is the product of the presented area of the component and the Pcd/h data. The total target vulnerable area is determined from the combined component vulnerable areas based upon various target damage definitions.

COVART is capable of modeling several penetrators: a single missile fragment, a set of missile fragments, a single Man Portable Air Defense (MANPAD) missile, a single Armor Piercing Incendiary (API) projectile, and a single High Explosive Incendiary (HEI) projectile. COVART is also capable of modeling the damage mechanisms induced by threat penetrators. Damage is modeled using several methods. Analysts' selection of the damage mechanism modeling method depends upon the penetrator type and failure modes of the equipment being modeled. Physical damage criteria, such as hole size or damage distance, are preferred because they can be directly related to tests. Distance criteria are used to model blast and hydrodynamic ram induced damage. Hole size criteria is used to model functional failures due to liquid leaking from a container. Air-gap distance criteria are used to model sustained fires from threat induced leaks of flammable materials. Other equipment damage is modeled using penetrator impact mass and velocity relationships. A given component may be vulnerable to several damage effects. The COVART model uses failure analysis trees (fault trees) to assess the cascading effects of damage. The fault trees use data obtained from ground simulators (flight controls simulators, hydraulic sys-

tem simulators, avionics coolant simulators, fuel system simulators, electrical power simulators) to enhance the robustness and quality of failure predictions.

COVART requires data characterizing the threat; velocity, material etc. The model also needs specific data on the materials and thicknesses of aircraft components. Required inputs for the critical components, for the kill level being analyzed, include Pcd/h data and fault tree data for redundant components. The COVART model assumes the penetrator or fragment travels along the shotline, ricochet and spall are not modeled, and blast effects are not considered. The COVART model determines the component and aircraft vulnerable areas as a function of the kill level for the specified attack directions. Numerous kill levels can be modeled [1].

2.9 Summary

Past efforts were limited by the video technology required to obtain the data to predict residual mass, residual velocity, and incendiary function based upon test characteristics of impact velocity, impact mass, material (ply) thickness, and angle of attack (obliquity). As a result, most past research focused on classification of flash effects versus characterization of the flash. Likewise, these same limitations hampered efforts to model flash size. The same aircraft vulnerability concerns that motivated past research efforts are still of concern today. However, current technologies are now sufficient to obtain the necessary data to provide more accurate flash characterization models.

While the current video technology allows for data collection to re-examine these past studies, the current effort focuses on building predictive flash characterization models. The next chapter provides the initial methodology along with model validation approaches.

3. Methodology

This chapter presents the methodology developed in this research. Section 3.1 discusses the development of the experiment employed by the 46th Test Group, Aerospace Survivability Analysis Branch. Section 3.2 examines how the test was conducted and addresses data collection procedures. Finally, Section 3.3 explains the various analysis procedures used to develop the response surface model yielding the ballistic impact flash boundary model.

3.1 Design of Experiment

This research investigates a method of modeling ballistic impact flash events for survivability analyses. Henninger (2010) made use of data which had already been collected according to a standard experimental design testing sequence and post-processed via the Bestard and Kocher [2] methods. Analyzing such data led Henninger to develop a quartic model, with time as the regressor, which yielded reasonably accurate predictions for flash radius in both the x-axis and y-axis. His equations, however, only predict flash radius as a function of time and do not express the radius as functions of the predictor (independent) variables that define the particulars of the flash event. That same designed experiment is used for current ballistic impact flash modeling efforts, and is described below. A subsequent experiment was defined during this research but not completed in time for its inclusion.

The independent variables associated with each shot are:

1. Panel Thickness,
2. Obliquity Angle,
3. Projectile Mass, and
4. Initial Velocity.

Each independent variable, or factor, was examined at a number of levels, or settings. Based upon previous testing, panel thickness and initial velocity were tested at three different settings, with obliquity angle and projectile mass tested at two levels. Table 1 shows the four factors, their associated levels for testing, and the units of measure for each.

Table 1 Designed Experiment Factors and Levels

Factor	Variable	Low	Med	High	Units
Panel Thickness	Thick	0.1	0.25	0.35	inches
Obliquity Angle	Angle	0	N/A	45	degrees
Projectile Mass	Mass	40	N/A	70	grams
Initial Velocity	Vel	4000	5500	7000	fps

With high-speed digital cameras, footage of each shot was captured and subsequently digitally processed, yielding response variables collected at discrete points in time throughout the duration of the flash. The response variables collected were the flash radius, in both the X-axis and Y-axis, displacement from the point of impact, in both X- and Y-direction, and orientation of the flash ellipse with respect to the shot line. Bestard and Kocher's methods [2] were used in collection of these responses.

A full factorial design includes all possible combinations of each level for every factor. In order to perform a full factorial investigation for this experiment $2^2 * 3^2$, or 36 test shots were required. Each test configuration was replicated twice to provide better estimates and estimate error. This brought the total number of test shots to 72, with the shots run in a random order. The designed experiment can be found in Appendix A.

3.2 Data Collection

The experiment outlined in the previous section was conducted by the 46th Test Group, Aerospace Survivability Analysis Branch, at Wright-Patterson AFB over the course of three weeks in 2009. All projectiles fired were steel fragments.

The target panels were a bismaleidmide resin (BMI) material roughly eight inches square. The test setup is illustrated in Figure 5.

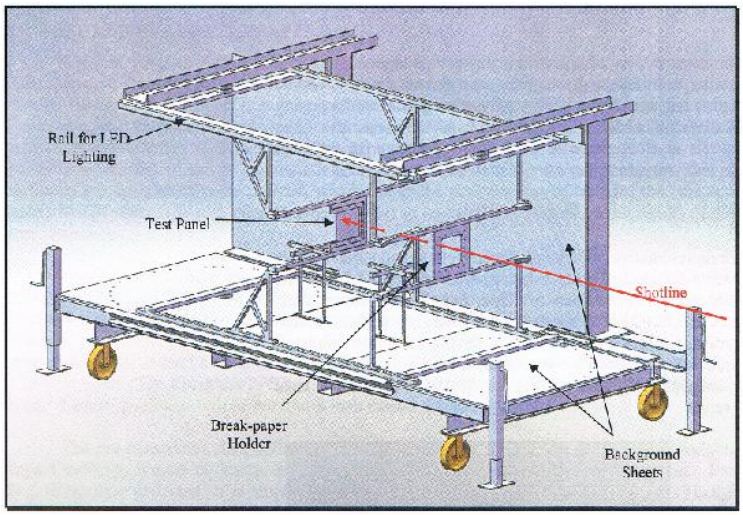

Figure 5 Model of Test Setup

Break paper was used to measure projectile velocity. As the projectile penetrates the paper, an electric current passing through the paper is disrupted, triggering a timing device. Knowing the distance between the gun, break paper, and target, and the time to travel that distance, a velocity is easily computed, allowing for verification of the designed velocity setting.

It is assumed that the tests were conducted with sufficient controls in place to ensure the actual factor settings accurately reflected the designed settings. It is also assumed that Bestard and Kocher's image processing methods provided data that adequately reflect the operational tests conducted.

Initial test results (found in Appendix A) showed that five projectiles (#'s 2, 29, 35, 37, 51) had a firing malfunction and failed to hit the panel. These test points were re-run to provide data for their corresponding test settings.

Test results also showed several cases where the entirety of the entry-side flash was not captured in the video frame, preventing video processing and accurate data from being collected for the entire shot event; using such truncated data would bias

any model building process. Additionally, the structure holding the target panel in place obstructed the view of part of the flash, a cause for concern primarily for smaller flashes. In both cases, these situations impacted the ability to accurately fit an ellipse to the flash, limiting the flash measurement and preventing data from being collected. These shots were not re-run. As a result, these test points were not considered when developing the empirical model. This significantly reduced the number of test points from the 72 shots run, to 21 usable shots. Discussions with subject matter experts deemed these 21 shots a sufficient sample for subsequent empirical model development. Table 2 contains the usable test points.

Table 2 Test Shot Data Used in Study

Test Number	Mass	Velocity	Thickness	Obliquity
T005	40	5500	0.1	45°
T025	40	4000	0.35	45°
T038	40	4000	0.1	0°
T039	75	5500	0.1	0°
T040	75	5500	0.1	0°
T042	75	4000	0.1	0°
T048	75	7000	0.1	0°
T049	40	4000	0.25	0°
T050	40	4000	0.25	0°
T051	75	4000	0.25	0°
T052	75	4000	0.25	0°
T055	75	5500	0.25	0°
T056	75	5500	0.25	0°
T057	40	7000	0.25	0°
T058	40	7000	0.25	0°
T059	75	7000	0.25	0°
T063	75	4000	0.35	0°
T065	40	5500	0.35	0°
T066	40	5500	0.35	0°
T067	75	5500	0.35	0°
T072	75	7000	0.35	0°

3.2.1 Data Validation. An empirical model is only as good as the data upon which it is based. The flash size data used in this research is based on the

post-processing of high speed digital video. The post-processing procedure resulted in very "noisy" data, so data validation was an important aspect of this research.

All 72 shots had video files of the impact and flash. These video files were processed by research interns using MATLAB signal processing routines. User settings defining the ellipses were found to impact the responses obtained by the image processing routine.

Each of the 72 video files were reviewed and examined with respect to the data provided for that shot. Particular attention was paid to the flash location (entry or exit side) and how well the data correlated to the flash.

This validation effort resulted in screening out shots deemed unusable. The effort also uncovered two data processing errors. First, sign reversals were found on some data; these were easily fixed. Second, user inputs pertaining to flash intensity were found to bias the radii measures, underestimating flash size early in the flash event and overestimating flash size near the end of the flash event. This latter error was due to an analysis original goal to examine flash size measures in an aggregate, or engineering, perspective. An empirical model building effort requires statistically-based, unbiased data. Flash radius calculations were re-accomplished using recommended approaches so that cleaner data were used in subsequent analyses.

3.3 Analysis Method

Henninger's [4] efforts led him to build a regression-based model to predict flash radius. The basic concept behind a regression model is the expression of (1) the tendency of the response variable(s) to vary with the predictors in a systematic fashion, and (2) to assess how responses vary around this tendency of statistical relationship, i.e. a deterministic and stochastic piece of the model. Henninger investigated multiple regression model forms to predict flash radius as a function of time and ultimately concluded that a quartic model adequately fit the observed data.

This approach models the flash radius for each shot as a function of time, but does not relate flash radius to the measured factors in the design. Henninger's approach is also limited to estimating flash radius at discrete test settings and would require vast amounts of testing to map flash radius over the range of ballistic impact conditions. An analytical model of a ballistic impact flash event must be a function of the parameters defining that event, such as, in the current setting, fragment speed, size and angle. The quartic model approach of modeling each shots' X-radius and Y-radius, along with models of the flash position in space and angle of movement, thus provide the response data for each experimental design point. This response data, coupled with the experimental design settings (Table 1) can be processed to produce a response surface for each of the X-radius and Y-radius data. This response surface is not your everyday surface since this response surface is used to generate the estimate time-series quartic model for the ballistic flash event. For both the X-radius and Y-radius, the quartic model coefficients are determined using the equation

$$\beta_i = b_0 + b_1 Thick + b_2 Angle + b_3 Mass + b_4 Vel, \;\; i = 1, .., 4. \tag{14}$$

This regression meta-model predicts the time-based quartic model regression coefficients from the factor settings and is the method of relating the factors to flash radius. All possible combinations of the four factors were analyzed; as few as zero and as many as four factors were used to predict the quartic model regression coefficients. Of these 16 possible combinations, the combination that provided the fit with the least amount of error was chosen.

Figure 6 graphically summarizes this methodology developed. Examining clockwise from the upper left corner, the experiment is run producing video of each event. The video is processed to provide a time-series summary of flash measurements. The X-radius and Y-radius time-series are then summarized in quartic models; the model coefficients are now the experimental responses. Response surface

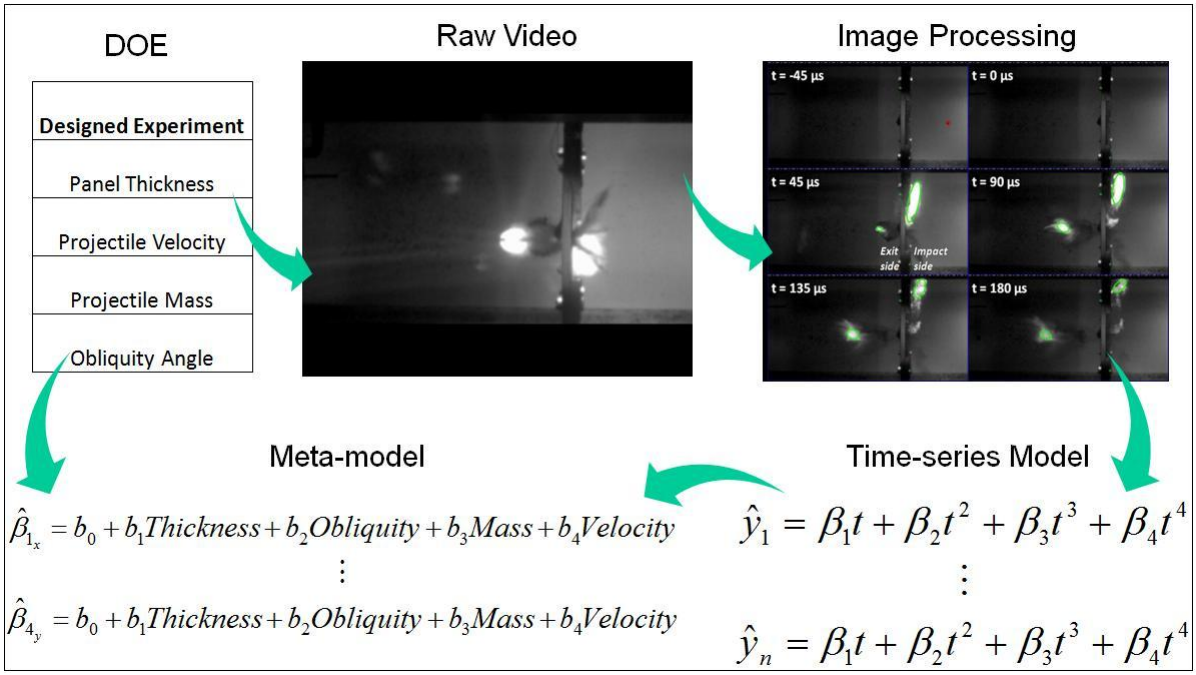

Figure 6 Summary of Methodology

meta-models are created to predict the quartic model coefficients. These meta-models constitute the ballistic impact flash event models.

The remaining flash characteristics, flash position (both X- and Y-directions), orientation, and duration were predicted in a similar fashion. For each characteristic, the data were analyzed and an appropriate regression model developed. Where appropriate, each regression coefficient was modeled as a function of the factor settings.

This provides a set of models that characterizes the size, position, orientation, and duration of a ballistic impact flash. When coupled with physics-based thermal energy models associated with a particular ballistic impact event, a simulation-based approach to the characterization of ballistic impact flash is available to support of system-level survivability analyses crucial for assessing weapon system survivability in hostile environments.

4. Results and Analysis

4.1 Flash Radius

4.1.1 Initial Investigation. Reynolds' [8] research used the four factors in Table 1 to derive formulas for incendiary function. As such, initial investigations for flash radius analysis considered predicting quatric model coefficients using all four factors. Since the goal was to generate a model to accurately characterize a flash, statistical significance was not of primary concern. For each X- and Y-radius, the quartic model

$$FlashRadius(t) = \beta_0 + \beta_1 t + \beta_2 t^2 + \beta_3 t^3 + \beta_4 t^4 \tag{15}$$

was fit to each of the 21 shots listed in Table 2, with no flash radius at time zero, i.e., the intercept, β_0, was set equal to zero. Appendix B contains the coefficient values for each shot (see Tables 7 and 9 for the X-radius and Y-radius quartic model coefficients, respectively). These data are the designed experiment response data.

Using Equation 14, a regression meta-model was created where the response variables were the regression coefficients from the quartic model and the regressors were the four test factors. The coefficients for the quartic model were predicted as a function of the test settings and the meta-model coefficients from Equation 14 are available in Appendix B, Tables 8 and 10 for the X-radius and Y-radius response surface, respectively.

Using the meta-model coefficient values, the factor levels for each shot were input to generate the quartic model coefficients. The observed times from testing were input into the quartic model to generate a predicted flash radius for the duration of the flash. The predicted flash radius was compared to the observed flash radius to assess model adequacy for each of the shots used in this research.

This initial approach provided adequate estimates for roughly one-third of the shots. Figure 7 illustrates a flash radius that was reasonably predicted by the model. The majority of the shots, however, had a predicted flash radius that vastly differed

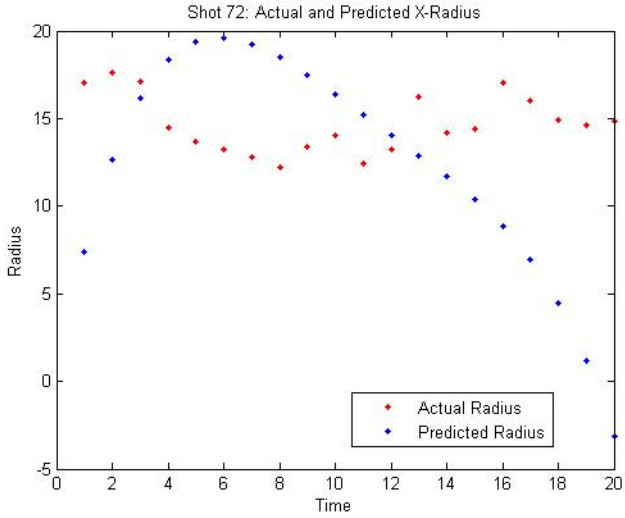

Figure 7 Shot 72 Predicted vs Actual Flash Radius

from the observed values, with errors that were several orders of magnitude greater than the actual flash radius. Figure 8 demonstrates such an occurrence.

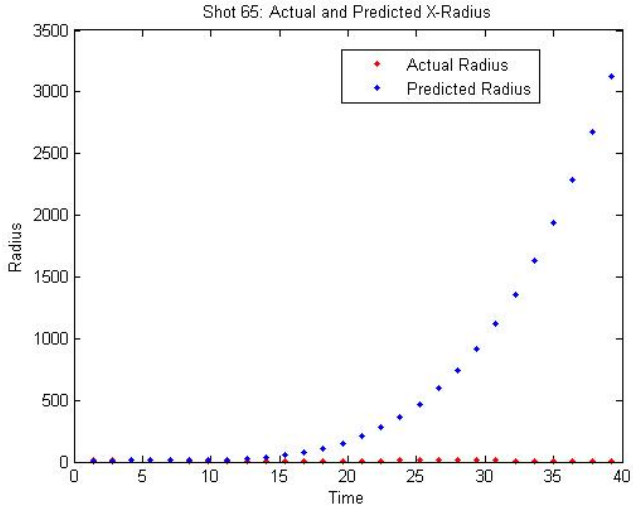

Figure 8 Shot 65 Predicted vs Actual Flash Radius

In contrast to conclusions from Reynolds' research, the results from this initial model indicate that flash radius cannot be predicted with sufficient fidelity when a model is developed using all four factors. Use of all four factors resulted in a model overspecification when predicting the quartic model coefficients, leading to large errors when predicting flash radius. This is unacceptable for survivability analysis purposes.

4.1.2 Finalized Radius Model. To find a more parsimonious and reasonable model, all 15 possible subsets of these four factors were considered and analyzed and the subset of factors that minimized the prediction error was selected for the meta-model. It was observed that when grouped by panel thickness, the flash radii exhibit similar behaviors. Figures 9, 10, and 11 demonstrate this phenomenon for each panel thickness considered in this experiment. The particular results from this fairly extensive model fitting effort are not included in this work.

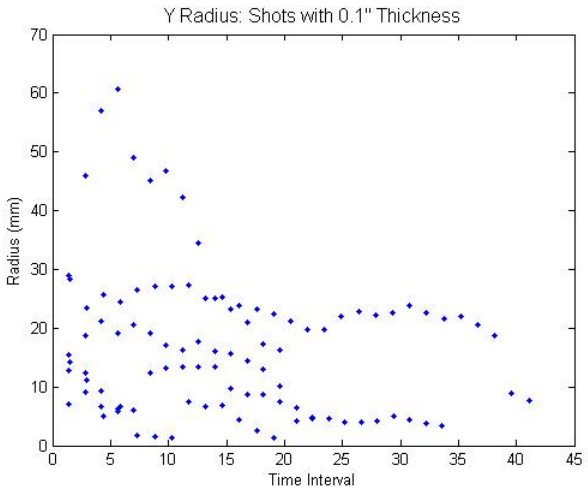

Figure 9 Y-Radius: Flash Radius vs Time, 0.1" Panel Thickness

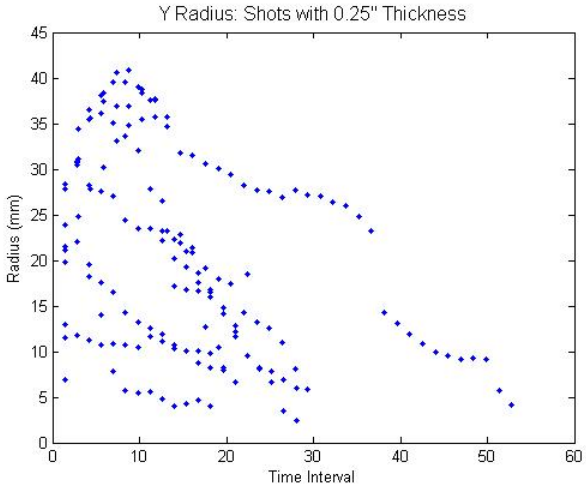

Figure 10 Y-Radius: Flash Radius vs Time, 0.25" Panel Thickness

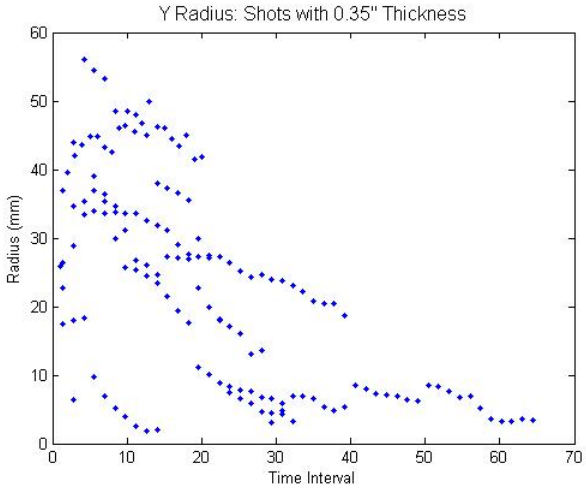

Figure 11 Y-Radius: Flash Radius vs Time, 0.35" Panel Thicnkess

The data were thus grouped into three categories based upon panel thickness. A quartic model was fit to each grouping, yielding three quartic models. Table 3 provides the radius coefficients for both the X-radius and Y-radius for each level of panel thickness.

Table 3 Quartic Model Coefficients by Panel Thickness

Panel Thickness	Radius	β_1	β_2	β_3	β_4
0.1	X	4.450814199	-0.440850217	0.015069162	-0.000170075
	Y	7.507448086	-0.761592921	0.026807665	-0.000307409
0.25	X	3.784029734	-0.309707491	0.008876397	-8.19E-05
	Y	7.451878212	-0.645630814	0.019119153	-0.000182598
0.35	X	2.67616226	-0.173142342	0.004094458	-3.21E-05
	Y	7.868621188	-0.534157888	0.012071884	-8.87E-05

Again, each coefficient of the quartic model was modeled as a function of the panel thickness for each shot using a regression model. The response variables were the regression coefficients from the quartic model and the sole regressor was the panel thickness, taking the form:

$$\beta_i = b_0 + b_1 Thick, \;\; i = 1, .., 4. \tag{16}$$

Table 4 contains the meta-model coefficients for both the X-radius and Y-radius quartic model prediction equation.

Table 4 Radius Meta-Model Coefficients

Radius	Coefficient	b_0	b_1
X	β_1	5.244465859	-6.889130548
	β_2	-0.554140103	1.055314656
	β_3	0.019541582	-0.043692468
	β_4	-0.000224115	0.000554559
Y	β_1	7.305658059	1.301390443
	β_2	-0.856882495	0.898951232
	β_3	0.032944706	-0.058336307
	β_4	-0.000396238	0.000871425

Developing a meta-model where the shots were grouped by panel thickness provided a model that more accurately predicted flash radius for both the X-radius and Y-radius for all shots. Figures 12 and 13 illustrate the improvement in the predictive capability of this model over the model initially considered. All such shot graphs were examined and are available in Appendix C.

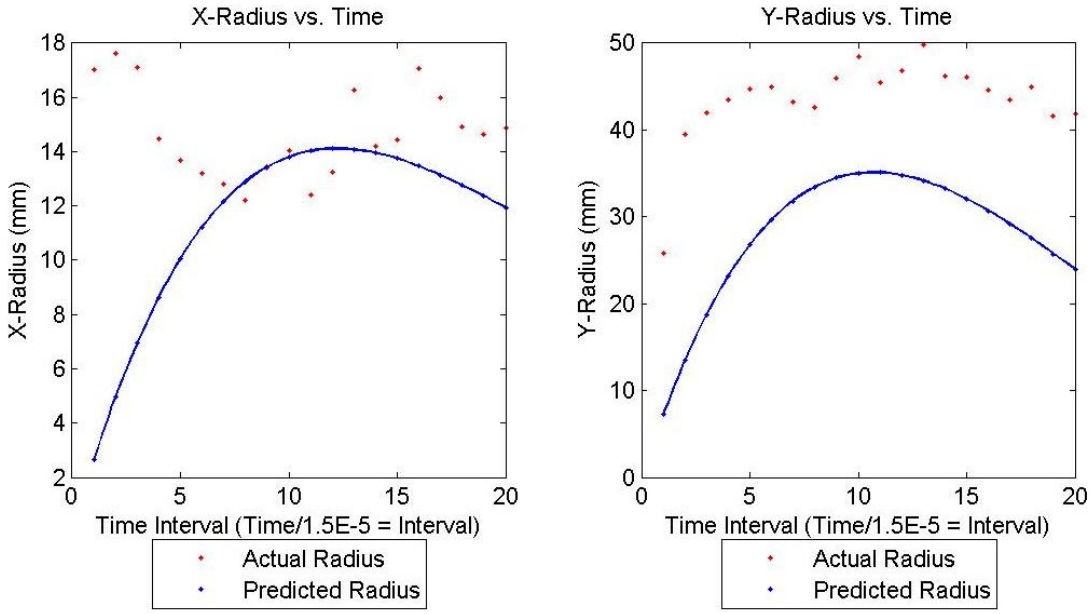

Figure 12 Shot 72 Predicted vs Actual Flash Radius

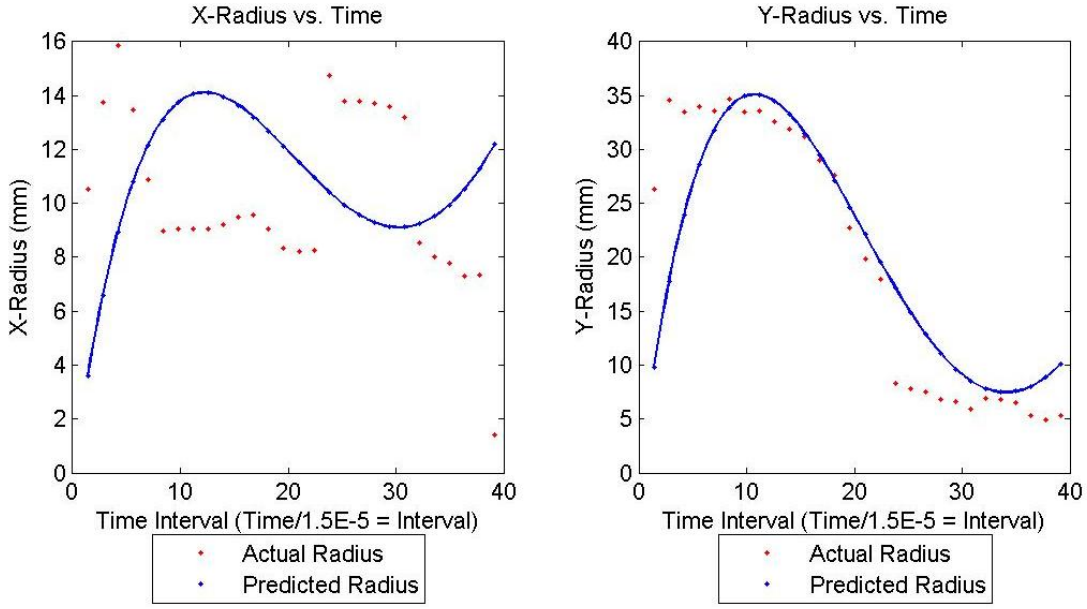

Figure 13 Shot 65 Predicted vs Actual Flash Radius

4.2 Flash Orientation

Bestard & Kocher's [2] research led them to conclude that orientation of the major axis of the flash with respect to the shot line was random, ranging between 0° and 90°. They recommended simplifying this variation to the average angle of the flash orientation over the duration of the flash. Figure 14 illustrates this random nature of the flash orientation. It is reasonable to conclude, then, that flash orientation is not time-dependent.

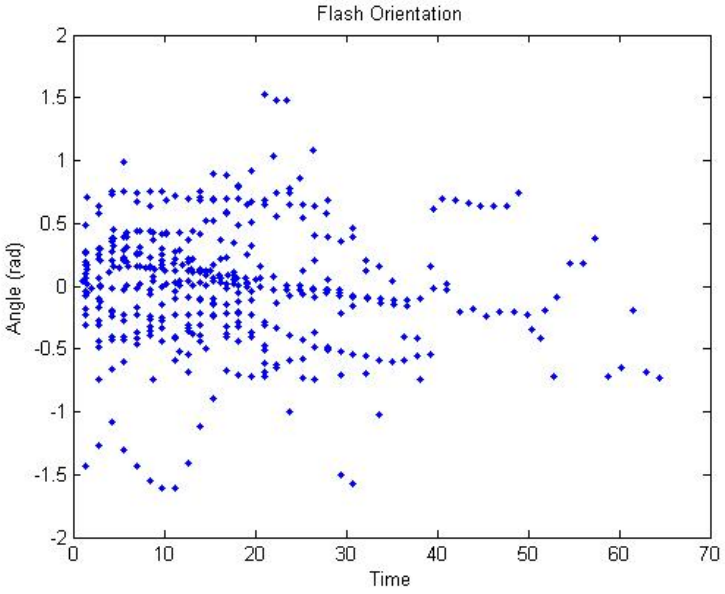

Figure 14 Flash Orientation: Angle of Orientation (rad) With Respect to Time

With no apparent dependency on time, it was hypothesized that flash orientation could vary based upon the various factor settings and was modeled accordingly. Initially, it was thought that trends in flash orientation may exist when categorized by some combination of the factor settings. If so, a theoretical distribution could be fit to the observed orientation angles. Flash orientation could then be modeled stochastically as a random draw from such a distribution and using that value as the orientation angle across the entirety of the flash instance.

The analysis indicated that the flash orientation angle shows no visible patterns when categorized by any combination of the factor settings. For all possible factor combinations, the angle between the major axis of the flash ellipse and the shot line varied significantly across all factor levels, as illustrated in Figure 15.

Further investigations observed that while flash orientation varied greatly with no observable patterns, the range of the orientation angle appeared centered around a zero radian angle. The initial concept of modeling flash orientation using a fitted distribution was applied to the full data set with positive results. Figure 16 displays

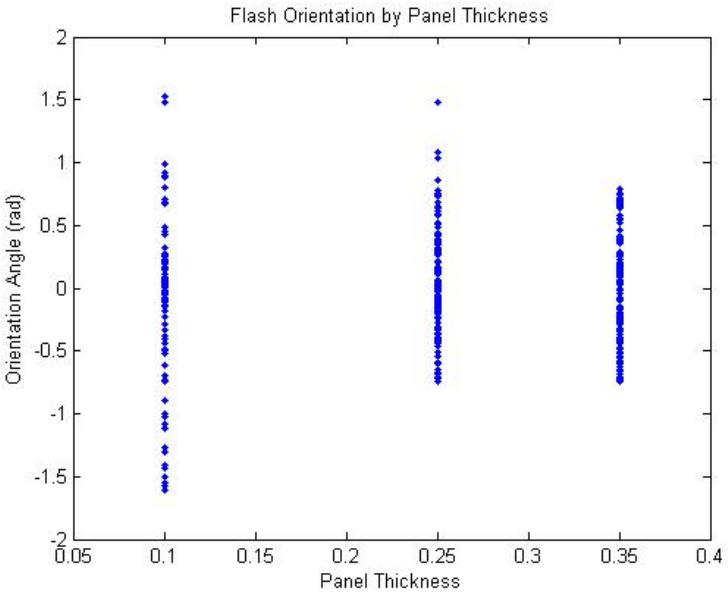

Figure 15 Flash Orientation: Angle of Orientation (rad) By Panel Thickness

a histogram of the orientation angles across the entire duration of the shot and across all factor levels.

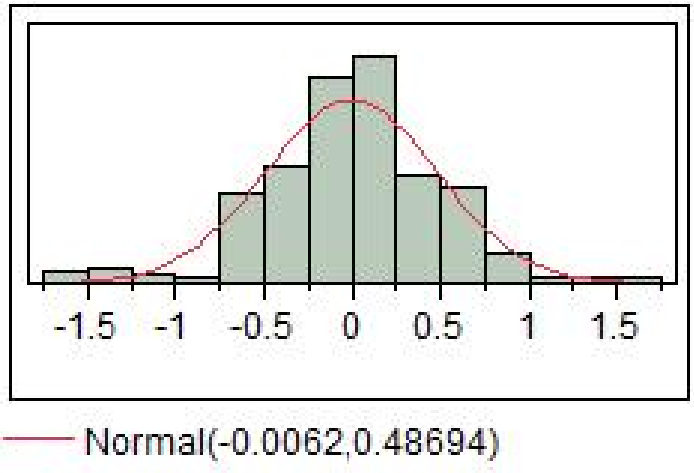

Figure 16 Flash Orientation Angle (rad) Fit With a Normal Distribution

This histogram indicates that the orientation appears to be a normally distributed random variable, with a mean of virtually 0 radians and a standard deviation of 0.48694 radians. A Kolmogorov-Smirnov goodness-of-fit test was performed to

validate this observation. With a test statistic of 0.052 and a corresponding p-value of 0.15, the null hypothesis that the orientation angle follows a normal distribution could not be rejected. As such, it seems appropriate to model this orientation angle as a random draw from this normal distribution and set this angle constant for the duration of the flash.

4.3 Flash Position

The position of the center of the ellipse with respect to the origin (i.e., the point of impact) tends to follow a pattern for each individual shot, but there was no apparent relationship between it and any combination of the factor settings, as shown in Figures 17 and 18. For current modeling efforts, position is modeled as a function of time:

$$Position = b_0 + b_1 Time. \tag{17}$$

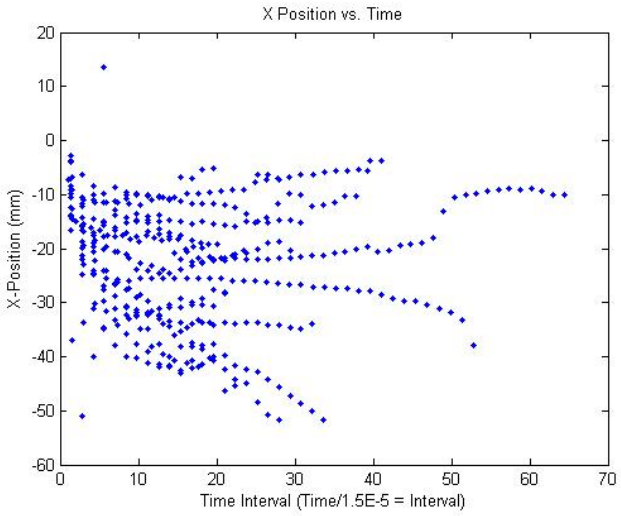

Figure 17 X Position of Center of Flash Over Time

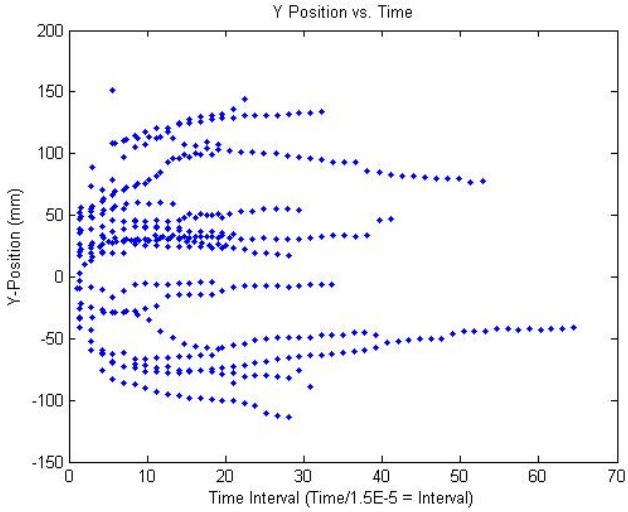

Figure 18 Y Position of Flash Over Time

Using Equation 17 for each axis, the position of the center of the ellipse was modeled across all shots as a function of time. Equations 18 and 19, below, capture the displacement from the orientation.

$$Position_x = \quad -22.56174 + 0.0025045 * t \tag{18}$$

$$Position_y = \quad 23.493393 - 0.4906371 * t \tag{19}$$

Predicted values for the X- and Y-position varied greatly from observed values.

4.4 Flash Duration

Initial attempts tried to model the duration of the flash instance as a function of panel thickness. Using the equation

$$Duration_i = b_0 + b_1 Thick_i \tag{20}$$

did not provide an accurate prediction of the observed flash durations. Additionally, when modeled this way, the predicted flash duration did not align well with the flash radius model.

Since the quartic model for flash radius and the duration of the flash are obviously related, it was determined that the most appropriate way to model flash duration was to determine the real, non-zero root of Equation 15. This provides the time when the flash radius dissipates and ceases to exist, i.e., the duration of the flash.

When modeling the flash radius, the magnitudes of the X-radius and Y-radius were assumed independent. While this is a reasonable assumption, this results in a different root for Equation 15 for each axis model, implying that a flash instance has a different duration in each axis, which is not logical.

To avoid two separate flash duration values, the minimum of the two roots is used. Once either the X-radius or Y-radius equals zero, there is no longer any area associated with the flash and it essentially does not exist, despite the mode prediction from the alternative radius model.

Another approach considered is to find the root of Equation 15 for each radius, select the minimum of the two and fix this time as the flash duration for both the x-radius and y-radius. A regression can then be performed where the roots are fixed at time zero and the specified duration, generating a different set of regression coefficients that are used to predict flash radius than discussed in section 4.1. This would resolve any discontinuities between the modeled flash radius and force the models for both the X-radius and Y-radius to align on their modeled duration of flash.

Figure 19 provides a flash event modeling algorithm based on the response surface models created. This algorithm can be computerized to yield a reasonable boundary model of a ballistic impact flash event. Additional work, separate but concurrent with this research, is developing a physics-based thermal energy model of the ballistic flash event. Coupling the boundary model with the thermal energy model will realize a first-ever ballistic flash event simulation.

- INPUT: User provides panel thickness
- STEP 1: Flash size model generated
  - Determine quartic model coefficients using the following:

$$\hat{\beta}_{1_x} = b_0 + b_1 Thickness$$
$$\vdots$$
$$\hat{\beta}_{4_y} = b_0 + b_1 Thickness$$

Radius	Coefficient	b_0	b_1
X	β_1	5.244465859	-6.889130548
	β_2	-0.554140103	1.055314656
	β_3	0.019541582	-0.043692468
	β_4	-0.000224115	0.000554559
Y	β_1	7.305658059	1.301390443
	β_2	-0.856882495	0.898951232
	β_3	0.032944706	-0.058336307
	β_4	-0.000396238	0.000871425

- STEP 2: Duration derived from root of quartic model equation
  - Minimum of X-radius and Y-radius root selected
- STEP 3: Random draw from *N*(-0.0062, 0.48694) to model orientation
- STEP 4: Model position of ellipse centroid

$$P_x(t) = b_{x0} + b_{x1}(t) \rightarrow -22.56174 + 0.00251t \qquad P_y(t) = b_{y0} + b_{y1}(t) \rightarrow 23.49339 - 0.49064t$$

- OUTPUT: Flash duration, size and shape of flash for any given time

Figure 19 Flash Event Modeling Algorithm

4.5 Summary

Systematic analysis of test data generated a set of parsimonious models for flash radius, duration, orientation, and position. Categorizing test shots by panel thickness provided a series of time-based quartic models whose parameters, when modeled as a function of panel thickness, provided a reasonable estimate of flash radius. Solving for the real, non-zero root of the quartic model for both the X- and Y-radius, the minimum of the two is taken as the modeled duration of the flash. Flash orientation is not time-dependent and follows a normal distribution. The orientation of the flash with respect to the shot line is modeled as random draw from this distribution and held constant for the duration of the flash. The center position of the flash exhibits no correlation with test scenario parameters but is dependent on time. The coordinates for its location with respect to the point of impact are modeled as linear functions of time. These collective models provide a complete characterization of impact flash.

5. *Conclusions, Recommendations, and Future Work*

Air forces are naturally concerned with the ability of their aircraft to withstand damage from hostile environments. Impact and penetration from armor-piercing incendiary projectiles and missile fragments encountered during combat operations generate ballistic impact flashes capable of igniting fires. The advent of high-speed digital video allows these flashes to be accurately captured. Image processing tools were used to characterize the size, shape and position, and duration of the impact flash. Using the processed test data obtained via live-fire testing, an empirical model was developed to estimate the characteristics of these impact flashes, to include flash size radii, flash position, flash size duration, and flash orientation, as a function of the test parameters. These ballistic flash event boundary models, when coupled with physics-based thermal models, provide a projectile impact flash cloud representation. This supplies the joint survivability community the ability to predict ballistic impact flash characteristics for survivability analyses, the first time such a capability exists.

In Chapter 3, the factors of interest were defined and an designed experiment generated. The 46th Test Group, Aerospace Survivability Analysis Branch, performed the live-fire testing of 72 shots and provided the time series parameters describing the ellipses enclosing the flash cloud. The data were validated and screened to eliminate test shots where video processing could not provide accurate data, reducing the usable data set to 21 shots. Regression analysis was performed to construct empirical models for flash radius (both X and Y directions), flash position, and flash orientation.

In Chapter 4, the time-based fourth-order regression models for flash radius were analyzed and response surface meta-models were developed to generate the fourth-order time-based model parameters as a function of panel thickness. This model accurately predicted flash size for most flashes from the test data. From this model, the duration of the flash was derived by finding the minimal non-zero root of

the fourth-order regression model. Test parameters did not exhibit any noticeable patterns on the position of the flash. Thus, no meta-model was constructed and a first-order time-based regression model used to predict position. No time dependency or test parameter dependency was evident in the orientation of the flash but the aggregate of the orientation angles appeared to follow a normal distribution. This was verified with a statistical goodness-of-fit test and orientation was modeled stochastically as a random draw from its normal distribution.

Additional testing by the 46th Test Group, Aerospace Survivability Analysis Branch, is underway to augment this research. That test design makes explicit use of the lessons learned in this research. Additional data will fill in gaps for various test parameters as well as for various projectiles and target materials. With additional test data, it is likely that the "noise" in the data can be reduced and a more accurate model realized. Using the same methodology approach as was discussed in this effort, time-based regression models can be developed. Test parameters can be analyzed for their significance and appropriate meta-models constructed to characterize ballistic impact flash.

A technical issue not addressed in this work is the nature of the model error. A deterministic model was constructed but the limited data and its "noisy" nature prevented robust analysis of model error. While a deterministic model may be sufficient for the needs of the survivability community, development of a stochastic model allows statistical testing to be performed and provides a confidence level on how well the model fits the empirical data. With the planned addition of more test data, this improvement is left to future efforts.

Appendix A. Designed Experiment Test Data

A.1 Test Matrix

Table 5 Designed Experiment Factors and Levels

Test Number	Projectile Mass	Velocity	Panel Thickness	Obliquity
T001	40	4000	0.1	45
T002	40	4000	0.1	45
T003	75	4000	0.1	45
T004	75	4000	0.1	45
T005	40	5500	0.1	45
T006	40	5500	0.1	45
T007	75	5500	0.1	45
T008	75	5500	0.1	45
T009	40	7000	0.1	45
T010	40	7000	0.1	45
T011	75	7000	0.1	45
T012	75	7000	0.1	45
T013	40	4000	0.25	45
T014	40	4000	0.25	45
T015	75	4000	0.25	45
T016	75	4000	0.25	45
T017	40	5500	0.25	45
T018	40	5500	0.25	45
T019	75	5500	0.25	45
T020	75	5500	0.25	45
T021	40	7000	0.25	45

Continued on Next Page...

Table 5 – Continued

Test Number	Projectile Mass	Velocity	Panel Thickness	Obliquity
T022	40	7000	0.25	45
T023	75	7000	0.25	45
T024	75	7000	0.25	45
T025	40	4000	0.35	45
T026	40	4000	0.35	45
T027	75	4000	0.35	45
T028	75	4000	0.35	45
T029	40	5500	0.35	45
T030	40	5500	0.35	45
T031	75	5500	0.35	45
T032	75	5500	0.35	45
T033	40	7000	0.35	45
T034	40	7000	0.35	45
T035	75	7000	0.35	45
T036	75	7000	0.35	45
T037	40	4000	0.1	0
T038	40	4000	0.1	0
T039	75	5500	0.1	0
T040	75	5500	0.1	0
T041	75	4000	0.1	0
T042	75	4000	0.1	0
T043	40	5500	0.1	0
T044	40	5500	0.1	0
T045	40	7000	0.1	0
T046	40	7000	0.1	0

Continued on Next Page...

Table 5 – Continued

Test Number	Projectile Mass	Velocity	Panel Thickness	Obliquity
T047	75	7000	0.1	0
T048	75	7000	0.1	0
T049	40	4000	0.25	0
T050	40	4000	0.25	0
T051	75	4000	0.25	0
T052	75	4000	0.25	0
T053	40	5500	0.25	0
T054	40	5500	0.25	0
T055	75	5500	0.25	0
T056	75	5500	0.25	0
T057	40	7000	0.25	0
T058	40	7000	0.25	0
T059	75	7000	0.25	0
T060	75	7000	0.25	0
T061	40	4000	0.35	0
T062	40	4000	0.35	0
T063	75	4000	0.35	0
T064	75	4000	0.35	0
T065	40	5500	0.35	0
T066	40	5500	0.35	0
T067	75	5500	0.35	0
T068	75	5500	0.35	0
T069	40	7000	0.35	0
T070	40	7000	0.35	0
T071	75	7000	0.35	0

Continued on Next Page...

Table 5 – Continued

Test Number	Projectile Mass	Velocity	Panel Thickness	Obliquity
T072	75	7000	0.35	0

A.2 Test Results

Table 6 Flash Data

Test Number	Time	X Position	Y Position	X Radius	Y Radius	Orientation
T005	2.20E-05	-0.036891	-0.021847	0.0047152	0.014143	0.70771
T005	4.40E-05	-0.033697	-0.032766	0.0074807	0.011093	0.20288
T005	6.60E-05	-0.030171	-0.028429	0.0030158	0.0050936	0.44466
T005	8.80E-05	-0.031657	-0.028923	0.0026655	0.0067523	0.42282
T005	0.00011	-0.034084	-0.027826	0.0038261	0.0016606	0.26099
T005	0.000132	-0.032973	-0.03099	0.0017698	0.0015483	-0.74795
T005	0.000154	-0.034885	-0.034691	0.0026488	0.0013671	0.6855
T005	0.000176	-0.038146	-0.044216	0.0036202	0.0073693	-0.51465
T005	0.000198	-0.039623	-0.049106	0.0032968	0.0065909	-0.37831
T005	0.00022	-0.040688	-0.054226	0.0046718	0.0068051	-0.49162
T005	0.000242	-0.041243	-0.056121	0.006311	0.0044344	0.22093
T005	0.000264	-0.041835	-0.057732	0.0057996	0.0026463	0.083859
T005	0.000286	-0.040194	-0.05873	0.0020767	0.0013793	0.25691
T025	4.20E-05	-0.050994	-0.043084	0.046969	0.0064772	-0.74364
T025	6.30E-05	-0.040008	-0.061463	0.010101	0.056088	0.7586
T025	8.40E-05	-0.034591	-0.068449	0.010936	0.054434	0.7535
T025	0.000105	-0.031226	-0.073117	0.011506	0.053314	0.74507

Continued on Next Page...

Table 6 – Continued

Test Number	Time	X Position	Y Position	X Radius	Y Radius	Orientation
T025	0.000126	-0.030939	-0.073944	0.012372	0.04843	0.74962
T025	0.000147	-0.032585	-0.071791	0.011971	0.046341	0.75305
T025	0.000168	-0.031839	-0.073389	0.011719	0.047903	0.72282
T025	0.000189	-0.032543	-0.072966	0.011599	0.044934	0.69692
T025	0.00021	-0.030834	-0.075806	0.012022	0.038	0.70568
T025	0.000231	-0.030905	-0.075777	0.011825	0.037258	0.69453
T025	0.000252	-0.030366	-0.075977	0.011707	0.036643	0.70042
T025	0.000273	-0.029301	-0.076891	0.011334	0.035498	0.69788
T025	0.000294	-0.027502	-0.079035	0.011422	0.029889	0.6673
T025	0.000315	-0.028198	-0.078165	0.010951	0.027135	0.64557
T025	0.000336	-0.021088	-0.080635	0.0070615	0.018231	0.55295
T025	0.000357	-0.020811	-0.079617	0.0059109	0.017107	0.65477
T025	0.000378	-0.020179	-0.080161	0.005611	0.016017	0.65396
T025	0.000399	-0.018977	-0.081234	0.0048283	0.013052	0.63388
T025	0.00042	-0.018676	-0.081482	0.0051608	0.013511	0.67925
T025	0.000441	-0.020325	-0.076292	0.0048559	0.0031114	-0.71269
T025	0.000462	-0.010138	-0.089573	0.00301	0.0048286	0.46531
T038	2.10E-05	-0.0028566	0.035292	0.0052598	0.0071365	-0.1829
T038	4.20E-05	-0.0063471	0.048726	0.0053408	0.012295	0.065883
T038	6.30E-05	-0.0084852	0.051314	0.0050668	0.0092384	0.27993
T038	8.40E-05	-0.0097629	0.055345	0.0045957	0.005819	0.992736327
T038	0.000105	-0.0085512	0.055498	0.003473	0.0060413	0.67211
T038	0.000126	-0.0095386	0.045629	0.0066712	0.01248	-0.032275
T038	0.000147	-0.0098396	0.045407	0.0073804	0.013143	-0.14382
T038	0.000168	-0.0099601	0.045666	0.0074844	0.013359	-0.23328

Continued on Next Page...

Table 6 – Continued

Test Number	Time	X Position	Y Position	X Radius	Y Radius	Orientation
T038	0.000189	-0.010282	0.0454	0.0074386	0.013433	-0.333
T038	0.00021	-0.011036	0.04576	0.007806	0.013376	-0.43974
T038	0.000231	-0.0067534	0.051078	0.004858	0.0096375	0.17274
T038	0.000252	-0.0069053	0.05113	0.0050331	0.0087061	0.22524
T038	0.000273	-0.0054082	0.049984	0.003525	0.0086704	0.010794
T038	0.000294	-0.0051961	0.048198	0.0033618	0.007456	-0.04517
T039	2.10E-05	-0.0083433	0.026865	0.0124	0.029011	0.06617
T039	4.20E-05	-0.018698	0.053231	0.015211	0.045885	0.21908
T039	6.30E-05	-0.024785	0.070197	0.019349	0.057025	0.2069
T039	8.40E-05	-0.027523	0.0784	0.01845	0.060766	0.21764
T039	0.000105	-0.033257	0.097346	0.018611	0.048994	0.15686
T039	0.000126	-0.035773	0.10496	0.018498	0.045218	0.14922
T039	0.000147	-0.037689	0.10787	0.017034	0.046834	0.16815
T039	0.000168	-0.038952	0.11278	0.016454	0.042186	0.22055
T039	0.000189	-0.041886	0.11752	0.015496	0.034491	0.18857
T039	0.00021	-0.041688	0.12444	0.014804	0.025143	0.6803
T039	0.000231	-0.042488	0.12835	0.013047	0.023263	0.892826327
T039	0.000252	-0.040668	0.12943	0.011707	0.020949	0.886646327
T039	0.000273	-0.041343	0.13135	0.011125	0.017247	0.806876327
T039	0.000294	-0.040017	0.13201	0.0090507	0.016291	0.920246327
T039	0.000315	-0.046389	0.13648	0.0084891	0.0065021	1.524807327
T039	0.000336	-0.04425	0.14382	0.0023552	0.0048125	1.481732327
T040	2.10E-05	-0.012332	0.020693	0.008396	0.01542	0.48
T040	4.20E-05	-0.011713	0.019687	0.0099684	0.0090832	-0.48641
T040	6.30E-05	-0.010163	0.019095	0.008065	0.0067032	-0.40184

Continued on Next Page...

Table 6 – Continued

Test Number	Time	X Position	Y Position	X Radius	Y Radius	Orientation
T040	8.40E-05	0.013529	0.15126	0.0030802	0.0062538	0.20143
T042	2.20E-05	-0.0068077	0.022062	0.0091979	0.028374	-0.052326
T042	4.40E-05	-0.010965	0.027793	0.013327	0.023381	0.0069686
T042	6.60E-05	-0.011512	0.031567	0.011848	0.025717	0.15324
T042	8.80E-05	-0.011513	0.031234	0.011618	0.024531	0.1874
T042	0.00011	-0.011433	0.030911	0.011581	0.026495	0.15248
T042	0.000132	-0.011656	0.030202	0.011781	0.027048	0.074854
T042	0.000154	-0.011887	0.029491	0.012308	0.027137	0.012127
T042	0.000176	-0.011106	0.031372	0.01153	0.027245	0.037125
T042	0.000198	-0.010478	0.033459	0.011644	0.025163	0.11202
T042	0.00022	-0.010545	0.033154	0.011749	0.025283	0.091943
T042	0.000242	-0.0099219	0.032481	0.011338	0.023865	0.062542
T042	0.000264	-0.0097768	0.03226	0.011285	0.023292	0.055314
T042	0.000286	-0.0095371	0.032146	0.010855	0.022483	0.02506
T042	0.000308	-0.009413	0.031696	0.010882	0.021211	0.058564
T042	0.00033	-0.0091951	0.03097	0.010732	0.019655	0.070598
T042	0.000352	-0.0091334	0.030456	0.010758	0.019831	0.0045633
T042	0.000374	-0.0076924	0.031395	0.0082157	0.021976	0.0012412
T042	0.000396	-0.0073528	0.03038	0.0075066	0.022886	-0.017014
T042	0.000418	-0.0070979	0.030739	0.0071312	0.022222	-0.031182
T042	0.00044	-0.0068126	0.030568	0.0066688	0.022618	-0.070953
T042	0.000462	-0.0064096	0.031305	0.006065	0.023765	-0.070904
T042	0.000484	-0.0062444	0.032797	0.005945	0.022532	-0.088083
T042	0.000506	-0.0059012	0.033201	0.005472	0.021686	-0.10242
T042	0.000528	-0.0056852	0.033347	0.0052365	0.021911	-0.11112

Continued on Next Page...

Table 6 – Continued

Test Number	Time	X Position	Y Position	X Radius	Y Radius	Orientation
T042	0.00055	-0.0056374	0.032881	0.0051014	0.020623	-0.11642
T042	0.000572	-0.0054153	0.034143	0.0043622	0.018711	-0.097524
T042	0.000594	-0.0037927	0.045556	0.0029253	0.0088886	-0.02246
T042	0.000616	-0.0036942	0.047073	0.0026025	0.0077731	0.018391
T048	2.10E-05	-0.010433	-0.025208	0.029348	0.01281	-1.430086327
T048	4.20E-05	-0.019938	-0.024797	0.033836	0.018799	-1.269316327
T048	6.30E-05	-0.024199	-0.026414	0.030286	0.021092	-1.084806327
T048	8.40E-05	-0.024027	-0.02822	0.027181	0.019115	-1.301306327
T048	0.000105	-0.02639	-0.028238	0.028689	0.020628	-1.431676327
T048	0.000126	-0.0276	-0.028116	0.026411	0.019142	-1.552909327
T048	0.000147	-0.028915	-0.025679	0.023451	0.017166	-1.612940327
T048	0.000168	-0.029614	-0.02382	0.023723	0.016252	-1.603174327
T048	0.000189	-0.033071	-0.015266	0.013681	0.017792	-1.411196327
T048	0.00021	-0.034428	-0.014842	0.012204	0.01613	-1.111176327
T048	0.000231	-0.035225	-0.01422	0.010034	0.015717	-0.889816327
T048	0.000252	-0.037425	-0.014685	0.0085109	0.014507	-0.38583
T048	0.000273	-0.038	-0.014589	0.0069576	0.013028	-0.28587
T048	0.000294	-0.037626	-0.01143	0.0054576	0.01013	0.31743
T048	0.000315	-0.039726	-0.0078531	0.0059778	0.0041718	-0.61052
T048	0.000336	-0.041623	-0.0073264	0.0035594	0.004621	-0.13168
T048	0.000357	-0.042437	-0.0073641	0.0043186	0.0046768	-0.997686327
T048	0.000378	-0.042838	-0.0075429	0.0048843	0.0039873	-0.72826
T048	0.000399	-0.044218	-0.0076524	0.0047813	0.0040168	-0.74516
T048	0.00042	-0.045544	-0.0077866	0.0056675	0.0042484	-0.5021
T048	0.000441	-0.04723	-0.0075196	0.0041434	0.0050634	-1.498865327

Continued on Next Page...

Table 6 – Continued

Test Number	Time	X Position	Y Position	X Radius	Y Radius	Orientation
T048	0.000462	-0.048686	-0.0064704	0.0034937	0.0044719	-1.575796727
T048	0.000483	-0.05005	-0.0064984	0.0028783	0.0038066	-0.69834
T048	0.000504	-0.051749	-0.0066813	0.003021	0.003359	-1.025706327
T049	2.10E-05	-0.0091437	0.016901	0.0070116	0.013016	-0.30641
T049	4.20E-05	-0.012117	0.025344	0.011903	0.011711	0.63937
T049	6.30E-05	-0.014488	0.026836	0.01217	0.011233	-0.19816
T049	8.40E-05	-0.015742	0.02764	0.013885	0.010789	-0.42301
T049	0.000105	-0.016696	0.028814	0.014582	0.010856	-0.40952
T049	0.000126	-0.017126	0.029401	0.015077	0.010749	-0.36083
T049	0.000147	-0.017729	0.030741	0.014257	0.01052	-0.27264
T049	0.000168	-0.016843	0.029833	0.015461	0.011658	-0.41839
T049	0.000189	-0.017347	0.030793	0.014331	0.011088	-0.35417
T049	0.00021	-0.017813	0.032096	0.013179	0.01038	-0.11076
T049	0.000231	-0.022086	0.031786	0.0076882	0.010112	-0.15175
T049	0.000252	-0.022414	0.032678	0.0064372	0.010033	-0.40888
T049	0.000273	-0.022626	0.032841	0.0056828	0.0097501	-0.43575
T049	0.000294	-0.022301	0.034043	0.0052864	0.0081715	-0.39948
T049	0.000315	-0.022135	0.034699	0.0042695	0.0066372	-0.68024
T050	2.10E-05	-0.0037494	-0.009342	0.0048145	0.011523	0.27079
T050	4.20E-05	-0.010608	0.012911	0.010475	0.030825	-0.10334
T050	6.30E-05	-0.011067	0.02061	0.010029	0.028278	-0.011933
T050	8.40E-05	-0.011444	0.019843	0.0090722	0.027531	-0.026574
T050	0.000105	-0.01125	0.018996	0.0086833	0.027027	-0.020545
T050	0.000126	-0.010049	0.026073	0.0076815	0.024389	0.15295
T050	0.000147	-0.010086	0.025735	0.0078592	0.023517	0.1468

Continued on Next Page...

Table 6 – Continued

Test Number	Time	X Position	Y Position	X Radius	Y Radius	Orientation
T050	0.000168	-0.010217	0.025226	0.0080701	0.023438	0.12855
T050	0.000189	-0.010567	0.024434	0.0087034	0.022208	0.11908
T050	0.00021	-0.010835	0.024619	0.0087676	0.020261	0.11763
T050	0.000231	-0.011164	0.02445	0.009131	0.019259	0.058712
T050	0.000252	-0.011592	0.02398	0.0096735	0.017577	-0.012888
T050	0.000273	-0.011592	0.023425	0.009572	0.016536	-0.12252
T050	0.000294	-0.011773	0.023655	0.010168	0.014779	-0.11648
T050	0.000315	-0.011976	0.023705	0.0098868	0.012869	-0.31428
T050	0.000336	-0.012289	0.021979	0.010482	0.0095637	0.74629
T050	0.000357	-0.01357	0.019529	0.0097662	0.0082766	-0.079921
T050	0.000378	-0.0062894	0.019216	0.0031347	0.007851	-0.058907
T050	0.000399	-0.006361	0.018493	0.002992	0.0069087	-0.089669
T050	0.00042	-0.0072047	0.017832	0.0021835	0.0060514	-0.023431
T051	2.20E-05	-0.0091649	0.037459	0.0096439	0.021146	0.021785
T051	4.40E-05	-0.015534	0.047894	0.012989	0.024784	0.20448
T051	6.60E-05	-0.018438	0.054492	0.013137	0.027815	0.31712
T051	8.80E-05	-0.019655	0.057348	0.013424	0.030158	0.31105
T051	0.00011	-0.020637	0.058779	0.013539	0.033031	0.31548
T051	0.000132	-0.021803	0.059956	0.013337	0.034797	0.36765
T051	0.000154	-0.022645	0.059784	0.012583	0.035502	0.43041
T051	0.000176	-0.023158	0.059815	0.013759	0.035693	0.43046
T051	0.000198	-0.023859	0.059035	0.012903	0.034632	0.43492
T051	0.00022	-0.020903	0.048492	0.01397	0.021928	0.51568
T051	0.000242	-0.020619	0.04772	0.014175	0.021357	0.36657
T051	0.000264	-0.021664	0.049983	0.013203	0.019199	0.10743

Continued on Next Page...

Table 6 – Continued

Test Number	Time	X Position	Y Position	X Radius	Y Radius	Orientation
T051	0.000286	-0.021434	0.050928	0.013591	0.017913	-0.0064611
T051	0.000308	-0.021867	0.051029	0.013376	0.017373	0.15841
T051	0.00033	-0.02123	0.052999	0.012491	0.014308	1.039036327
T051	0.000352	-0.020356	0.05291	0.011183	0.013182	1.479764327
T051	0.000374	-0.015175	0.054856	0.007109	0.012513	0.856236327
T051	0.000396	-0.014348	0.054764	0.00576	0.010996	1.078336327
T051	0.000418	-0.011691	0.055201	0.0040044	0.0080775	0.57867
T051	0.00044	-0.0098584	0.053667	0.0029311	0.0057929	-0.026417
T052	2.20E-05	-0.012717	0.056041	0.00835	0.023906	0.12971
T052	4.40E-05	-0.022866	0.089468	0.0094526	0.034411	-0.11824
T052	8.80E-05	-0.025513	0.10864	0.0122	0.037398	0.0039148
T052	0.00011	-0.026103	0.11116	0.013144	0.036861	0.018156
T052	0.000132	-0.025959	0.11251	0.01285	0.03687	0.035112
T052	0.000154	-0.025576	0.11361	0.012445	0.038331	0.02326
T052	0.000176	-0.025425	0.11373	0.012088	0.037554	0.0031755
T052	0.000198	-0.025503	0.11261	0.011544	0.035664	0.0028738
T052	0.00022	-0.025472	0.10789	0.01141	0.031833	0.0082338
T052	0.000242	-0.025404	0.10615	0.011231	0.031464	0.026355
T052	0.000264	-0.025473	0.10402	0.011426	0.030602	0.020962
T052	0.000286	-0.025397	0.10306	0.011507	0.03004	0.013345
T052	0.000308	-0.025434	0.10205	0.011679	0.029417	-0.0043328
T052	0.00033	-0.025921	0.10159	0.012026	0.028237	-0.024829
T052	0.000352	-0.026019	0.10141	0.011952	0.027662	-0.031785
T052	0.000374	-0.026054	0.10067	0.011751	0.027596	-0.024588
T052	0.000396	-0.026124	0.10009	0.011613	0.026928	-0.025488

Continued on Next Page...

Table 6 – Continued

Test Number	Time	X Position	Y Position	X Radius	Y Radius	Orientation
T052	0.000418	-0.026342	0.098519	0.011714	0.02765	-0.052291
T052	0.00044	-0.026585	0.097657	0.011608	0.027197	-0.051287
T052	0.000462	-0.026753	0.096217	0.011444	0.027028	-0.086334
T052	0.000484	-0.02706	0.094704	0.011616	0.026362	-0.10514
T052	0.000506	-0.027216	0.093375	0.011556	0.025943	-0.13774
T052	0.000528	-0.027394	0.092924	0.01137	0.024764	-0.14399
T052	0.00055	-0.027345	0.093524	0.011478	0.023265	-0.15957
T052	0.000572	-0.027756	0.08564	0.012915	0.014302	-0.74695
T052	0.000594	-0.027836	0.084421	0.013897	0.013052	0.61658
T052	0.000616	-0.028553	0.083207	0.013286	0.011945	-0.024458
T052	0.000638	-0.029161	0.082135	0.013406	0.010853	-0.20312
T052	0.00066	-0.02961	0.081487	0.013465	0.0099337	-0.18092
T052	0.000682	-0.029602	0.080602	0.013499	0.0095871	-0.23447
T052	0.000704	-0.030297	0.080124	0.013199	0.0091364	-0.20298
T052	0.000726	-0.031073	0.079841	0.012583	0.0092143	-0.20088
T052	0.000748	-0.031919	0.080008	0.011778	0.0091807	-0.22238
T052	0.00077	-0.033162	0.076847	0.012494	0.0056973	-0.41745
T052	0.000792	-0.037882	0.077727	0.0097681	0.0041254	-0.71795
T055	2.10E-05	-0.014031	-0.033798	0.010381	0.021468	-0.22916
T055	4.20E-05	-0.024837	-0.059059	0.014294	0.030451	-0.30648
T055	6.30E-05	-0.031007	-0.075486	0.014504	0.036516	-0.427
T055	8.40E-05	-0.034926	-0.082539	0.01439	0.03617	-0.40171
T055	0.000105	-0.03791	-0.086118	0.014241	0.035046	-0.36689
T055	0.000126	-0.039887	-0.087326	0.017844	0.033603	-0.38874
T055	0.000147	-0.040126	-0.08979	0.017474	0.031991	-0.44216

Continued on Next Page...

Table 6 – Continued

Test Number	Time	X Position	Y Position	X Radius	Y Radius	Orientation
T055	0.000168	-0.041197	-0.093345	0.017692	0.027873	-0.59134
T055	0.000189	-0.041403	-0.095341	0.017173	0.026466	-0.6844
T055	0.00021	-0.041984	-0.096544	0.024848	0.017155	0.75476
T055	0.000231	-0.042928	-0.097844	0.023713	0.016829	0.68585
T055	0.000252	-0.042093	-0.098556	0.022497	0.016625	0.59375
T055	0.000273	-0.041416	-0.099027	0.021979	0.01602	0.49006
T055	0.000294	-0.040654	-0.10001	0.021051	0.014206	0.5111
T055	0.000315	-0.042297	-0.10056	0.019422	0.012154	0.68222
T055	0.000336	-0.045408	-0.1028	0.0078942	0.018547	-0.64695
T055	0.000357	-0.044969	-0.10492	0.015458	0.0081402	0.77664
T055	0.000378	-0.048396	-0.11055	0.0099247	0.0065813	0.12691
T055	0.000399	-0.050695	-0.11234	0.0075605	0.0034228	0.20616
T055	0.00042	-0.051758	-0.11331	0.0077592	0.0023895	0.050437
T056	2.10E-05	-0.009021	-0.0027529	0.0084497	0.019825	0.26255
T056	4.20E-05	-0.015881	-0.0077848	0.013604	0.022082	0.57723
T056	6.30E-05	-0.01753	-0.01025	0.01396	0.019595	0.73212
T056	8.40E-05	-0.014985	-0.016229	0.012305	0.014051	-0.60386
T056	0.000105	-0.012813	-0.011142	0.012561	0.0078656	-0.45937
T056	0.000126	-0.014377	-0.0061234	0.0058254	0.0056746	-0.066146
T056	0.000147	-0.014763	-0.0054096	0.0059935	0.005443	0.30295
T056	0.000168	-0.01522	-0.0060254	0.005467	0.0055691	-0.095025
T056	0.000189	-0.016403	-0.0058382	0.005702	0.0048213	-0.53927
T056	0.00021	-0.017128	-0.0049687	0.0048902	0.0040402	-0.39482
T056	0.000231	-0.017655	-0.0050413	0.0043446	0.0042888	-0.1399
T056	0.000252	-0.018379	-0.0044111	0.0037083	0.0046328	-0.6683

Continued on Next Page...

Table 6 – Continued

Test Number	Time	X Position	Y Position	X Radius	Y Radius	Orientation
T056	0.000273	-0.019886	-0.0040251	0.0037206	0.004046	-0.7029
T057	2.10E-05	-0.016631	0.046802	0.014325	0.027894	0.1743
T057	4.20E-05	-0.021896	0.055408	0.015102	0.0307	0.29516
T057	6.30E-05	-0.024657	0.061281	0.014166	0.035518	0.38352
T057	8.40E-05	-0.026965	0.06695	0.01563	0.038028	0.39617
T057	0.000105	-0.028772	0.070377	0.013257	0.039598	0.43662
T057	0.000126	-0.030582	0.073718	0.012918	0.039594	0.43953
T057	0.000147	-0.031706	0.076012	0.013605	0.03897	0.4136
T057	0.000168	-0.034941	0.081741	0.012052	0.037553	0.28019
T057	0.000189	-0.03758	0.09317	0.011775	0.023209	0.21343
T057	0.00021	-0.039893	0.096296	0.0098577	0.022311	0.11199
T057	0.000231	-0.038062	0.097205	0.0078425	0.020938	0.040654
T057	0.000252	-0.038098	0.098741	0.007869	0.018645	0.016685
T057	0.000273	-0.038662	0.099291	0.0083151	0.016809	-0.052762
T058	2.20E-05	-0.014536	0.048801	0.013351	0.028371	0.1743
T058	4.40E-05	-0.019425	0.057573	0.014168	0.031102	0.29516
T058	6.60E-05	-0.02221	0.063255	0.014129	0.0356	0.37916
T058	8.80E-05	-0.024132	0.069336	0.014772	0.038344	0.39617
T058	0.00011	-0.025759	0.072415	0.013133	0.040611	0.43343
T058	0.000132	-0.027274	0.075405	0.012631	0.040871	0.42799
T058	0.000154	-0.028542	0.078891	0.012837	0.038724	0.41588
T058	0.000176	-0.03155	0.084494	0.011133	0.037759	0.28237
T058	0.000198	-0.033985	0.096311	0.010828	0.023268	0.21293
T058	0.00022	-0.035971	0.099316	0.0088417	0.022837	0.11719
T058	0.000242	-0.034517	0.10071	0.0072559	0.02081	0.032597

Continued on Next Page...

Table 6 – Continued

Test Number	Time	X Position	Y Position	X Radius	Y Radius	Orientation
T058	0.000264	-0.033104	0.10913	0.0065448	0.012669	0.34897
T058	0.000286	-0.03363	0.10741	0.0062421	0.010461	0.64572
T059	2.10E-05	-0.004046	0.0028586	0.002847	0.0068787	0.024766
T059	4.20E-05	-0.015772	0.023011	0.01143	0.030498	-0.27601
T059	6.30E-05	-0.020618	0.033437	0.021436	0.018177	0.35976
T059	8.40E-05	-0.024041	0.036604	0.023912	0.017578	-0.028022
T059	0.000105	-0.026731	0.038967	0.025285	0.016449	-0.16475
T059	0.000126	-0.030611	0.040492	0.023604	0.01427	-0.23576
T059	0.000147	-0.031461	0.040603	0.023173	0.013252	-0.33177
T059	0.000168	-0.032054	0.040704	0.020962	0.012548	-0.40831
T059	0.000189	-0.031176	0.038725	0.01888	0.011908	-0.30465
T059	0.00021	-0.03046	0.038301	0.017247	0.010687	-0.30877
T059	0.000231	-0.029233	0.037054	0.01436	0.010107	-0.23982
T059	0.000252	-0.03003	0.036811	0.013814	0.0087241	-0.32275
T059	0.000273	-0.030525	0.036409	0.013295	0.0082573	-0.31832
T059	0.000294	-0.030706	0.035639	0.013779	0.007963	-0.3655
T059	0.000315	-0.028096	-0.085573	0.0079145	0.011698	-0.51433
T063	2.10E-05	-0.0084632	-0.03327	0.0059248	0.017457	-0.075897
T063	4.20E-05	-0.015917	-0.052553	0.010615	0.028865	-0.16971
T063	6.30E-05	-0.019636	-0.062293	0.012348	0.035435	-0.2004
T063	8.40E-05	-0.02004	-0.069702	0.011658	0.036905	-0.22699
T063	0.000105	-0.020697	-0.073068	0.01184	0.035388	-0.23381
T063	0.000126	-0.021004	-0.070308	0.01138	0.029862	-0.31834
T063	0.000147	-0.023878	-0.076349	0.0099683	0.025753	-0.0041101
T063	0.000168	-0.024009	-0.077027	0.0097631	0.025436	0.032648

Continued on Next Page...

Table 6 – Continued

Test Number	Time	X Position	Y Position	X Radius	Y Radius	Orientation
T063	0.000189	-0.02464	-0.077621	0.010367	0.024531	0.04275
T063	0.00021	-0.024499	-0.078247	0.010334	0.024646	0.033873
T063	0.000231	-0.023781	-0.07655	0.010408	0.027272	-0.10506
T063	0.000252	-0.02326	-0.075765	0.010676	0.027176	-0.14401
T063	0.000273	-0.022387	-0.074427	0.011062	0.027017	-0.21128
T063	0.000294	-0.021907	-0.07393	0.011153	0.027326	-0.2334
T063	0.000315	-0.021658	-0.072582	0.011362	0.027384	-0.28154
T063	0.000336	-0.021809	-0.07136	0.011152	0.027351	-0.3294
T063	0.000357	-0.021923	-0.069841	0.011221	0.026349	-0.39002
T063	0.000378	-0.022065	-0.068515	0.011415	0.025161	-0.43055
T063	0.000399	-0.022064	-0.067068	0.011258	0.024364	-0.48814
T063	0.00042	-0.021868	-0.066025	0.010972	0.024624	-0.50548
T063	0.000441	-0.021652	-0.064846	0.010924	0.024	-0.52249
T063	0.000462	-0.021433	-0.063805	0.011087	0.023689	-0.54113
T063	0.000483	-0.021292	-0.063089	0.011165	0.023134	-0.56023
T063	0.000504	-0.021176	-0.062372	0.01136	0.022226	-0.58754
T063	0.000525	-0.020845	-0.061488	0.011693	0.020841	-0.60127
T063	0.000546	-0.020483	-0.060197	0.011901	0.020503	-0.59397
T063	0.000567	-0.020232	-0.059449	0.011776	0.020469	-0.55327
T063	0.000588	-0.019661	-0.057728	0.011748	0.01877	-0.5417
T063	0.000609	-0.020505	-0.053242	0.01876	0.0084315	0.69407
T063	0.00063	-0.020368	-0.052208	0.018853	0.0079977	0.68246
T063	0.000651	-0.019497	-0.050995	0.017848	0.0073165	0.65957
T063	0.000672	-0.01923	-0.050464	0.017559	0.0070513	0.64233
T063	0.000693	-0.018929	-0.05015	0.017244	0.006998	0.63778

Continued on Next Page...

Table 6 – Continued

Test Number	Time	X Position	Y Position	X Radius	Y Radius	Orientation
T063	0.000714	-0.017919	-0.049752	0.017117	0.006409	0.64225
T063	0.000735	-0.013182	-0.046283	0.01105	0.0062314	0.7433
T063	0.000756	-0.010622	-0.044377	0.0054148	0.0085141	-0.3394
T063	0.000777	-0.010161	-0.044041	0.0048703	0.0083029	-0.19361
T063	0.000798	-0.0098513	-0.043622	0.0046839	0.0076964	-0.088314
T063	0.000819	-0.0093723	-0.042088	0.0040458	0.0067429	0.1849
T063	0.00084	-0.0090483	-0.04206	0.003635	0.006856	0.18361
T063	0.000861	-0.0088225	-0.043093	0.0038993	0.0051469	0.38017
T063	0.000882	-0.0090104	-0.042275	0.0044932	0.003547	-0.72413
T063	0.000903	-0.008998	-0.04256	0.0043733	0.0032995	-0.64693
T063	0.000924	-0.009274	-0.041879	0.003786	0.0032927	-0.19
T063	0.000945	-0.0099613	-0.041548	0.0026202	0.0035383	-0.6803
T063	0.000966	-0.009971	-0.040937	0.0021638	0.0033594	-0.72557
T065	2.10E-05	-0.0098179	-0.040679	0.010525	0.026346	-0.041892
T065	4.20E-05	-0.016556	-0.05259	0.013739	0.034573	-0.17501
T065	6.30E-05	-0.018832	-0.059342	0.015846	0.033508	-0.23791
T065	8.40E-05	-0.017841	-0.062499	0.013453	0.03397	-0.27676
T065	0.000105	-0.01616	-0.061245	0.010891	0.033541	-0.1749
T065	0.000126	-0.015299	-0.067022	0.0089944	0.034684	-0.26717
T065	0.000147	-0.015022	-0.066361	0.0090659	0.033527	-0.2469
T065	0.000168	-0.014772	-0.065188	0.0090496	0.033596	-0.2288
T065	0.000189	-0.014858	-0.065193	0.0090627	0.032627	-0.22893
T065	0.00021	-0.014812	-0.064412	0.009226	0.031874	-0.21757
T065	0.000231	-0.015057	-0.064377	0.0095072	0.031154	-0.22233
T065	0.000252	-0.01539	-0.064027	0.0095541	0.02899	-0.22187

Continued on Next Page...

Table 6 – Continued

Test Number	Time	X Position	Y Position	X Radius	Y Radius	Orientation
T065	0.000273	-0.015048	-0.063224	0.0090549	0.027608	-0.20469
T065	0.000294	-0.015551	-0.057415	0.0083211	0.02276	-0.3738
T065	0.000315	-0.015616	-0.055301	0.0082299	0.019878	-0.47905
T065	0.000336	-0.015966	-0.054639	0.0082784	0.018006	-0.62314
T065	0.000357	-0.015056	-0.051553	0.014757	0.0083353	0.74138
T065	0.000378	-0.015058	-0.050096	0.01378	0.0077628	0.54276
T065	0.000399	-0.015245	-0.049479	0.01379	0.007555	0.40698
T065	0.00042	-0.014827	-0.049151	0.013709	0.0068161	0.39359
T065	0.000441	-0.014726	-0.048773	0.013593	0.0066279	0.36057
T065	0.000462	-0.015307	-0.049029	0.013189	0.0059574	0.39361
T065	0.000483	-0.012259	-0.047113	0.0085363	0.0069292	0.20817
T065	0.000504	-0.011963	-0.046857	0.008008	0.0068448	0.15767
T065	0.000525	-0.011564	-0.04676	0.0077665	0.0065367	0.036113
T065	0.000546	-0.010252	-0.045495	0.0073053	0.0053723	-0.40339
T065	0.000567	-0.010361	-0.045531	0.007354	0.0049066	-0.41477
T065	0.000588	-0.0055376	-0.046933	0.0014314	0.0053367	0.16222
T066	2.10E-05	-0.0071342	0.039277	0.0059632	0.022704	0.095188
T066	4.20E-05	-0.014223	0.038752	0.010257	0.017953	-0.44251
T066	6.30E-05	-0.01708	0.040723	0.011645	0.018306	-0.65873
T066	8.40E-05	-0.015115	0.046448	0.013612	0.0098088	0.2838
T066	0.000105	-0.01378	0.045417	0.011726	0.0068616	0.2515
T066	0.000126	-0.010646	0.04513	0.0097084	0.0052143	0.64168
T066	0.000147	-0.013521	0.040276	0.0054516	0.0040205	0.20471
T066	0.000168	-0.013985	0.039813	0.005285	0.0024567	-0.044286
T066	0.000189	-0.013875	0.039566	0.00403	0.0018651	-0.087029

Continued on Next Page...

Table 6 – Continued

Test Number	Time	X Position	Y Position	X Radius	Y Radius	Orientation
T066	0.00021	-0.014683	0.039713	0.003376	0.0020077	-0.096041
T067	2.10E-05	-0.013844	0.052553	0.01005	0.036867	0.19164
T067	4.20E-05	-0.021369	0.07407	0.012904	0.043977	0.25068
T067	8.40E-05	-0.029781	0.10888	0.013311	0.039109	0.22625
T067	0.000105	-0.031165	0.11018	0.013544	0.036429	0.2655
T067	0.000126	-0.032329	0.11427	0.01356	0.033757	0.23054
T067	0.000147	-0.032348	0.11762	0.014083	0.031226	0.24735
T067	0.000168	-0.032221	0.12028	0.014234	0.026816	0.27814
T067	0.000189	-0.0322	0.12083	0.013713	0.0261	0.36534
T067	0.00021	-0.033393	0.12334	0.013609	0.023504	0.41297
T067	0.000231	-0.033799	0.12482	0.013526	0.021466	0.52125
T067	0.000252	-0.033935	0.1261	0.013627	0.019348	0.57995
T067	0.000273	-0.0338	0.12797	0.012631	0.017633	0.7854
T067	0.000294	-0.034128	0.12902	0.016979	0.011146	-0.71567
T067	0.000315	-0.03366	0.12849	0.017039	0.010008	-0.71437
T067	0.000336	-0.033861	0.13055	0.015915	0.0087758	-0.64338
T067	0.000357	-0.033791	0.13133	0.015223	0.0074977	-0.58608
T067	0.000378	-0.033749	0.13059	0.015089	0.0066462	-0.57983
T067	0.000399	-0.034175	0.13114	0.0088462	0.0058958	-0.37393
T067	0.00042	-0.034167	0.13147	0.0074272	0.0046814	-0.48335
T067	0.000441	-0.034549	0.13251	0.0061359	0.0044798	-0.2134
T067	0.000462	-0.034954	0.13324	0.0049097	0.0043506	-0.15379
T067	0.000483	-0.033929	0.13363	0.0041714	0.0032229	0.12117
T072	1.50E-05	-0.0073643	-0.0093767	0.017013	0.025856	0.04439
T072	3.00E-05	-0.014913	0.0099229	0.017614	0.039498	-0.014826

Continued on Next Page...

Table 6 – Continued

Test Number	Time	X Position	Y Position	X Radius	Y Radius	Orientation
T072	4.50E-05	-0.016821	0.01637	0.017124	0.041946	-0.00052099
T072	6.00E-05	-0.016153	0.024046	0.014477	0.04352	0.11567
T072	7.50E-05	-0.016575	0.02833	0.013673	0.044771	0.14217
T072	9.00E-05	-0.017472	0.028989	0.01322	0.044902	0.15681
T072	0.000105	-0.017735	0.029489	0.012825	0.043255	0.15696
T072	0.00012	-0.017477	0.029284	0.012213	0.042589	0.14919
T072	0.000135	-0.018149	0.029477	0.013407	0.046016	0.13656
T072	0.00015	-0.018615	0.029584	0.014047	0.048496	0.12309
T072	0.000165	-0.01765	0.033663	0.012424	0.045446	0.18165
T072	0.00018	-0.018077	0.0329	0.013249	0.046777	0.1667
T072	0.000195	-0.018452	0.032149	0.016269	0.04985	0.13767
T072	0.00021	-0.018156	0.030257	0.014191	0.046193	0.13408
T072	0.000225	-0.0183	0.028942	0.014431	0.046092	0.11803
T072	0.00024	-0.020167	0.02873	0.017051	0.044545	0.093058
T072	0.000255	-0.019739	0.027665	0.015988	0.043475	0.082431
T072	0.00027	-0.018842	0.025385	0.014927	0.04492	0.067081
T072	0.000285	-0.019114	0.026147	0.014623	0.041555	0.067956
T072	0.0003	-0.019066	0.02507	0.014875	0.04188	0.056008

Appendix B. Initial Analysis Results

Table 7 X-Radius Quartic Model Coefficients

Test Number	β_1	β_2	β_3	β_4
T005	4.141734044	-0.994820016	0.080879664	-0.002086535
T025	6.769693381	-0.836762301	0.036746955	-0.000542552
T038	2.234116227	-0.309172285	0.020066167	-0.000499415
T039	8.476241477	-1.216687917	0.067099043	-0.001314448
T040	9.758630952	-3.285378401	0.47241861	-0.032033094
T042	3.322257406	-0.266895975	0.007915706	-8.19E-05
T048	12.27789349	-1.495262549	0.060359018	-0.000796562
T049	4.578690023	-0.401331356	0.009737554	-2.74E-05
T050	3.776893093	-0.504714483	0.026495342	-0.000474902
T051	4.69609934	-0.513369171	0.022682874	-0.000361832
T052	2.710480703	-0.186201085	0.004884323	-4.29E-05
T055	4.058552323	-0.282740498	0.00914351	-0.000142371
T056	8.487230991	-1.662028169	0.113279351	-0.002585742
T057	8.748661923	-1.534404766	0.100432143	-0.002273186
T058	8.005232074	-1.336790904	0.083420566	-0.001813698
T059	6.59385199	-0.551083346	0.011985957	2.00E-05
T063	1.672499221	-0.08124767	0.001713456	-1.34E-05
T065	3.905853765	-0.409818602	0.015940698	-0.000204954
T066	5.166033745	-0.547073867	-0.001228626	0.001093603
T067	4.239139719	-0.423966921	0.017676171	-0.000266121
T072	9.89349106	-1.893492443	0.133060646	-0.003079546

Table 8 X-Radius Meta-Model Coefficients

Coefficient	b_0	b_1	b_2	b_3	b_4
β_1	-3.812572097	0.023430592	0.001781702	-5.211148555	0.023121875
β_2	0.720211848	-0.004726494	-0.000344999	2.224227573	-0.006858821
β_3	-0.033848169	0.000789154	2.35E-05	-0.333506028	0.000539945
β_4	-0.000808308	-5.76E-05	-6.17E-07	0.022453432	-7.19E-06

Table 9 Y-Radius Quartic Model Coefficients

Test Number	β_1	β_2	β_3	β_4
T005	7.523318012	-1.819366852	0.146299821	-0.003761859
T025	14.48490397	-1.347428025	0.045518325	-0.000549831
T038	3.992036635	-0.561197399	0.036502359	-0.00089027
T039	24.96284554	-3.557658061	0.182457867	-0.003264407
T040	29.86039286	-18.59656888	4.08912172	-0.300870731
T042	8.373640774	-0.781425164	0.026974155	-0.000312741
T048	6.811290682	-0.683327249	0.023598237	-0.000274192
T049	6.479546281	-1.090178574	0.069674173	-0.001516555
T050	10.65591413	-1.264124817	0.054325678	-0.000807266
T051	11.04085928	-1.121343389	0.041221863	-0.000531354
T052	7.526255032	-0.480290054	0.011201962	-9.10E-05
T055	15.0076694	-1.934833057	0.088301027	-0.001370875
T056	15.07403669	-3.408423177	0.255631481	-0.006236951
T057	16.33897387	-2.094299698	0.096782149	-0.001555773
T058	15.8947773	-1.988835182	0.093611594	-0.001661448
T059	10.71478196	-1.771619858	0.103264304	-0.002009228
T063	5.329685258	-0.27930942	0.005143112	-3.24E-05
T065	10.54620501	-0.910836772	0.026892579	-0.000266581
T066	18.58473503	-5.141225772	0.475899525	-0.014515006
T067	15.10049362	-1.755957088	0.069666548	-0.000922933
T072	21.7376585	-3.388625039	0.212517243	-0.004633975

Table 10 Y-Radius Meta-Model Coefficients

Coefficient	b_0	b_1	b_2	b_3	b_4
β_1	-3.44709873	0.068932473	0.002209376	3.096587222	0.011169786
β_2	-0.355792791	-0.026931182	-0.000524742	9.108905413	0.006503613
β_3	0.258277344	0.006251715	4.89E-05	-2.508318117	-0.001788019
β_4	-0.022560761	-0.000491609	-2.10E-06	0.195631682	0.000134148

Appendix C. Predicted and Modeled Flash Radius For All Test Shots

Shot 5: Actual and Predicted Radius

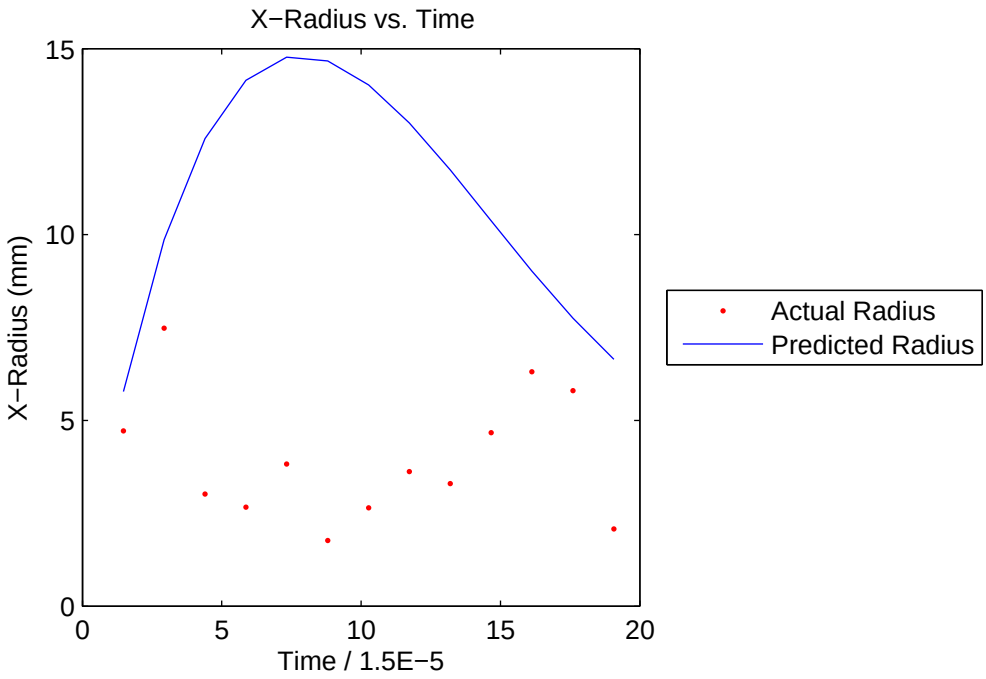

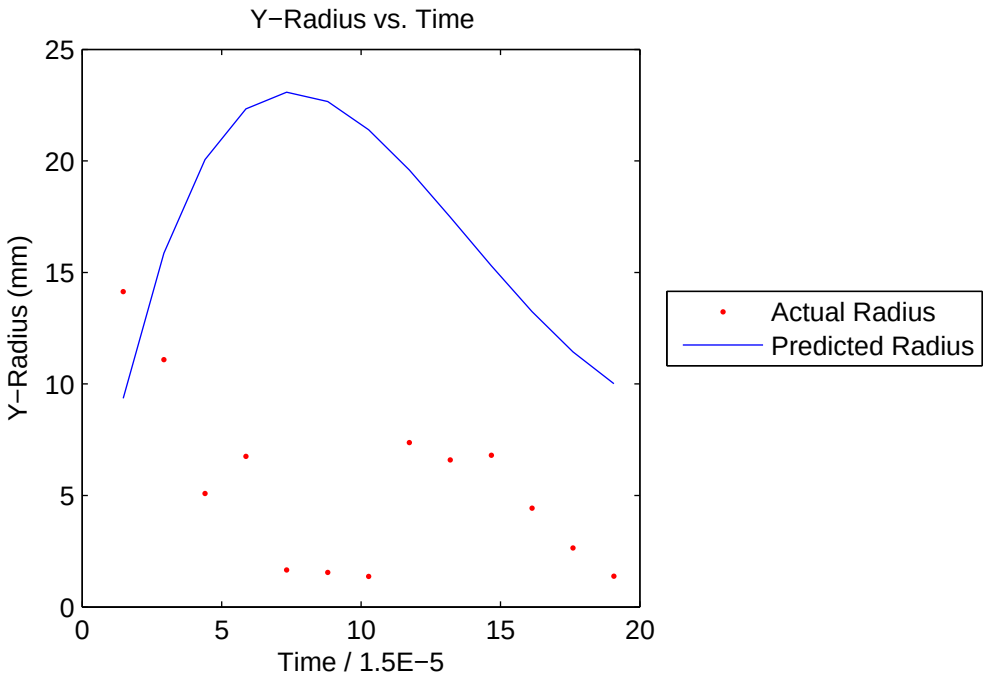

Shot 25: Actual and Predicted Radius

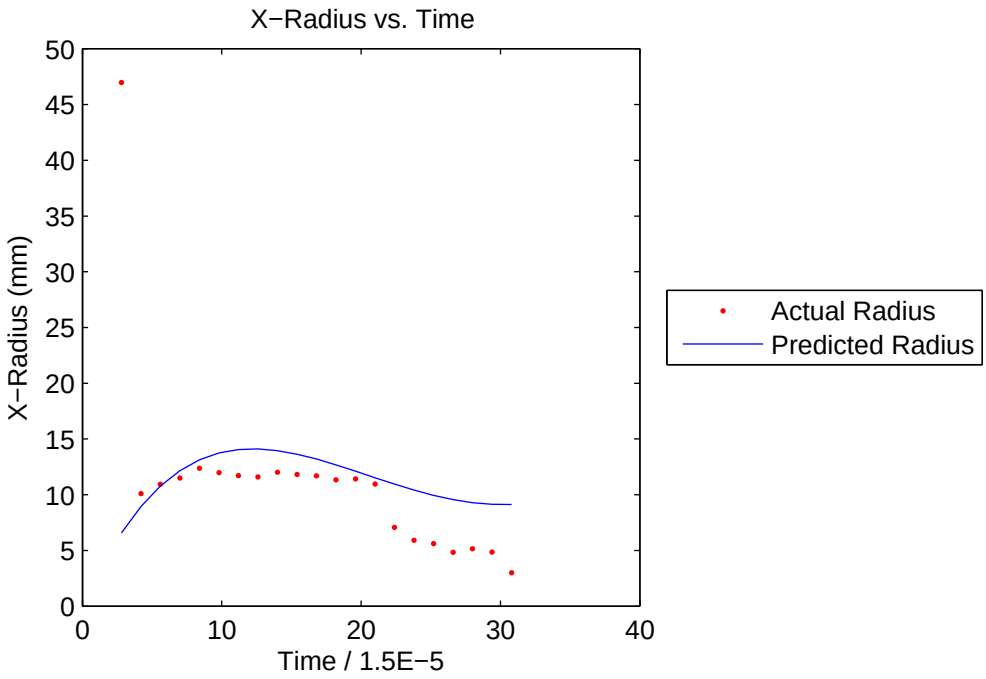

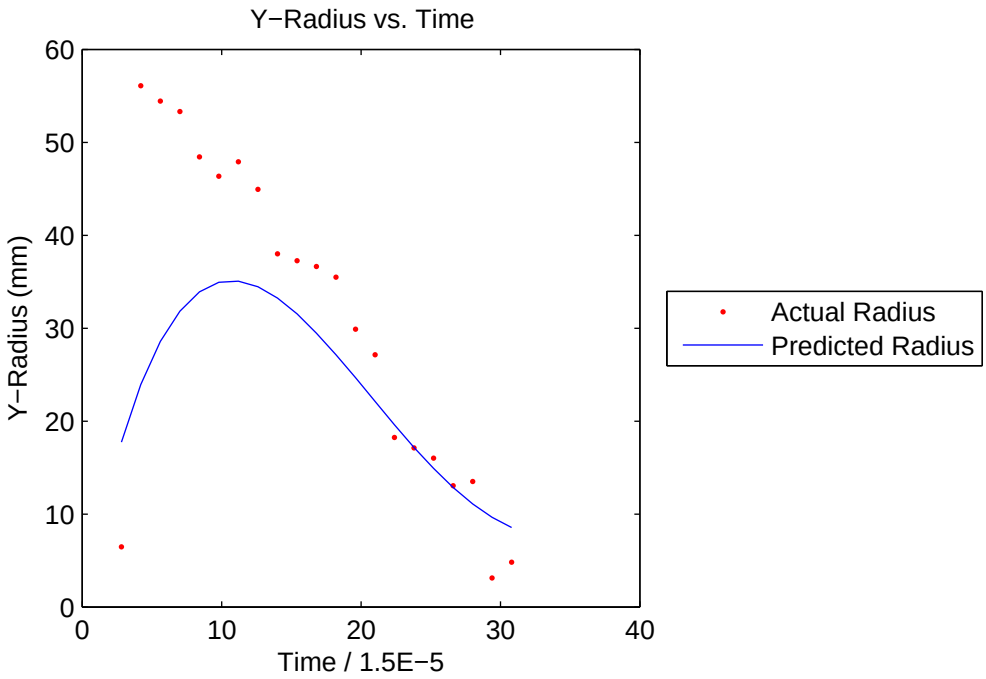

Shot 38: Actual and Predicted Radius

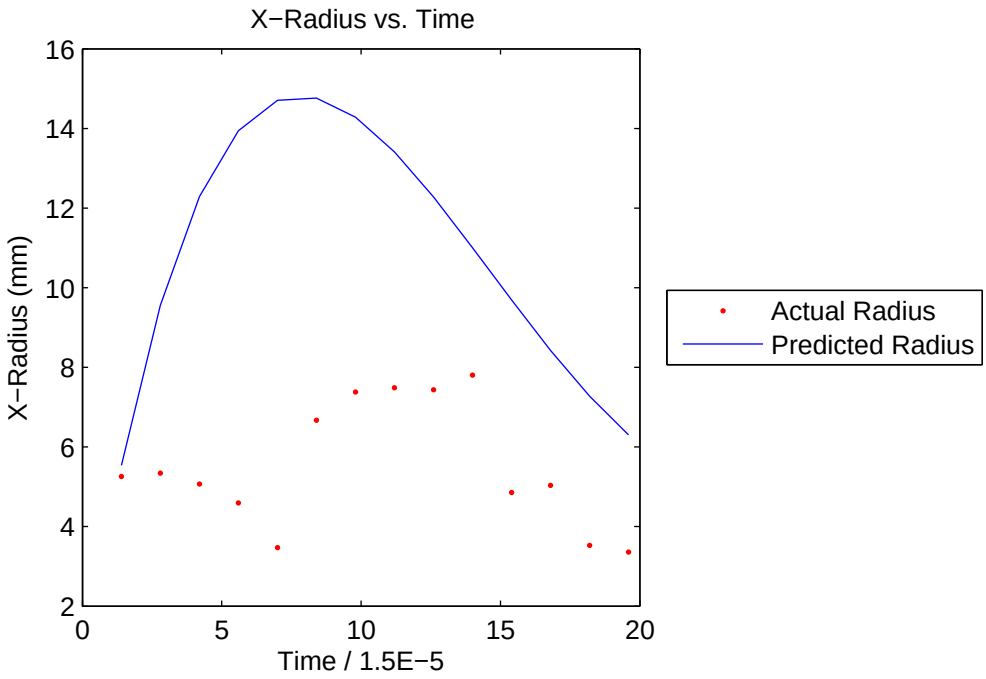

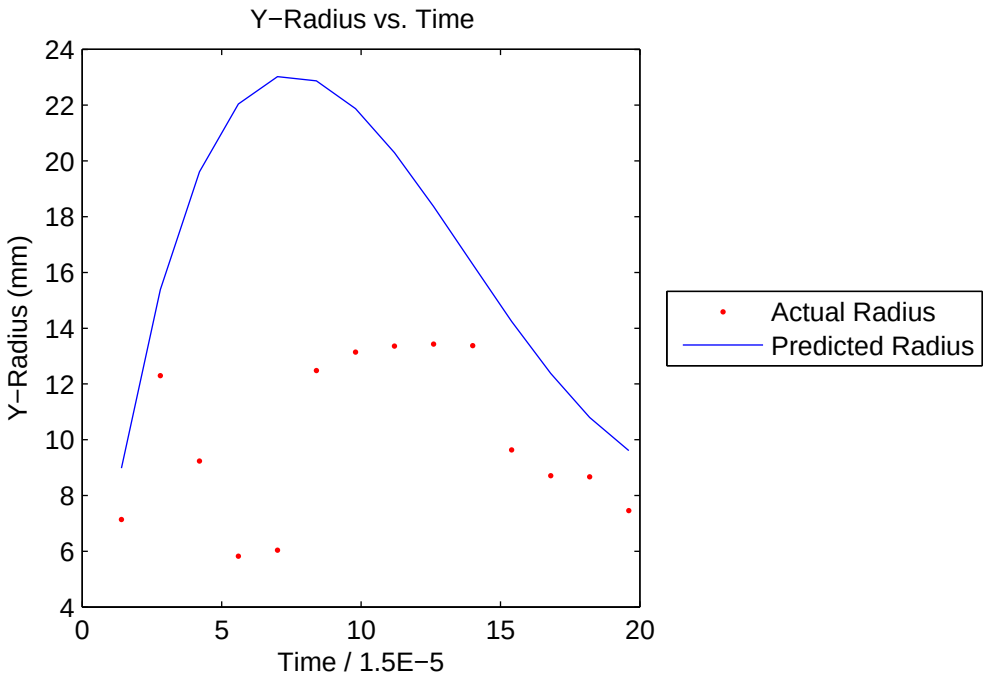

Shot 39: Actual and Predicted Radius

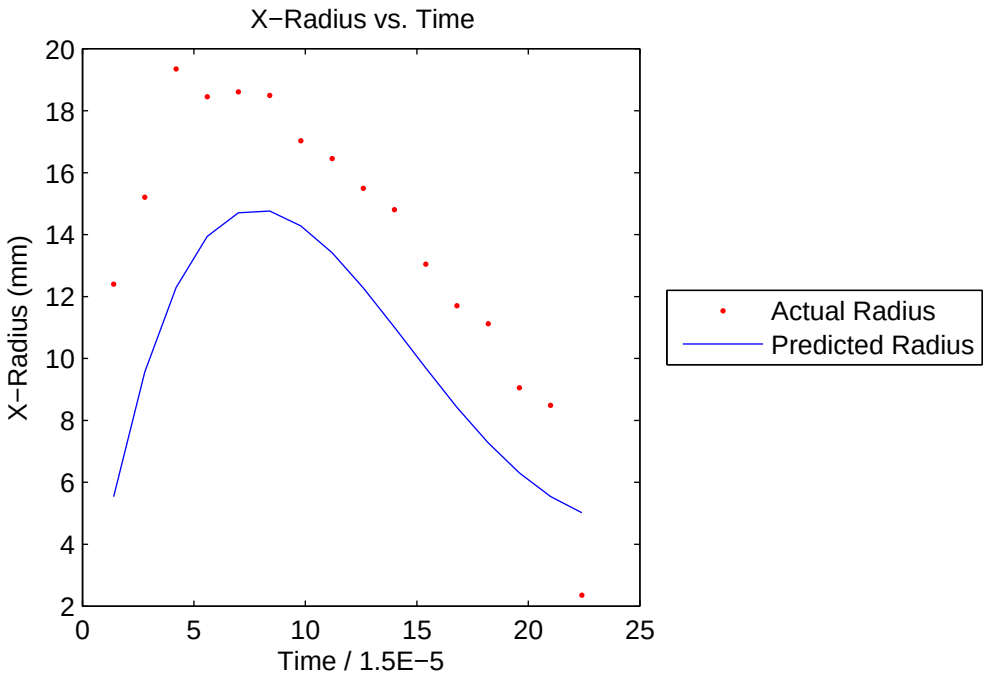

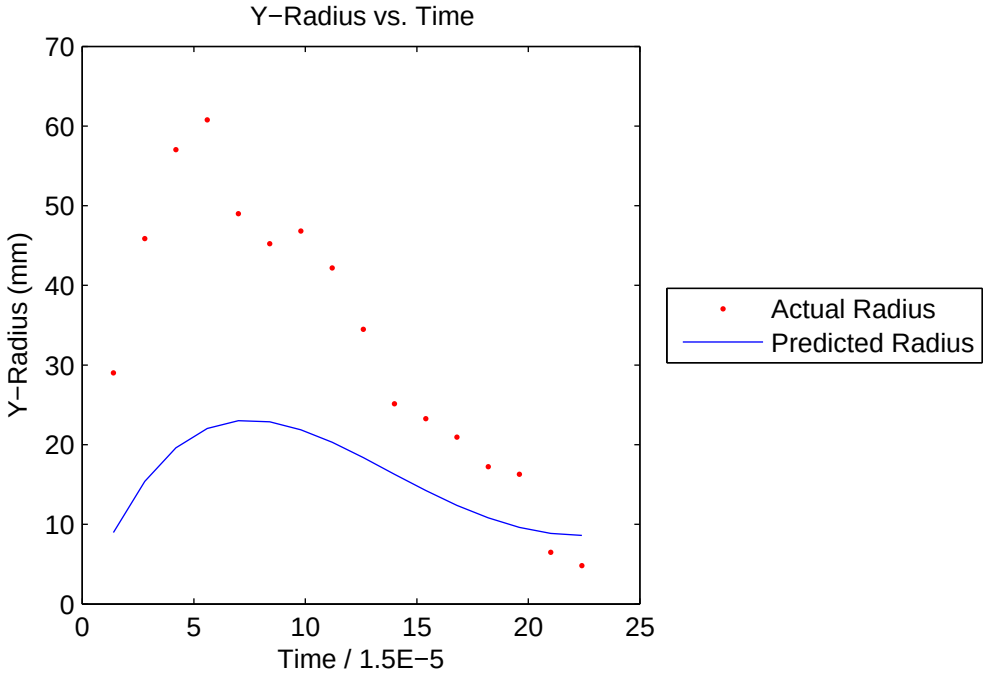

Shot 40: Actual and Predicted Radius

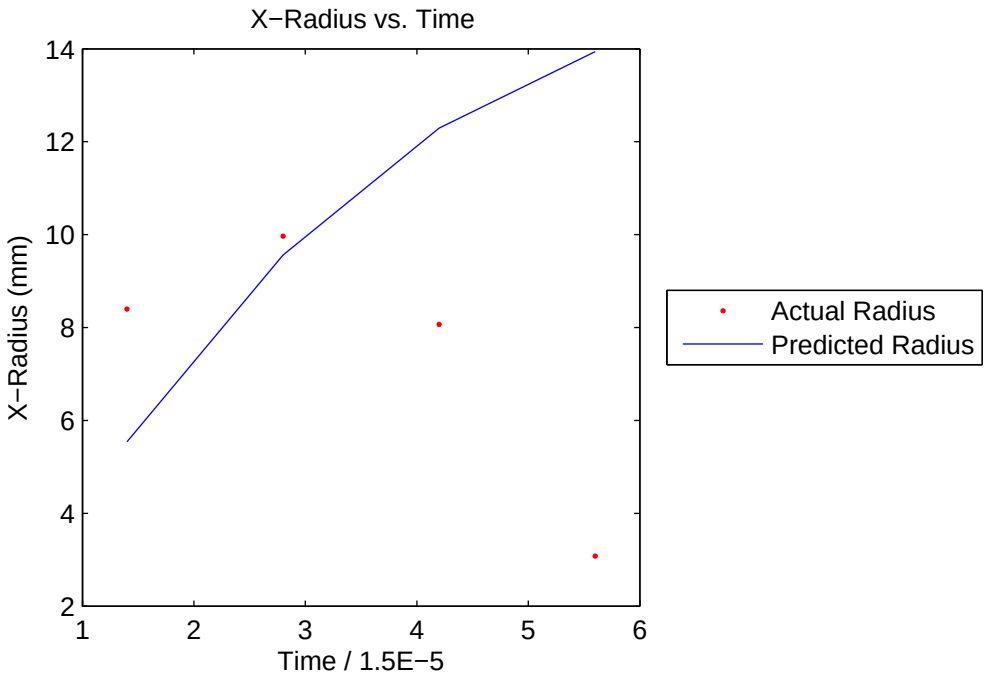

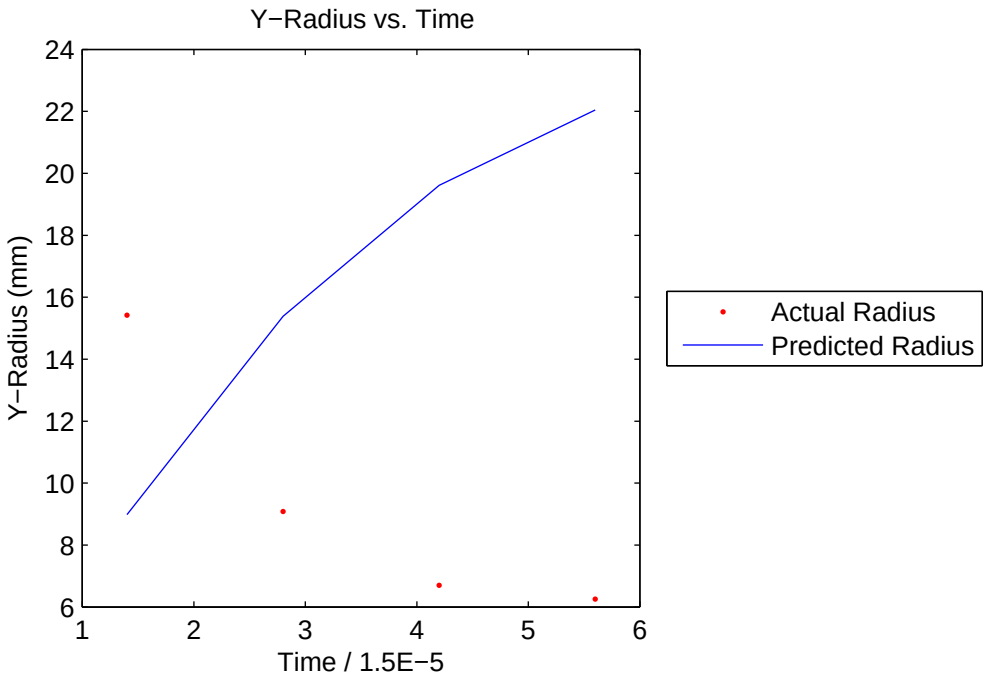

Shot 42: Actual and Predicted Radius

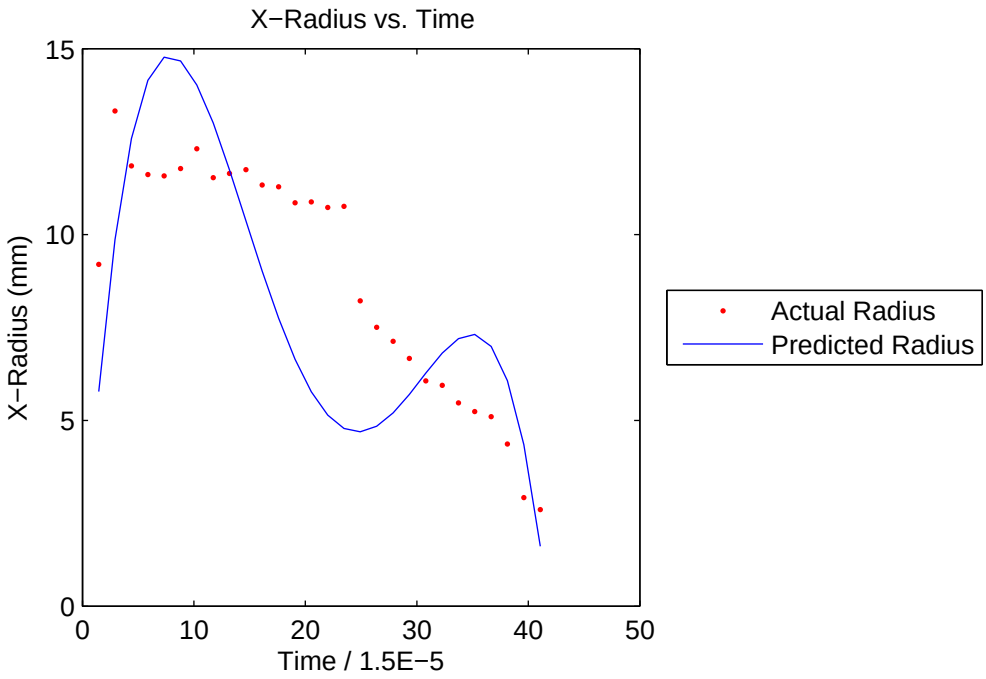

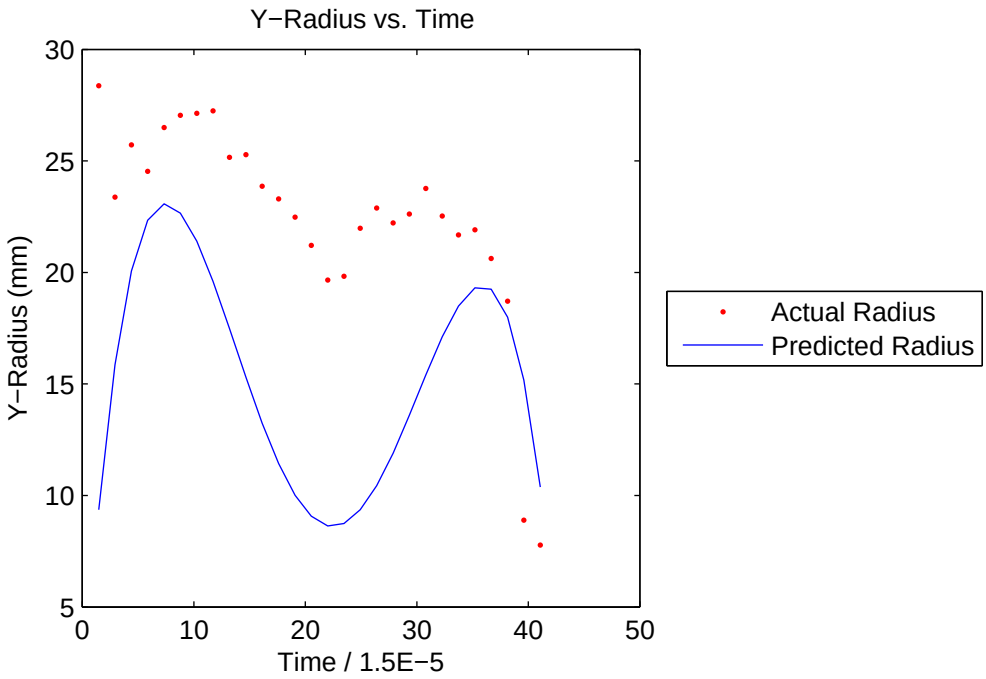

Shot 48: Actual and Predicted Radius

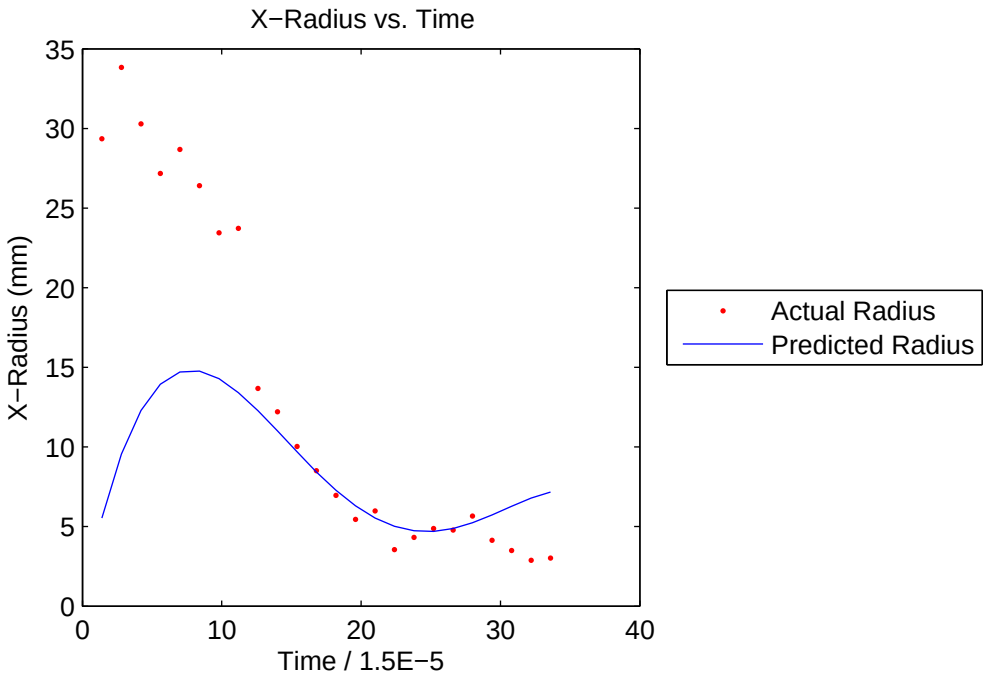

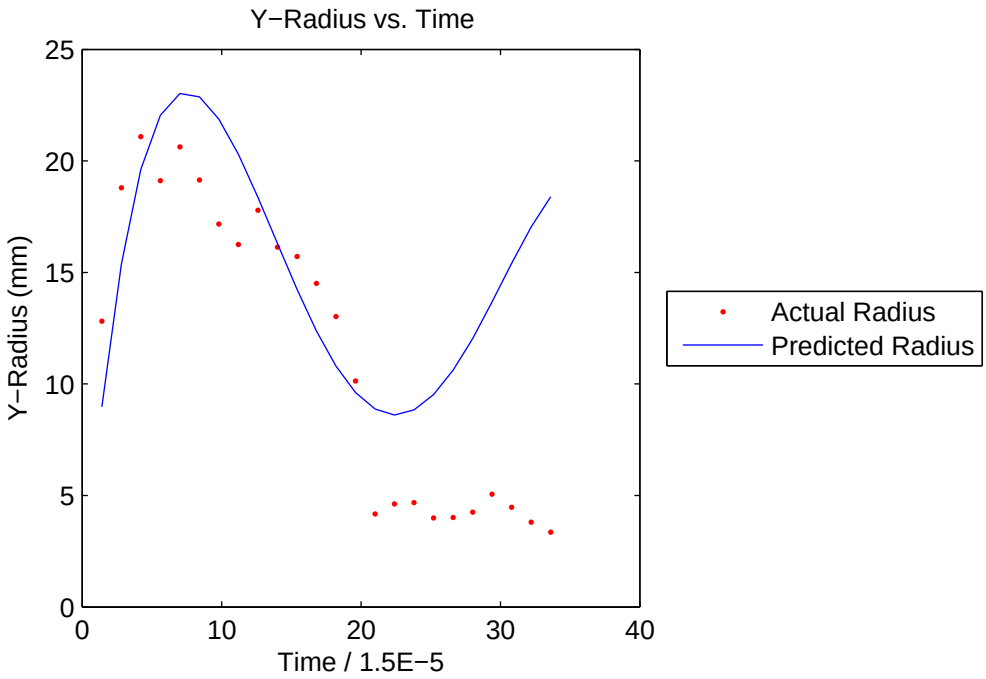

Shot 49: Actual and Predicted Radius

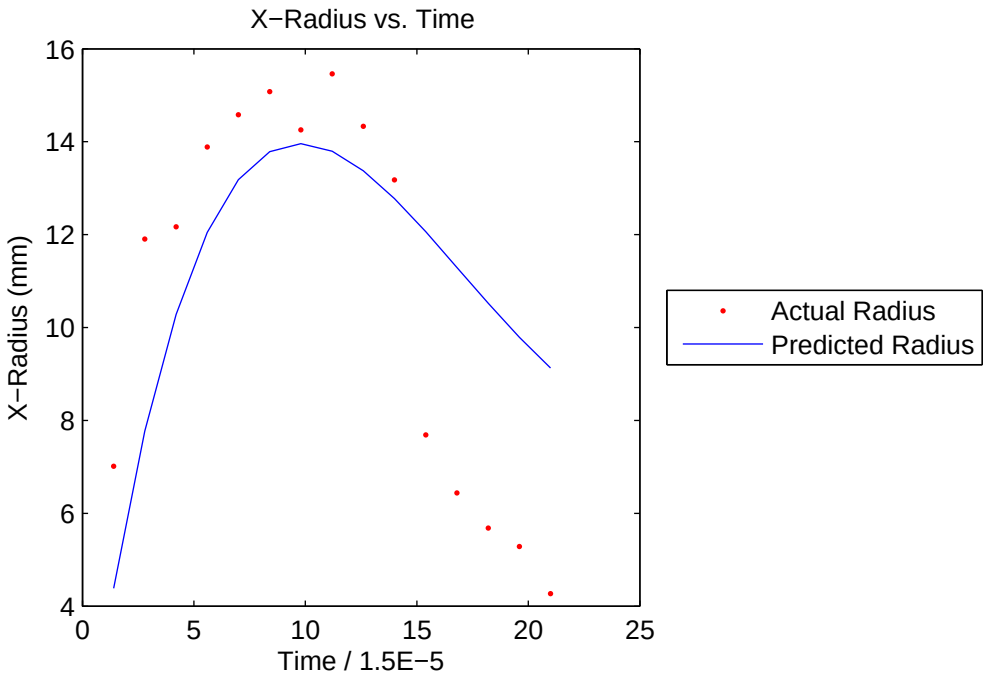

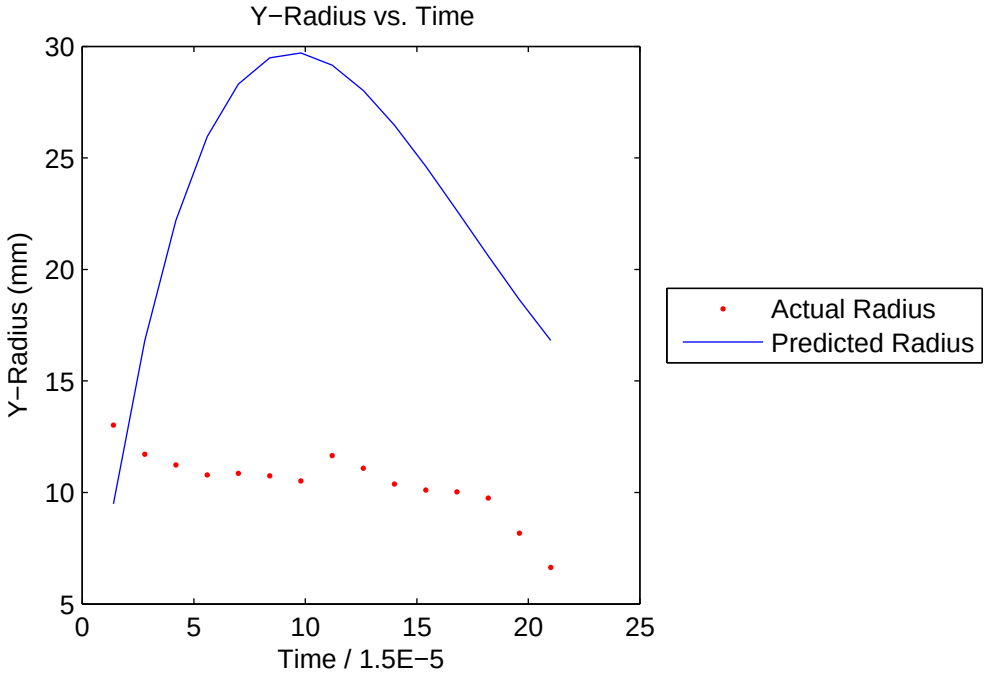

Shot 50: Actual and Predicted Radius

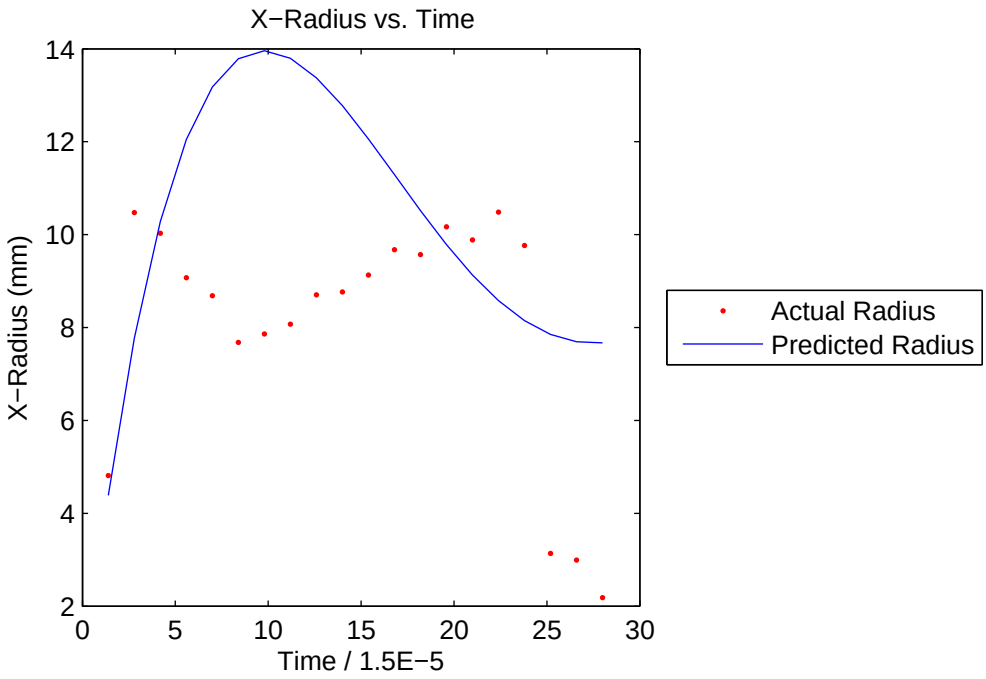

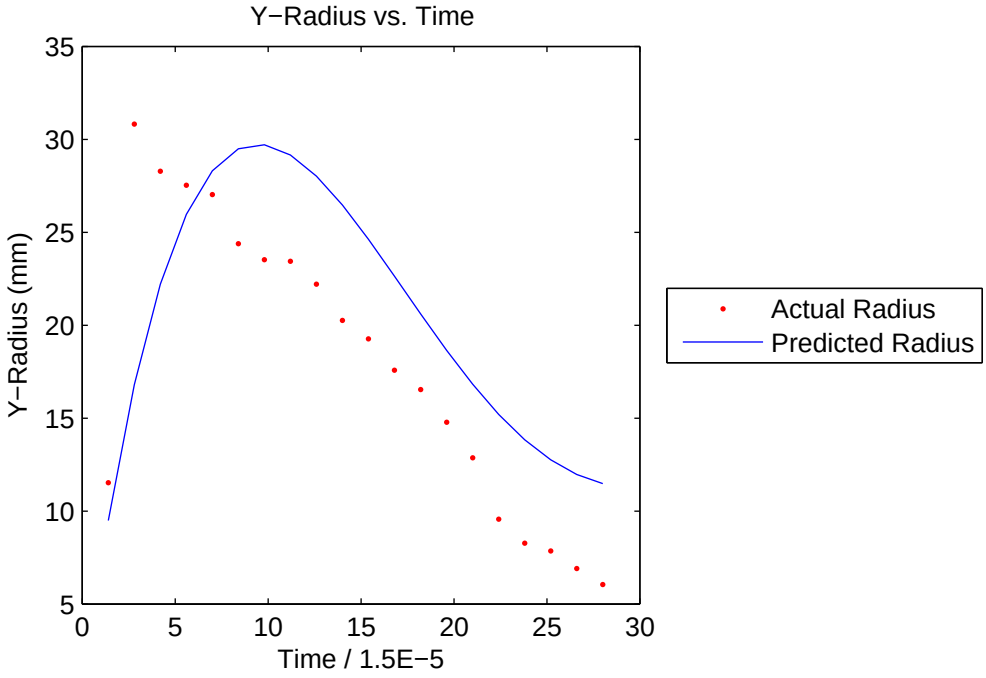

Shot 51: Actual and Predicted Radius

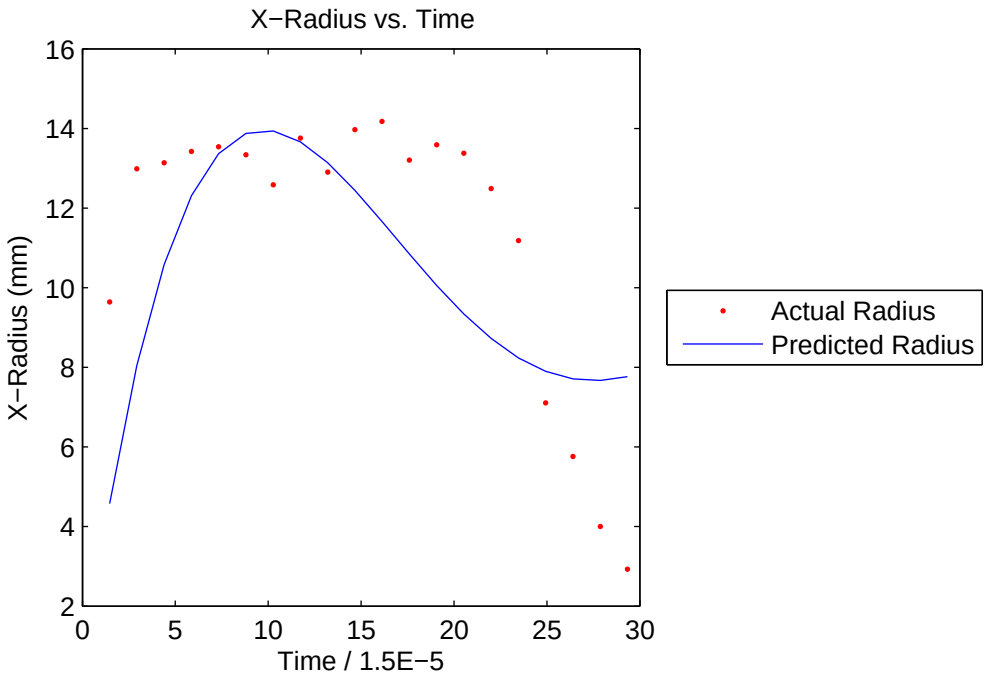

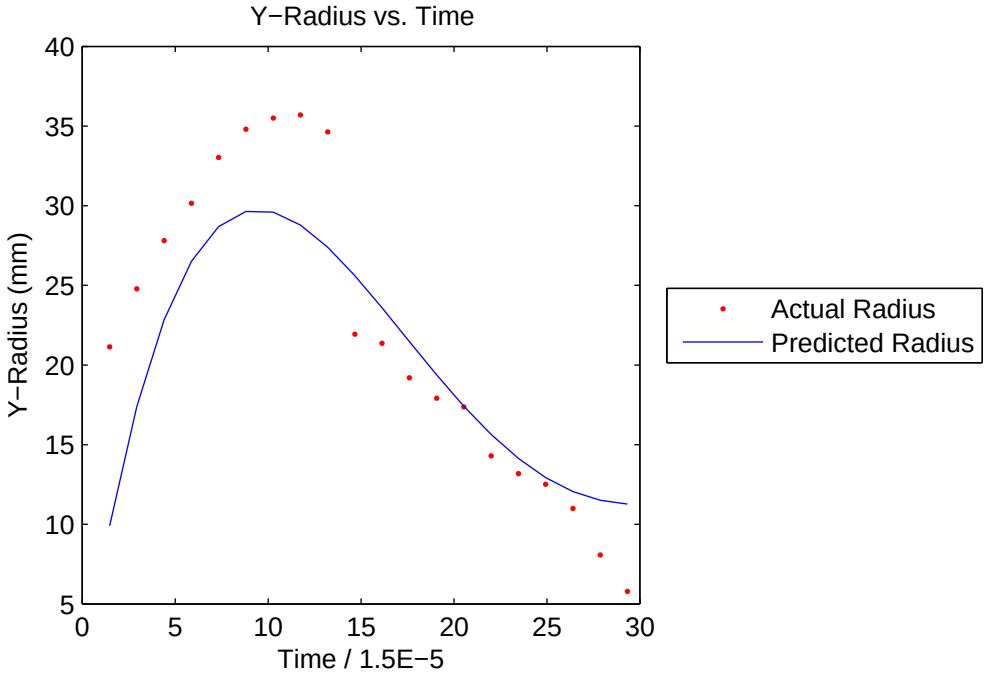

Shot 52: Actual and Predicted Radius

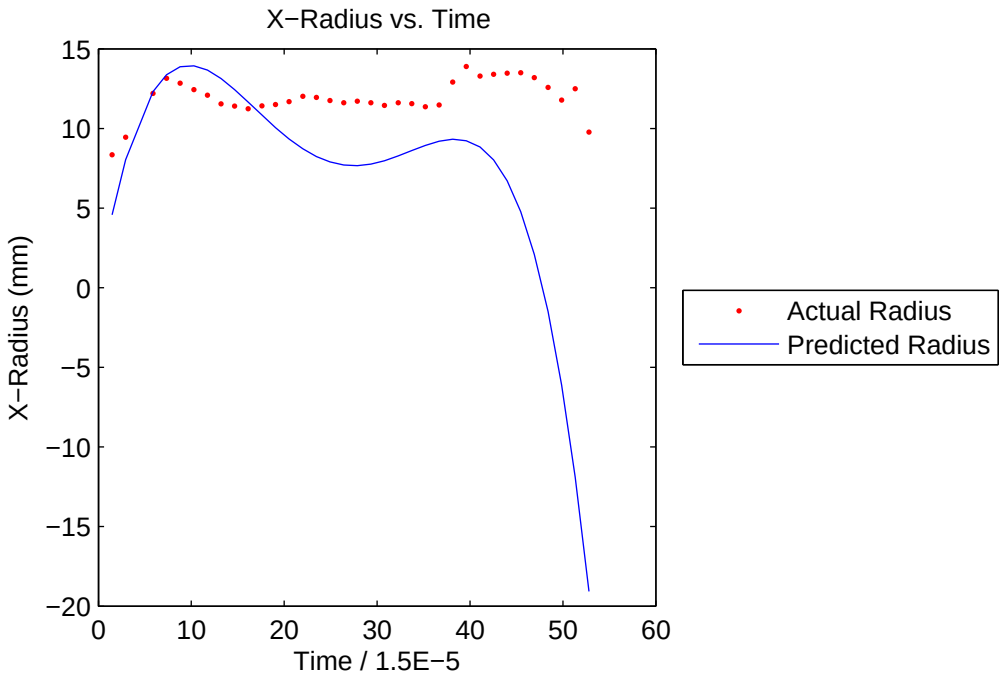

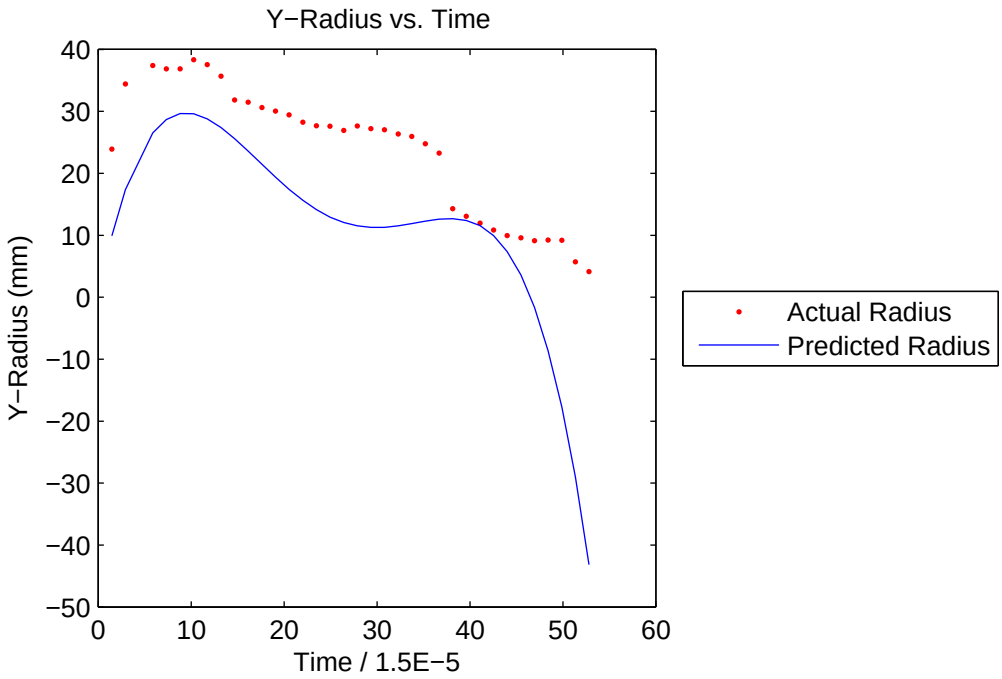

Shot 55: Actual and Predicted Radius

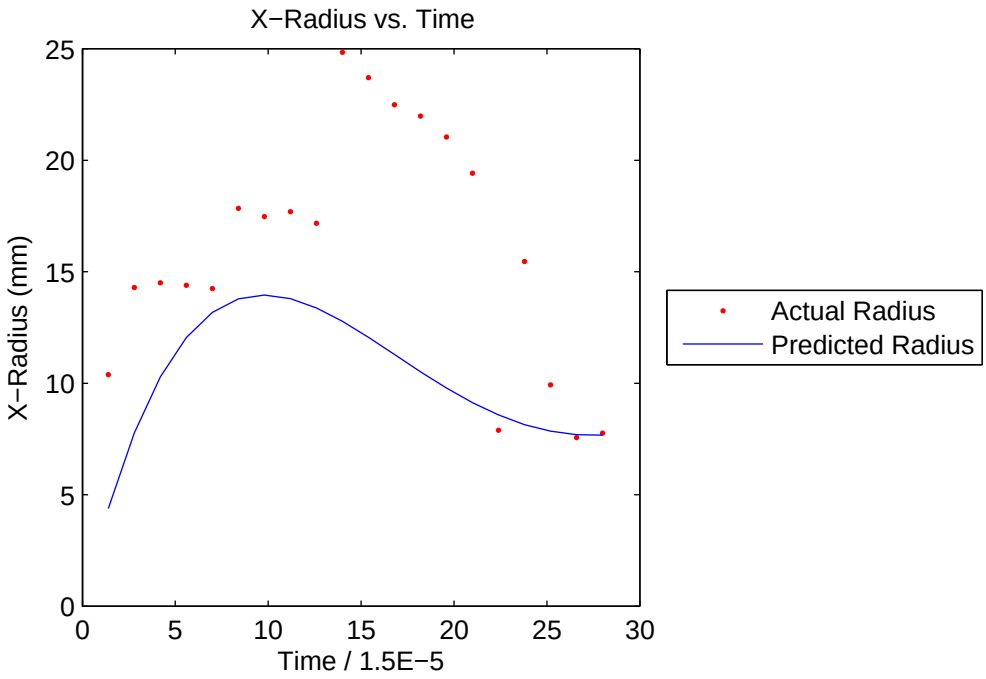

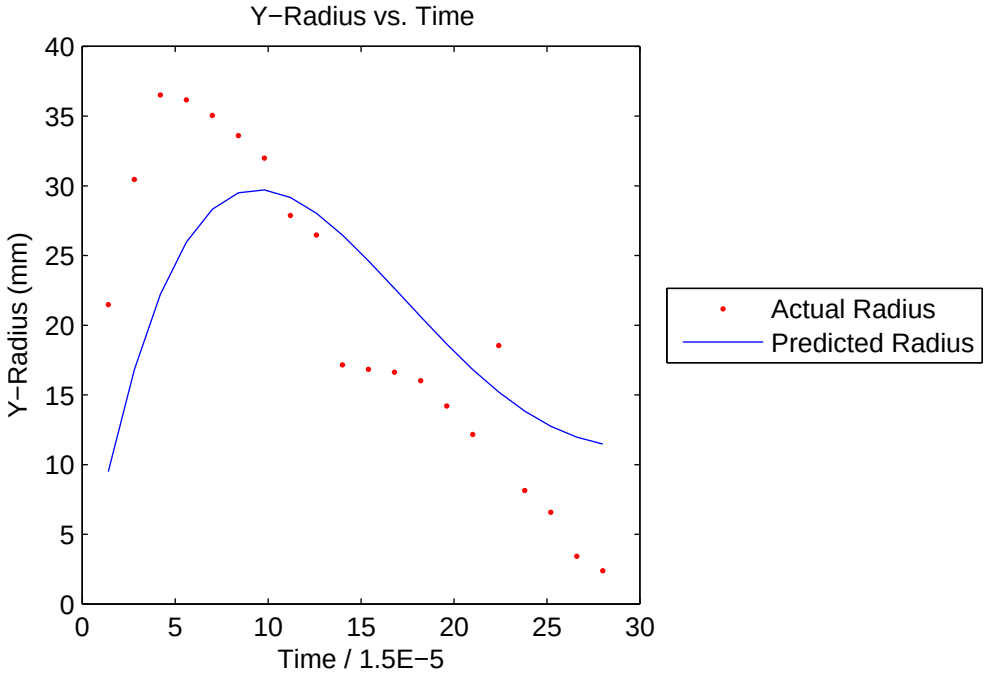

Shot 56: Actual and Predicted Radius

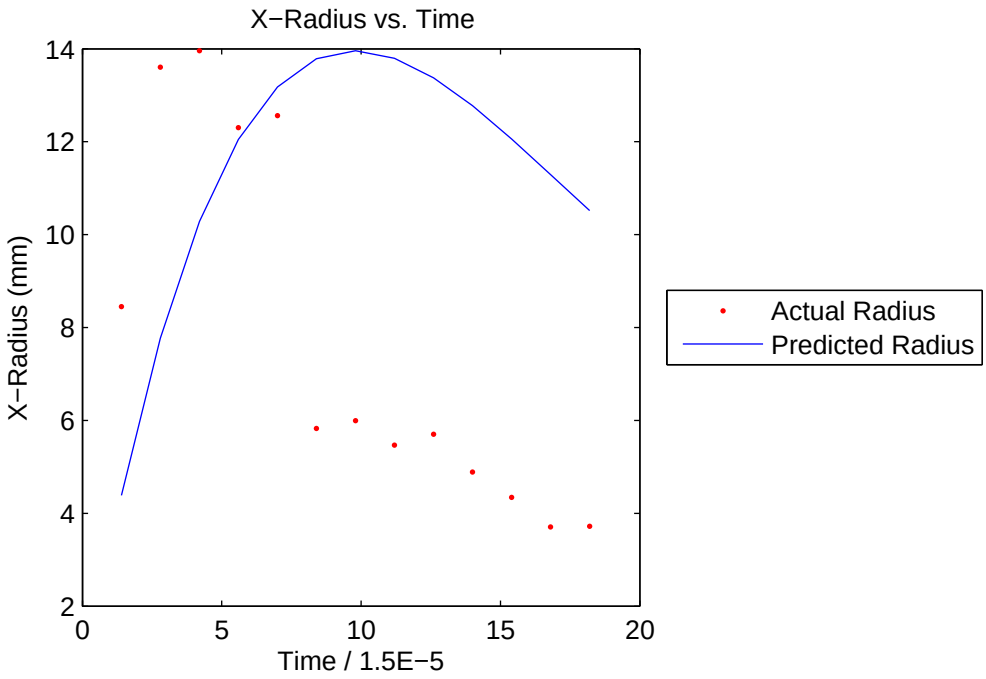

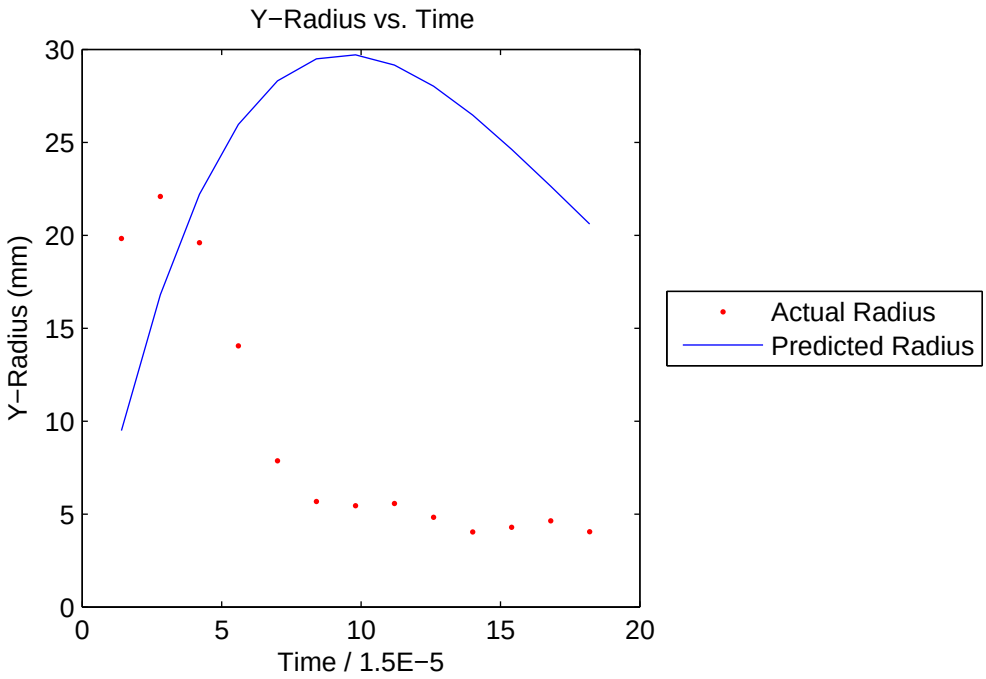

Shot 57: Actual and Predicted Radius

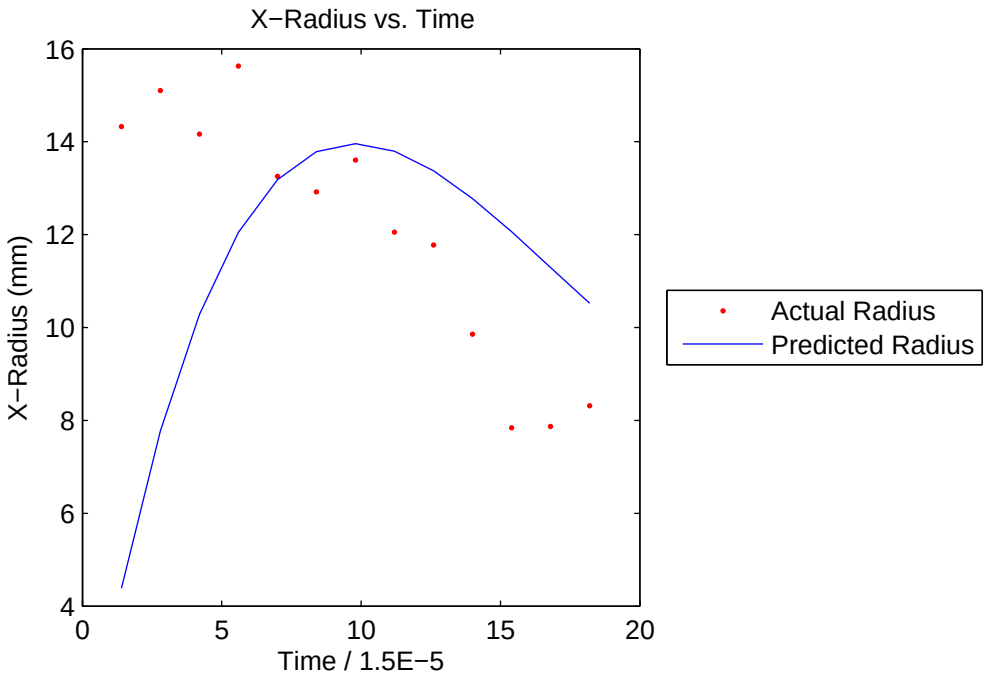

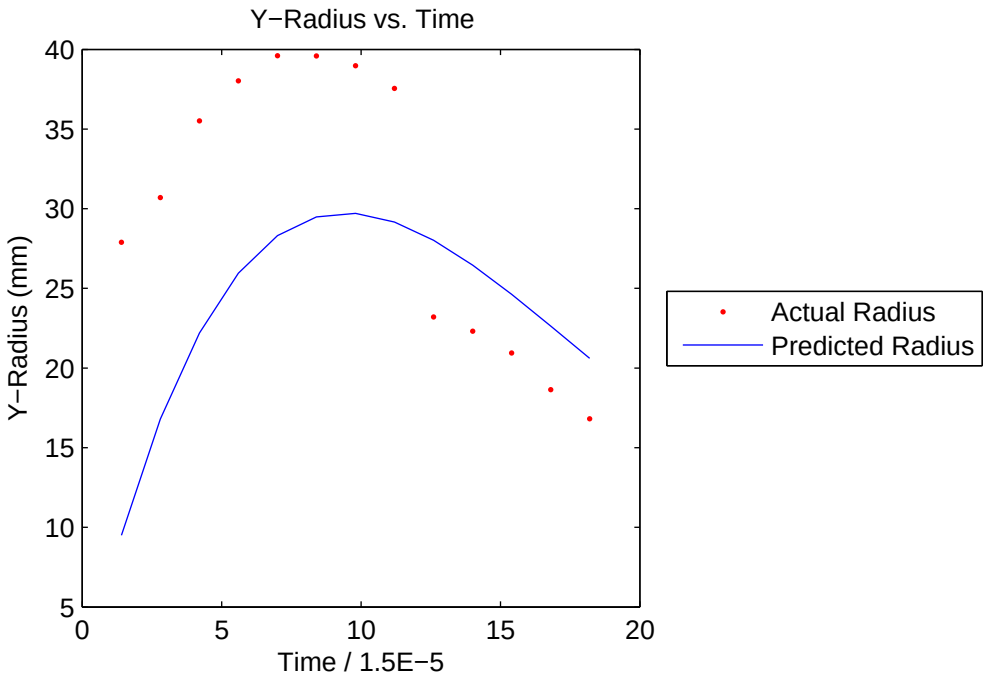

Shot 58: Actual and Predicted Radius

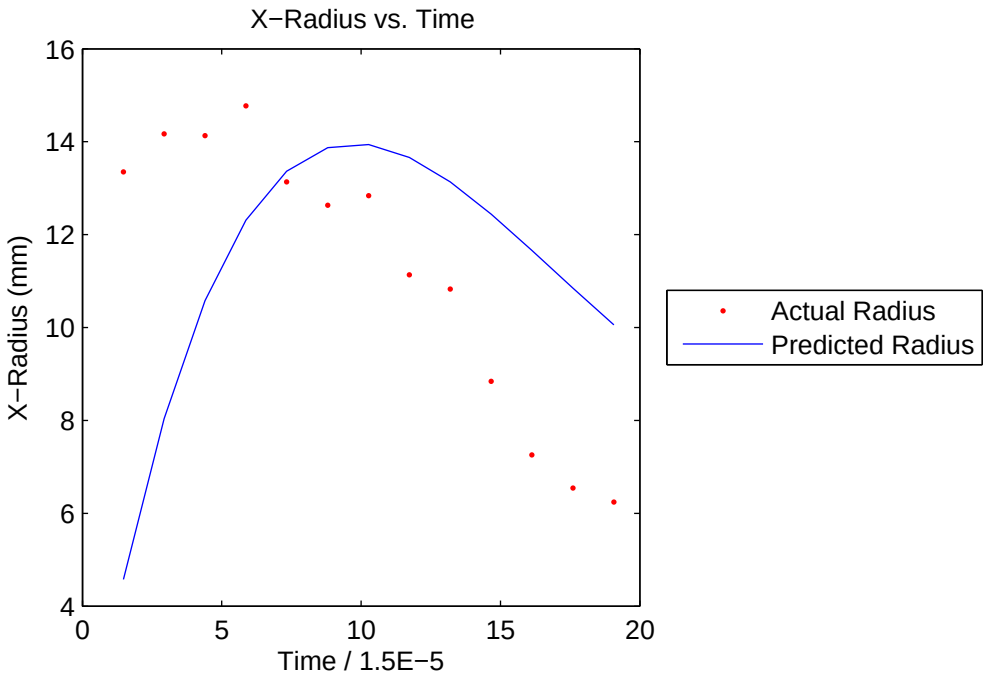

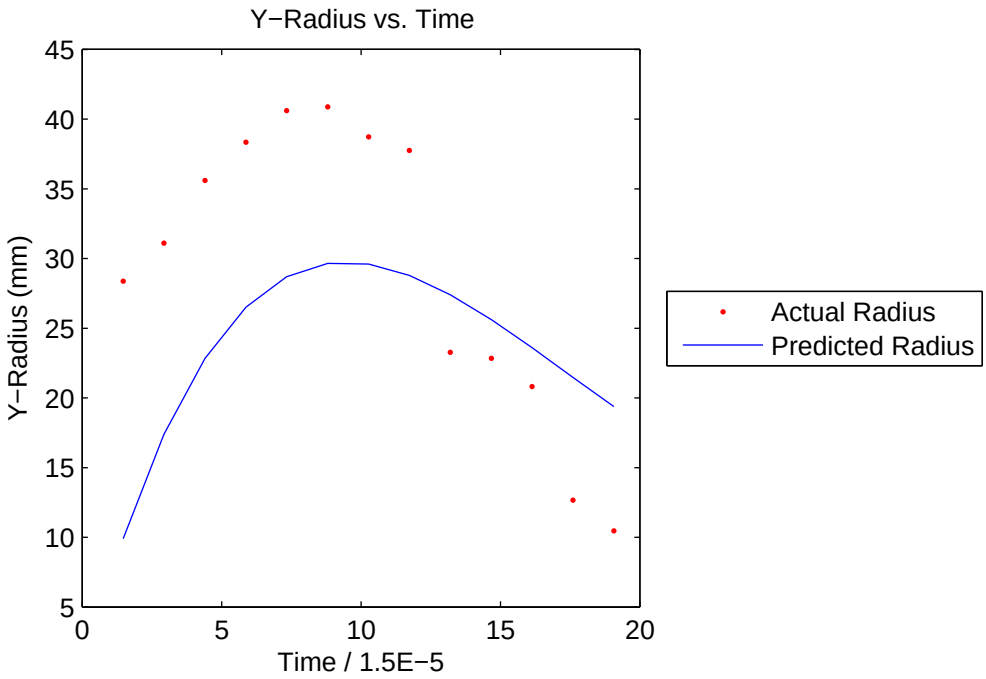

Shot 59: Actual and Predicted Radius

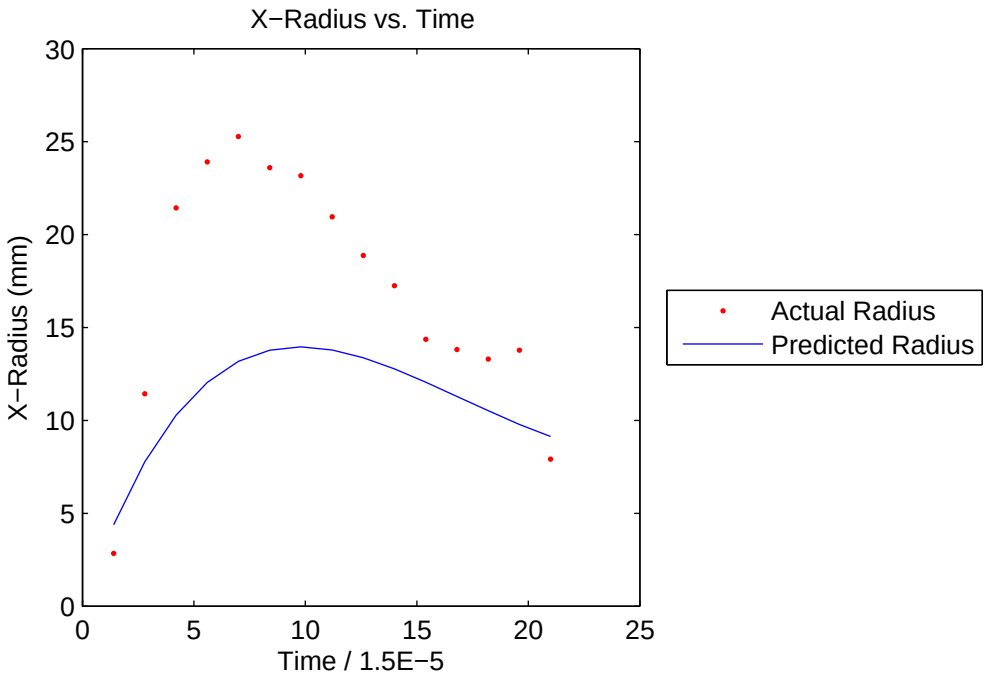

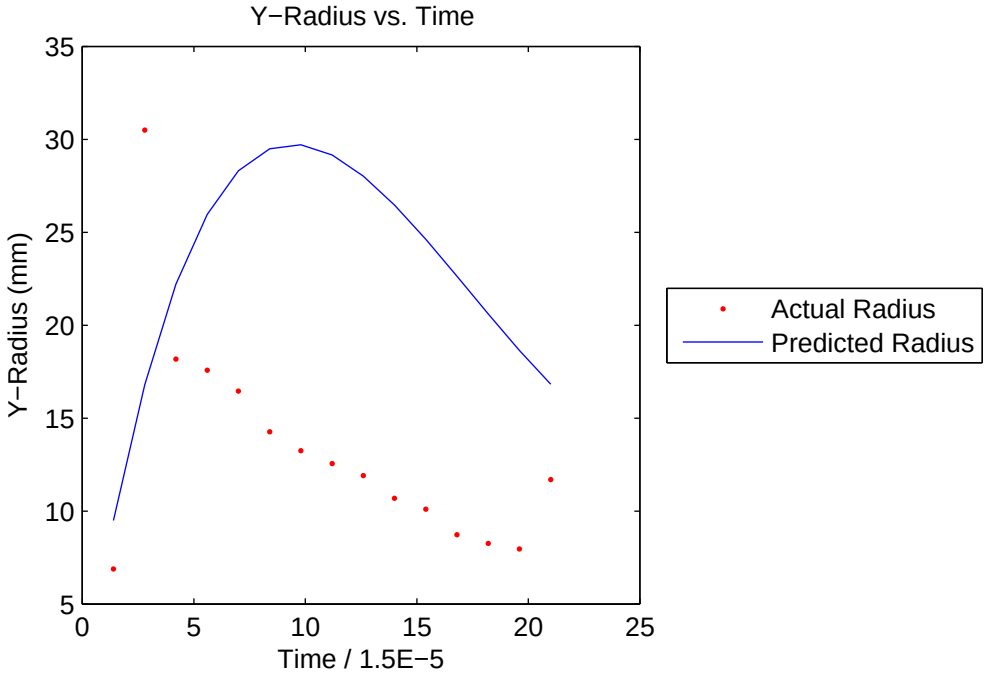

Shot 63: Actual and Predicted Radius

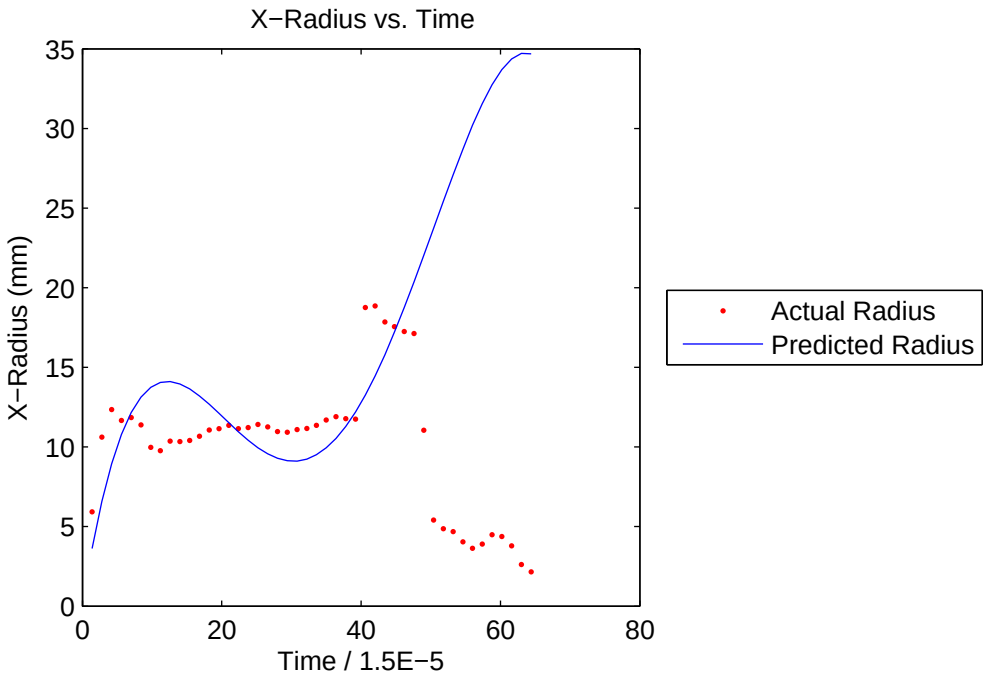

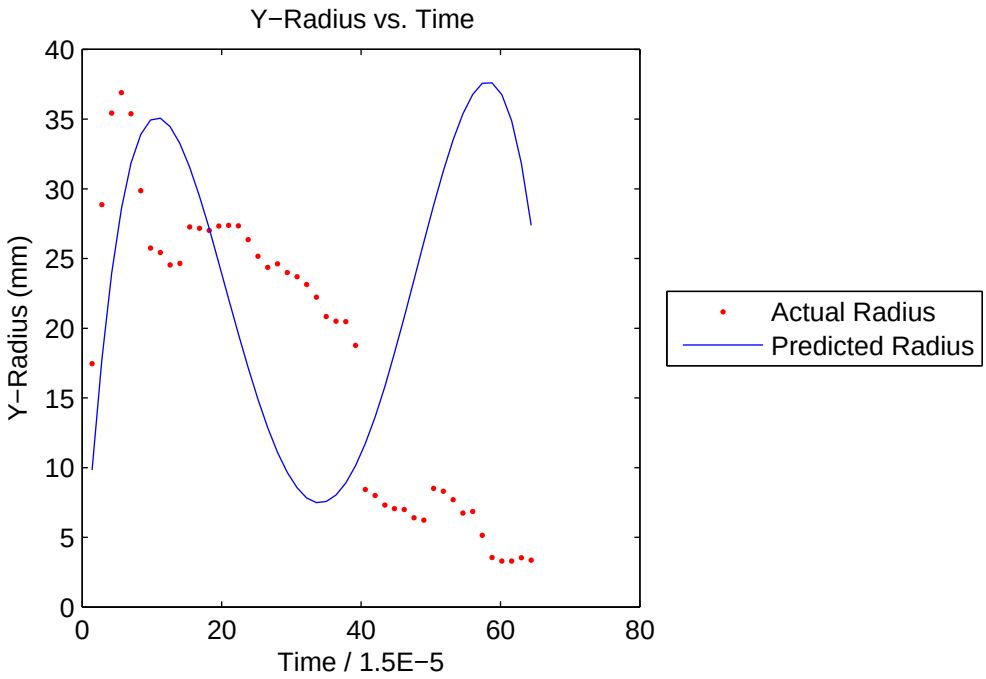

Shot 65: Actual and Predicted Radius

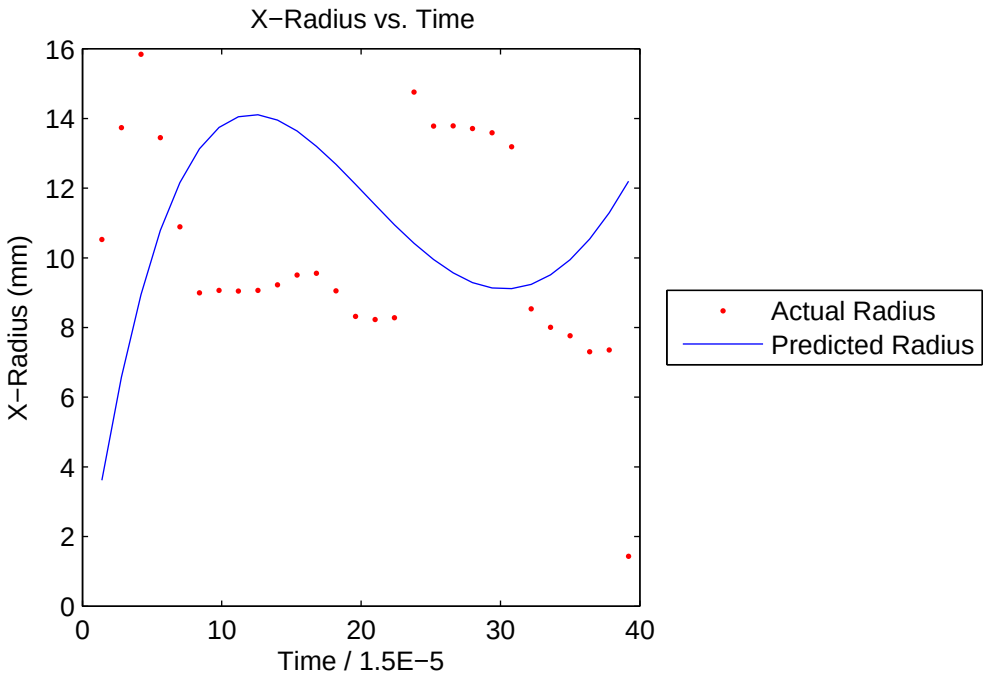

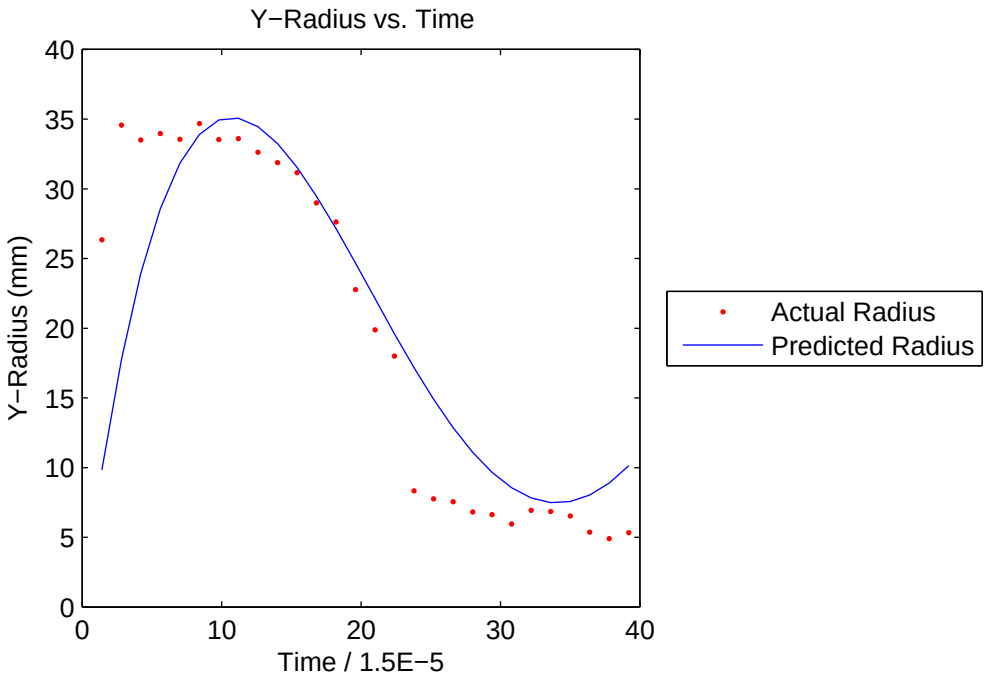

Shot 66: Actual and Predicted Radius

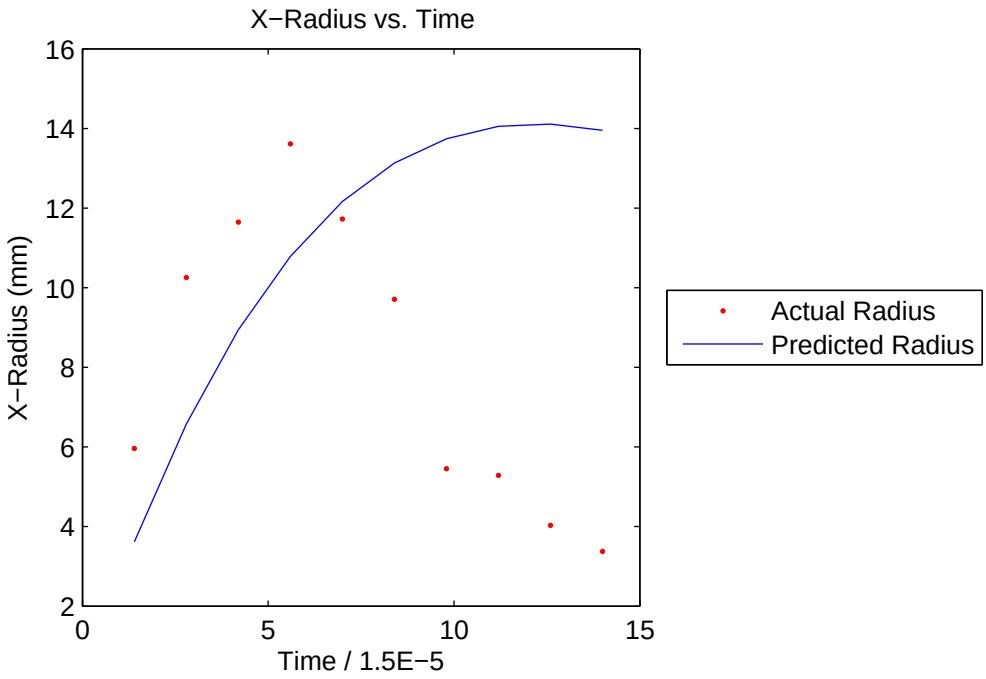

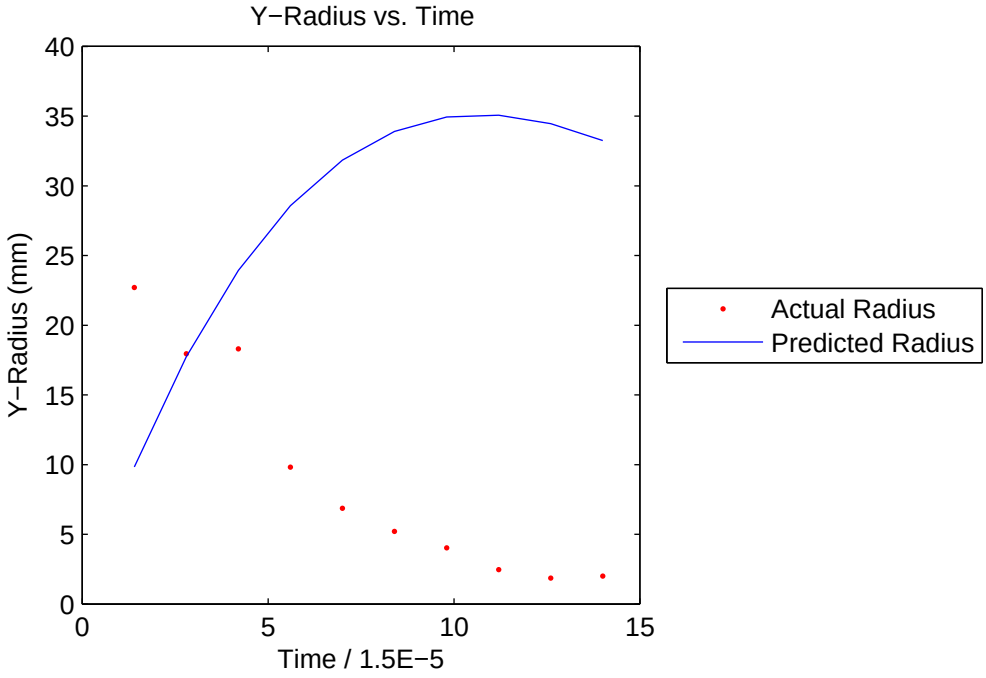

Shot 67: Actual and Predicted Radius

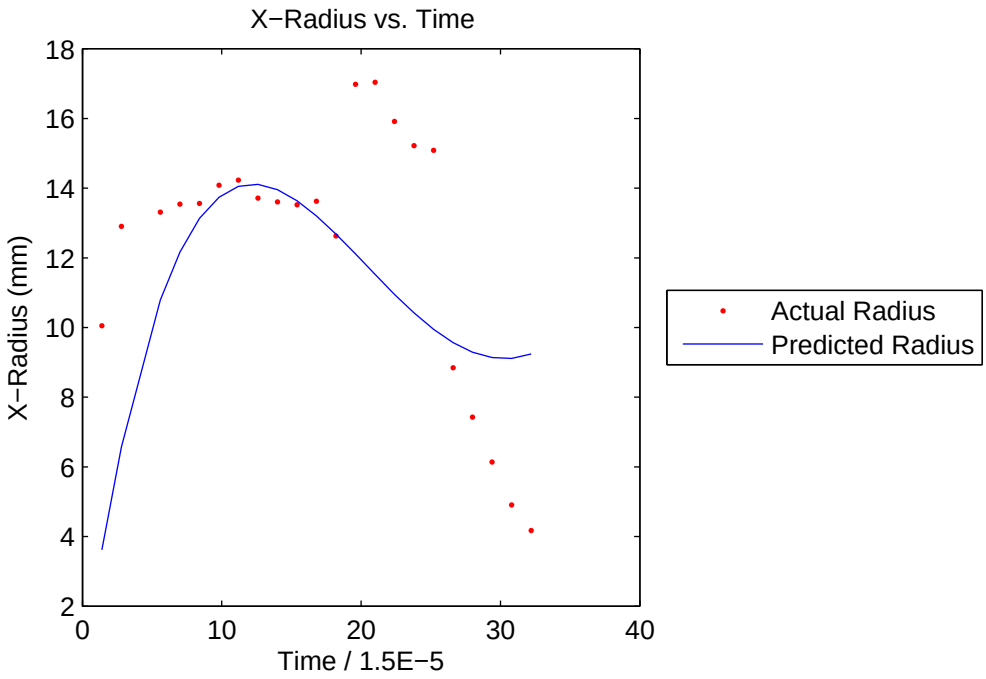

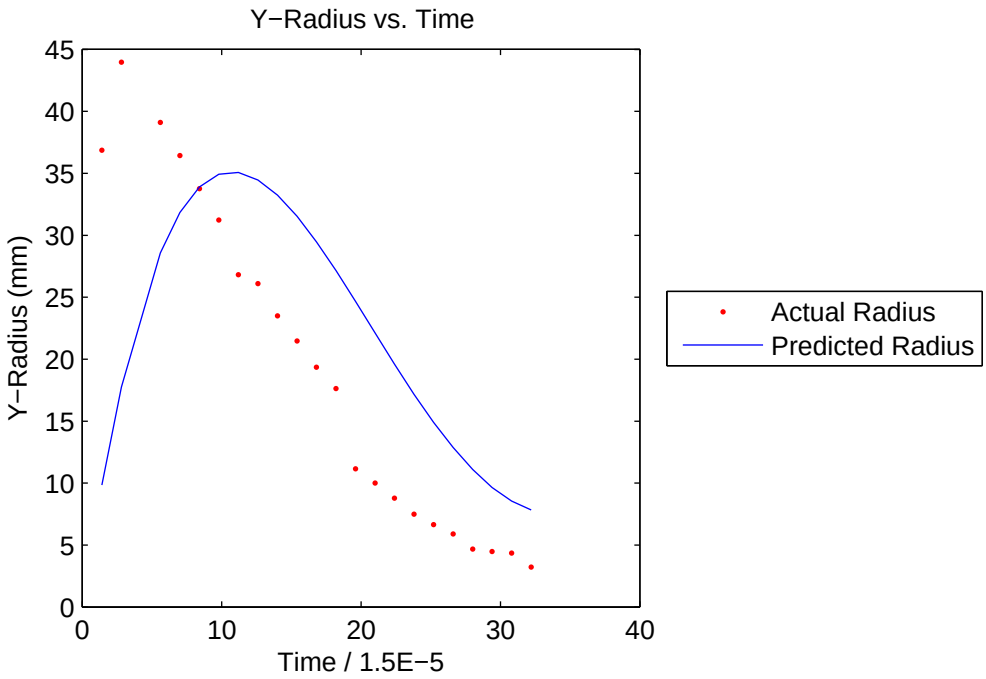

Shot 72: Actual and Predicted Radius

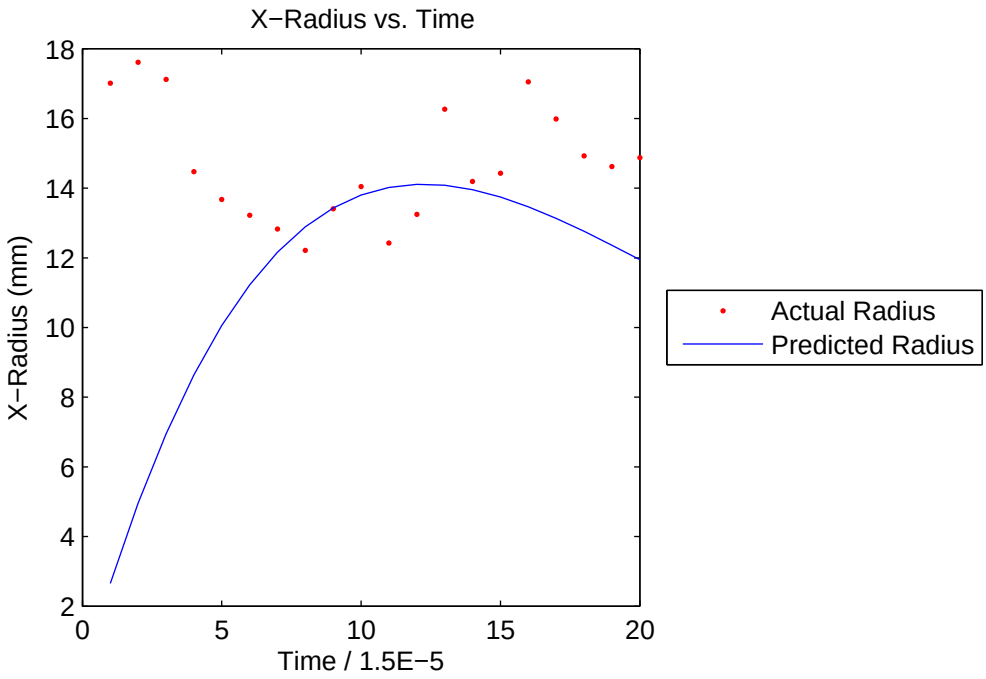

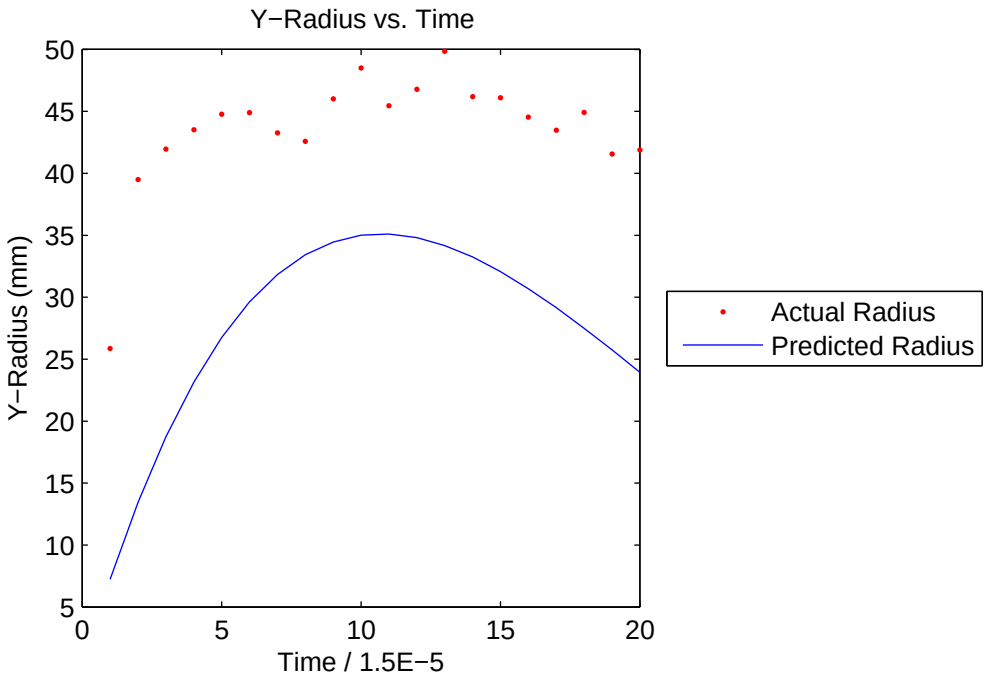

Appendix D. Blue Dart

Fires onboard aircraft are leading mechanisms for mishaps and losses during peacetime and combat operations. Typical ignition sources causing fires onboard aircraft include electrical sparks and hot surfaces. However, impact and penetration of common threats encountered during combat operations, such as armor piercing incendiary projectiles and missile fragments, generate short-lived, but thermally-intense clouds (flashes) capable of igniting fires. Fire simulations supporting system-level survivability analyses depend on accurate characterization of these flash clouds, however, such accurate representations are not currently available. This work provides the first such model to predict the flash characteristics of impact flash events.

This research presents the modeling approach developed to estimate boundary model representations of impact flashes. The research presents generalized meta-modeling approaches to estimate flash size radii (in both the X and Y dimension), flash size duration, flash position, and flash orientation. The empirical model was developed using actual test data obtained via live-fire testing conducted by the 46th Test Group, Aerospace Survivability Analysis Branch. The time series response data from a set of live-fire test events were validated, analytical methods used to develop that response data based on impact event image processing were refined, and the data were then used to create time series models of the response data for each of the test events. The collective of these time series models were then characterized by their parameter sets and a meta-model of those parameterizations was built as a function of test event setup parameters (e.g., projectile mass, projectile speed, angle of attack, and impact material) These final models were transitioned to the customer and are being linked to physics-based thermal models to realize a first-ever simulation of a ballistic flash event suitable for survivability analyses. This research directly supports the Joint Survivability Working Group and the Aerospace Survivability Flight of the 46th Test Group, sponsors of this research.

Appendix E. Storyboard

Empirical Characterization of Ballistic Impact Flash

1st Lt Thomas Talafuse
Advisor: Dr. Raymond Hill
Reader: Maj Shay Capehart
Department of Operational Sciences (ENS)
Air Force Institute of Technology

Research Objectives:

1. **Need for accurate ballistic impact flash characterization model for valid ignition probabilities and fire predictions.**
2. **Apply experimental design to live-fire-tests**
3. **Develop a ballistic impact event meta-model, enhancing survivability analyses**

Ballistic Impact Flash

- Incendiary ammunition or missile fragments strike aircraft
- Kinetic energy transferred through material deformation, friction, and heat
- Small pieces of material (spall) may also oxidize from intense heat
- Energy dissipated by heat produces flash capable of igniting flammable liquids and starting fires

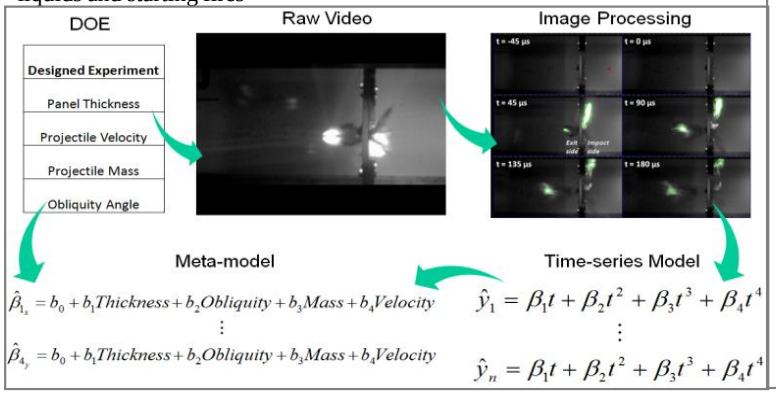

Significance

- First-ever empirical boundary model characterizing ballistic impact flash available
- Boundary model is better alternative than current flash models
- Capable of being easily updated/improved as more data collected
- Model can be coupled with thermal flash model
- Enables more accurate ignition probabilities and improve fire predictions
- Usable throughout the joint survivability community

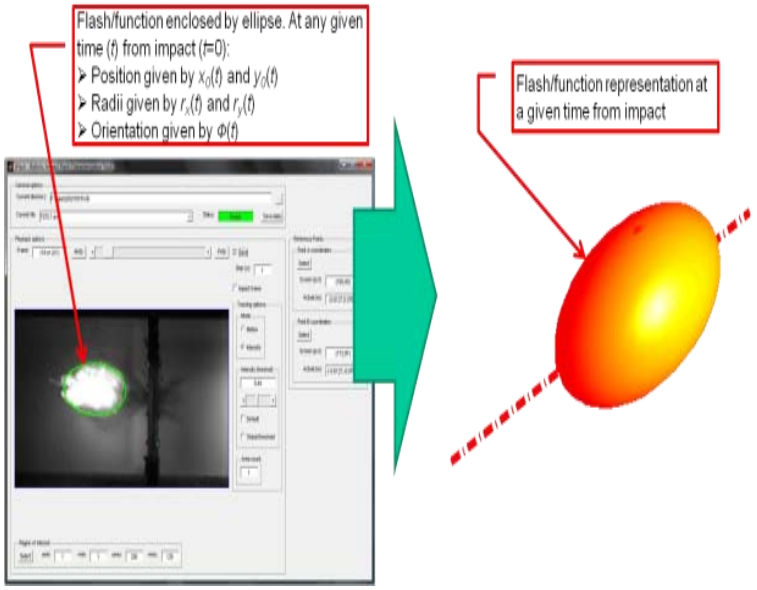

Algorithm

- INPUT: User provides panel thickness
- STEP 1: Flash size model generated
  - Determine quartic model coefficients using the following:

$$\hat{\beta}_{1_x} = b_0 + b_1 Thickness$$
$$\vdots$$
$$\hat{\beta}_{4_y} = b_0 + b_1 Thickness$$

Radius	Coefficient	b_0	b_1
X	β_1	5.244465859	-6.889130548
	β_2	-0.554140103	1.055314656
	β_3	0.019541582	-0.043692468
	β_4	-0.000224115	0.000554559
Y	β_1	7.305658059	1.301390443
	β_2	-0.856882495	0.898951232
	β_3	0.032944706	-0.058336307
	β_4	-0.000396238	0.000871425

- STEP 2: Duration derived from root of quartic model equation
  - Minimum of X-radius and Y-radius root selected
- STEP 3: Random draw from $N(-0.0062, 0.48694)$ to model orientation
- STEP 4: Model position of ellipse centroid

$$P_x(t) = b_{x0} + b_{x1}(t) \rightarrow -22.56174 + 0.00251t \qquad P_y(t) = b_{y0} + b_{y1}(t) \rightarrow 23.49339 - 0.49064\ t$$

- OUTPUT: Flash duration, size and shape of flash for any given time

Results

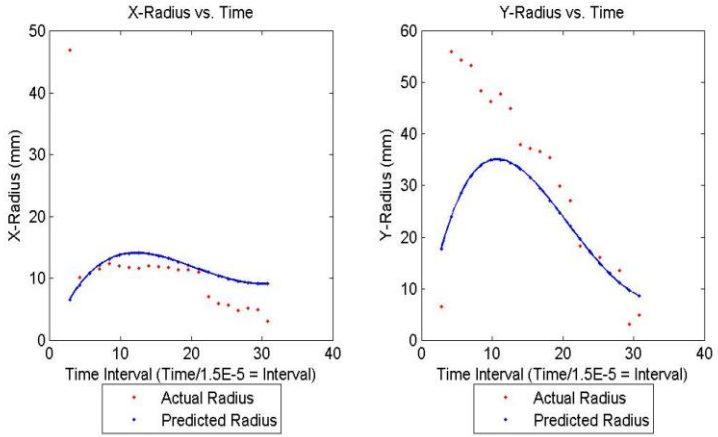

References

Ball, R. *The Fundamentals of Aircraft Combat Survivability Analysis and Design (2nd ed.).* New York, NY. American Institute of Aeronautics and Astronautics. 2003.

Bestard, J., and Kocher,, B. *Ballistic Impact Flash Characterization.* AIAA Conference. 2010.

Henninger, T. *Characterization of Ballistic Impact Flash: An Initial Investigation and Methods Development.* MS Thesis, Air Force Institute of Technology. 2010.

Montgomery, D. *Design and Analysis of Experiments (7th ed.).* New York, NY. John Wiley and Sons. 2009.

AFIT
AIR FORCE INSTITUTE OF TECHNOLOGY

Bibliography

1. Ball, Robert E. *The Fundamentals of Aircraft Combat Survivability Analysis and Design* (Second Edition). American Institute of Aeronautics and Astronautics, 2003.

2. Bestard, Jaime J. and Brian Kocher. "Ballistic Impact Flash Characterization," *AIAA-2010-2573* (2010).

3. Blythe, Robert M. *Preliminary Expirical Characterization of Steel Fragment Projectile Penetration of Graphite/Epoxy Composite and Aluminum Targets*. MS thesis, Air Force Institute of Technology, Wright-Patterson AFB, Ohio, 1993.

4. Henninger, Todd A. *Characterization of Ballistic Impact Flash: An Initial Investigation and Methods Development*. MS thesis, Air Force Institute of Technology, Wright-Patterson AFB, Ohio, 2010.

5. Knight, Earl E. *Predicting Armor Piercing Incendiary Projectile Effects After Impacting Composite Material*. MS thesis, Air Force Institute of Technology, Wright-Patterson AFB, Ohio, 1992.

6. Lanning, Jeffrey W. *Predicting Armor Piercing Incendiary Projectile Effects After Impacting Two Composite Panels*. MS thesis, Air Force Institute of Technology, Wright-Patterson AFB, Ohio, 1993.

7. Montgomery, Douglas C. *Design and Analysis of Experiments* (Seventh Edition). John Wiley & Sons. Inc., 2009.

8. Reynolds, Jon K. *A Response Surface Model for the Incendiary Functioning Characteristics of Soviet API Projectiles Impacting Graphite Epoxy Composite Panels*. MS thesis, Air Force Institute of Technology, Wright-Patterson AFB, Ohio, 1991.

REPORT DOCUMENTATION PAGE

Form Approved
OMB No. 074-0188

1. REPORT DATE *(DD-MM-YYYY)*	**2. REPORT TYPE**	**3. DATES COVERED** *(From – To)*
03-24-2011	**MASTER'S THESIS**	Jun 2010 – Mar 2011

4. TITLE AND SUBTITLE

EMPIRICAL CHARACTERIZATION OF BALLISTIC IMPACT FLASH

5a. CONTRACT NUMBER

5b. GRANT NUMBER

5c. PROGRAM ELEMENT NUMBER

6. AUTHOR(S)

THOMAS P. TALAFUSE, 1st Lt, USAF

5d. PROJECT NUMBER

5e. TASK NUMBER

5f. WORK UNIT NUMBER

7. PERFORMING ORGANIZATION NAMES(S) AND ADDRESS(S)
Air Force Institute of Technology
Graduate School of Engineering and Management (AFIT/EN)
2950 Hobson Street, Building 642
WPAFB OH 45433-7765

8. PERFORMING ORGANIZATION REPORT NUMBER

AFIT-OR-MS-ENS-11-23

9. SPONSORING/MONITORING AGENCY NAME(S) AND ADDRESS(ES)
46th TG OL-AC
Attn: Mr. Jaime Bestard
2700 D Street, Bldg 1661 DSN: 785-6302 x231
WPAFB OH 45433 e-mail: Jaime.bestard@wpafb.af.mil

10. SPONSOR/MONITOR'S ACRONYM(S)

11. SPONSOR/MONITOR'S REPORT NUMBER(S)

12. DISTRIBUTION/AVAILABILITY STATEMENT

APPROVED FOR PUBLIC RELEASE; DISTRIBUTION UNLIMITED.

13. SUPPLEMENTARY NOTES

14. ABSTRACT

Fires onboard aircraft are leading mechanisms for mishaps and losses during peacetime and combat operations. Typical ignition sources causing fires onboard aircraft include electrical sparks and hot surfaces. However, impact and penetration of common threats encountered during combat operations, such as armor piercing incendiary projectiles and missile fragments, generate short-lived, but thermally-intense clouds (flashes) capable of igniting fires. Fire simulations supporting system-level survivability analyses depend on accurate characterization of these flash clouds, however, such accurate representations are not currently available.

This research presents the modeling approach developed to estimate the boundary model representations of impact flashes. The research presents generalized meta-modeling approaches to estimate flash size radii (in both the X and Y dimension), flash position, flash size duration, and flash orientation. The empirical model was developed using actual test data obtained via live-fire testing conducted by the 46th Test Group, Aerospace Survivability Analysis Branch. The time series response data from a set of live-fire test events were validated, analytical methods used to develop that response data based on impact event image processing were refined, and the data were then used to create fourth-order time series models of the response data for each of the test events. The collective of these time series models were then characterized by their parameter sets and a meta-model of those parameterizations was built as a function of test event setup parameters (e.g., projectile speed, angle of attack, and impact material) These final models were transitioned to the customer and are being linked to physics-based thermal models. The end result will be a first-ever projectile impact flash cloud representation suitable for survivability analyses.

15. SUBJECT TERMS
Survivability, Operations Research, Empirical Modeling, Design of Experiments

16. SECURITY CLASSIFICATION OF:			**17. LIMITATION OF ABSTRACT**	**18. NUMBER OF PAGES**	**19a. NAME OF RESPONSIBLE PERSON**
a. REPORT	**b. ABSTRACT**	**c. THIS PAGE**			Raymond R. Hill, Ph.D.
U	**U**	**U**	**UU**	96	**19b. TELEPHONE NUMBER** *(Include area code)* (937) 255-6565, ext 4314; e-mail: raymond.hill@afit.edu